Doctoral Thesis

Developing Multi-functional Nanoplatforms Using Protein Architectures

Hyojin Moon

Department of Biological Sciences

Graduate School of UNIST

2017

Developing Multi-functional Nanoplatforms Using Protein Architectures

Hyojin Moon

Department of Biological Sciences

Graduate School of UNIST

ULSAN NATIONAL INSTITUTE OF SCIENCE AND TECHNOLOGY

Developing Multi-functional Nanoplatforms Using Protein Architectures

A thesis submitted to the Graduate School of UNIST
in partial fulfillment of the requirements
for the degree of Doctor of Science

Hyojin Moon

04. 26. 2017

Approved by

Advisor

Sebyung Kang

ULSAN NATIONAL INSTITUTE OF SCIENCE AND TECHNOLOGY

Developing Multi-functional Nanoplatforms Using Protein Architectures

Hyojin Moon

This certifies that the thesis of Hyojin Moon is approved.

04.26.2017 of submission

Advisor: Sebyung Kang

Sung You Hong

Taejoo Park

Hyun-Woo Rhee

Moonil Kim

Abstract

A variety of nano-sized materials are developed in the biotechnology fields. Developing nano-sized particles have become a critical issue in biomedical applications because they are closely related to quantum yield, large surface area and EPR effects. Despite these advantages of nanoparticles, it has become indispensable to use more advanced nanoparticles due to their chemical complexity, heterogeneity, difficulty in precisely controlling the size, and toxicity *in vivo* applications. In this regard, protein-based nanoparticles have biocompatibility, uniform size, shape, composition and stability, and they are quite suitable as multifunctional nanoplatforms. In addition, the structures of protein nanoparticles are based on the atomic resolution crystal structure allowing genetic and chemical modifications at the molecular level.

The aim of this thesis was to describe of developing the multi-functional protein nanoparticles using protein cages and monomeric fusion proteins. Thus, *Thermotoga maritima* encapsulin protein cage whose outer diameter 24 nm was developed as *in vitro* theranostic nanoplatform. A novel protein cage, encapsulin have not been used for targeted delivery system before, and was prepared as a versatile template for targeted delivery through SP94 peptide insertion which known to bind with hepatocellular carcinoma cells. Functional plasticity and versatility of the engineered encapsulin allow us to apply for specifically detecting and effective treatment of diseases.

Relatively small lumazine synthase which isolated from *Aquifex aeolicus* (AaLS) protein cage nanoparticles with outer diameter of 15.4 nm have been utilized to develop as uniform layer by layer assemblies. High ordered structures of two complementary AaLS protein cages were successfully constructed using simple recognition of histag and Ni-NTA.

Furthermore, fluorescent imaging modular toolkits were established using monomeric fusion proteins and ligation proteins by giving cancer cell targeted capability of affibody and visualizing cancer cells of fluorescent proteins. These affibody-fluorescent protein conjugations are post-translationally generate, allowing simple and rapid binding between affibodies and fluorescent proteins.

A variety of protein nanoparticles demonstrated that they have potential to be utilized as a multifunctional nanoplatforms in biomedical and biotechnology fields.

Contents

List of figures

Chapter 1. Introduction

Chapter 2. Encapslin Protein Cage as a Targeted Delivery Nanoplatform

Chapter 3. Cell Imaging Modular Toolkits using SpyTag/SpyCatcher

Chapter 4. Layer-by-layer Assemblies with Protein Cage via His-tag/metal Recognition

Appendix A. Analytical techniques

Appendix B. Encapsulin fusion protein cage

Abbreviations

AaLS : Aquifex aeolicus lumazine synthase

AFM : Atomic force microscopy

ATRP : Atom transfer radical polymerization

CCMV : Cowpea chlorotic mottle virus

CPMV : Cowpea mosaic virus

DLS : Dynamic light scattering

EGFR : Epidermal growth factor receptor

EPR : Enhanced permeability and retention

ESI-TOF MS : Electrospray ionization-time of flight Mass spectrometry

eYFP : enhanced yellow fluorescent protein

FcBP : Fc binding peptide

GFP : Green fluorescent protein

HCC : hepatocellular carcinoma

HER2 : Human epidermal growth factor receptor 2

His_6 : Hexa Histidine

Hsp : Heat shock protein

LbL : Layer by yayer

LHRH : Hormone releasing hormone receptor

MjHsp : *Methanocuccus jannaschii* heat shock protein

PfFn : Pyrococcus furiosus ferritin

QCM : Quartz crystal microbalance

SEC : Size exclusion chromatography

SMCC : Succinimidyl 4-(N-maleimidomethyl) cyclohexane-1-carboxylate

SPR : Surface plasmon resonance

TEM : Transmission electron microscopy

TFP : teal fluorescent protein

VLP : Virus like particles

ZnPc : Zinc phthalocyanine

Chapter 1. Introduction

1.1 Applications of Multi-functional Nanoplatforms

1.1.1 Targeted Cell Imaging and Drug delivery

The development of various nanotechnology has been widely applied to the diagnosis, treatment and prevention of diseases, and these technologies are changing the scientific atmosphere.

Thus, more techniques are used to develop faster and more accurate diagnosis and treatment techniques of which targeted imaging systems enable this process. Techniques for imaging specific cancer cells have played a significant role in understanding the functions, behavior, and mechanisms of cells.[1-2]

In addition, targeted imaging of specific cancer cells means to diagnostic and treat of cancers rapidly, and effective, and the concept of simultaneous diagnosis and treatment is called theranostics and has been studied for decades.[3] Although non-target therapies have generally caused critical side effects to normal cells or tissues, specific targeted delivery techniques can reduce these side effects. This targeted imaging and delivery system allows cells and tissues to be simply visualized a more faster and reliably, thus they can be treated more effectively with fewer side effects. In these targeted cancer cell imaging, antibodies, antibody mimics, peptide or chemical ligands have been explored and studied in a wide range of applications.[4-10]

Targeted imaging and therapy using these targeted moieties (antibody, antibody mimics, peptide and chemical ligands) not only enable rapid diagnosis and treatment of disease, but also allows the drugs to stay a little longer in the bloodstream of the body.[11] Conventional diagnostic probes or drugs tend to spread rapidly and are easily dispersed throughout the body, but therapeutics with a target functions are conjugated, they can be delivered effective and localized disease treatments by transferring the therapeutic agent to the desired site. This concept is challenging but still considered a valuable and promising task.

Passive and active targeting of tumors

Cell targeting systems can be divided into passive targeting and active targeting, and it is important to decide the nanoparticle size in passive targeting. Bloodstream of tumors is limited by angiogenesis, which makes nutrient uptake and oxygen delivery difficult. In addition, angiogenesis leads to a lack of cells around the blood vessels, which reduces the diffusion of the targeted drug because the internal pressure of the tumor is higher and causes fluidic flow. Nano-size particles can be trapped in the tumor through enhanced permeability and retention (EPR) effects.[12] Passive targeting can also induce targeting using the intrinsic characters of nanoparticles, such as cationic liposomes are bound by electrostatic

interaction with negatively charged phospholipid head groups that are preferentially expressed in tumor endothelial cells.[13-14]

Active targeting involves using conjugated target sites to enhanced delivery of the nanoparticle system. Targeting site is important for the cell uptake mechanism, and the long cycle time enables the nanoparticle to be efficiently transported to the tumor site through the EPR effect, and the targeted molecules can endocytose in cells readily.[15-18] As drug loaded nanoparticles endocytose, the therapeutic effect can be increased. Therefore, in most cases, endocytosis of nanoparticles plays a key role in biotherapeutics such as effective delivery of certain anticancer drugs, and gene delivery.[19]

Targeting to Breast cancer

The number of cancer patients is steadily increasing every year, especially breast, lung, prostate and colorectal cancers accounting for the largest percentage.

The most commonly used strategy for drug delivery is to target the HER2 receptor, which is particularly overexpressed in breast cancers. The efficacy of therapeutics targeted poly (lactic-co-glycolic acid, PLGA) nanoparticles loaded with a model toxin against HER2 positive tumors was recently studied.[20] N-hydroxysuccinimide presenting nanoparticles were chemically conjugated with primary amine groups on the humanized anti-HER2 antibody fragments and to target BT-474 cells compared MCF7 cells, HER2 negative cell. In another group, targeting to SK-BR-3 cells of antibody binding domain genetically inserted protein cage bound with anti-HER2 antibody was estimated using confocal microscope and flow cytometry.

Folate receptor has also been utilized for the improved therapy. Folate acid conjugated magnetite nanoparticles target with BT-20 breast cancer cells *in vitro* studies.[21] The hormone releasing hormone (LHRH) receptor is another target which has been widely investigated for targeted delivery of imaging agents and treatment of localized breast cancer. Iron oxide nanoparticles conjugated with LHRH and interacted with MDA-MB-435S.luc breast cancer cells and demonstrated the accumulation of targeted nanoparticles to tumor tissues.[22]

1.1.2 High-ordered Structure

The development of uniform nanostructures, including biomolecules, has received much attention in many applications due to their technical and scientific importance in terms of space control and effective space utilization. Molecular structures with well-defined particle sizes and shapes are used in a variety of applications ranging from imaging agents, thin films, multi-layer films[23-25], nanoelectronics to biological sensing devices.[26-28] Therefore, it is important to produce uniform nanostructures with functional nanomaterials and biomacromolecules. The multi-layer arrangement of functional

biomolecules provides little specificity and/or activity, their spontaneous or directed assembly being achieved by the covalent interaction of the components to produce larger structures from the bottom-up.

Using the surface properties of two or more biomaterials, it is called layer-by-layer (LbL) assembly to make an arranging or stacking several layers uniformly without any aggregation.[29-30] Furthermore, a specific recognition is needed to bind two or more materials. Considering these points, a protein-based nanoparticle that is uniform in size and regular and capable of producing assemblies through chemical or genetic modification is suitable, and can be applied *in vivo* because it is a biomaterial.

In particular, the layer-by-layer assembly has been used for biomineralization and drug delivery system using biodegradable materials such as protein cages which have interior cavity. Therefore, protein-based nanoparticles such as protein cages can be used to make a uniform high-ordered structure while retaining the characteristics of a multi-layer arrangement, or a complex assembly can be formed by adding various functions to each protein cage could be used in many fields.

Proteins can also be used in biofilms, biosensors, and drug delivery systems using LbL assembly. One of the main trends in biology applications of the LbL assembly is the use of bioactive proteins to form thin films into electronic devices, sensors, drug delivery, cell seeding and growth, and tissue engineering. The main concern is to make films that are stable and bioactive after stacked in multi layers. One example was that a multilayer film containing the enzyme glucose oxidase (GOD) was prepared by alternative adsorption of anionic glucose oxidase and anionic PDDA or PEI. The reacted enzyme activity was measured using D-glucose, peroxidase, and DA67 dye to test the bioactivity of GOD.[31] The formation of such a charged multilayer structure has also been demonstrated in other group, they showed combination of positively charged myoglobin and negatively charged lysozyme can be used. This approach has confirmed that multiple structures also apply to proteins, but there is a limitation that such weak adsorption cannot proceed naturally between proteins and poly ions of the same charge.

Protein cage are useful tool to overcome limitations and to create a more rigid and fixed assembly structure. CCMV[32], CPMV[33] and ferritin[34-35] were exploited for nano-building blocks with strong binding using streptavidin and biotin interactions[32-38] (Figure 1.1). In the case of CCMV, it was confirmed that multi-layer could be formed through labeling different fluorescein on each particle. It demonstrated that CCMV can be utilized as multifunctional nanoplatform to enhance the signal in the imaging system.[38]

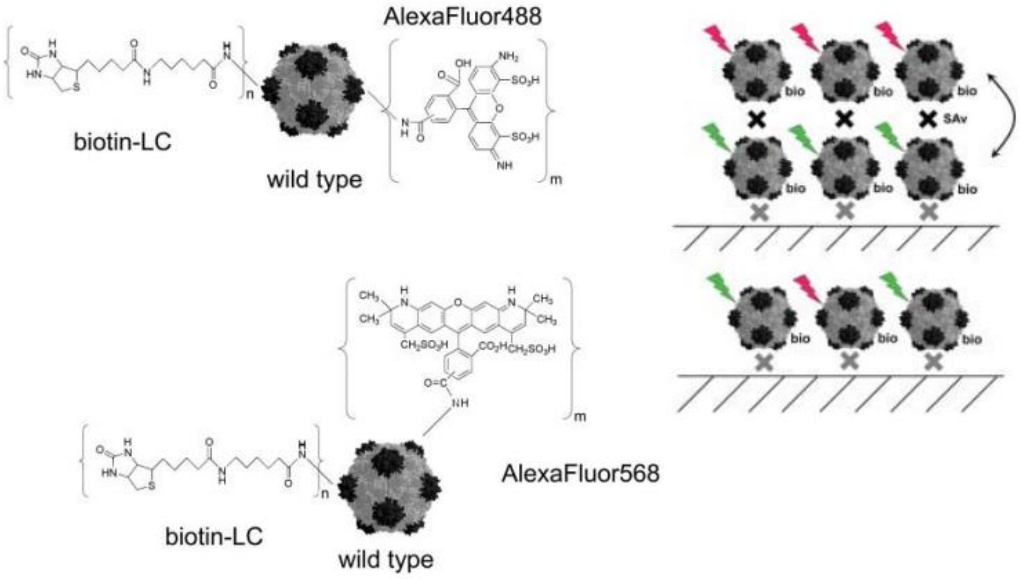

Figure 1.1 Representation of chemically modified CPMV: CPMVBIO-AF488 and CPMVBIO-AF568 (left), diagrammatic representation of layer structures (right).[39]

1.2 Protein-based Nanoplatforms

A wide variety of nanoparticles have been exploited for various applications to diagnose diseases or detect cancers *in vitro*/*in vivo*. Especially, for *in vivo* imaging, a variety of nanoscale delivery platforms, the nanometer-range size and manipulation of nanoplatforms generally result in enhanced permeability and retention (EPR) effects that allow deep penetration of delivered cargoes, such as therapeutics and diagnostics, and a long circulation time in the blood stream, and consequently these nanoparticles have a promising potential because they could provide effective clues to help to make right decision in therapy.[40-41] However, nanoscale delivery platforms such as inorganic and polymeric nanoparticles, liposomes and micelles have chemical complexity and heterogeneity often make it difficult to control their size, shape, and composition in a precise way. In addition, although some nanoplatform such as gold nanoparticles, carbon nanotubes or photosensitizer-based nanoparticles can be utilized for therapy, their depth penetration are limited, obstructing their clinical purpose.

To overcome these drawbacks, natural-derived protein-based nanoparticles can be used, which are well-controlled and have a biocompatibility and solubility by effectively chemical and genetic manipulating the surface of proteins. Also, they have symmetric protein structures and consist of identical subunits with a highly uniform size distribution. Moreover, they were already identified their

atomic resolution structures, and allow us to rationally design and genetically modified the desired site to give multiple functions. Therefore, proteins are considerable to be one of the excellent candidates for multi-functional nanoplatforms for various applications. Here, two kinds of proteins, protein cages and monomeric proteins will be discussed.

1.2.1 Protein Cage Architectures

Over the past few decades, a wide range of protein cages nanoparticles, such as ferritin[8, 42-45], heat shock proteins (Hsps)[7, 46-49], and virus-like particles (VLPs)[40-41, 50-64], have been investigated for biotechnology applications. Protein cages are precisely self-assembled into macromolecules from multiple copies of a limited number of protein subunits. Therefore, they have very uniform size and composition also biocompatibility because they are built by nature. Thus, they do not have toxic as in *vitro*/*in vivo* materials. Furthermore, they are very stable itself, chemical or genetic manipulations are enable. Protein cages have a compartment of exterior, interior and interfaces allowing to give various functions as multi-functional nanoplatforms (Figure 1.2).

Most of them are made up of spherical spheres that have a certain symmetric shape and thus have cavity inside of cages. This cavity can accommodate a variety of guest molecules, cargoes such as drugs or imaging probes, and enzymes which are needed to protect from the harsh conditions. Taking advantages of these protein cages, many groups continue to be actively researched for use in a wide range of biomedical, materials, biosensor applications, and will be used in more applications in the future.[65]

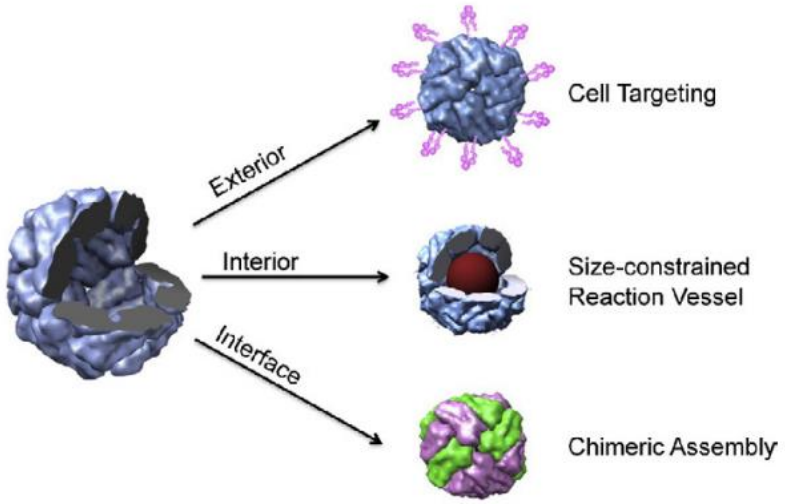

Figure 1.2 A schematic illustration of the three interfaces of a protein cage that can be exploited to impart designed functionalities.[66]

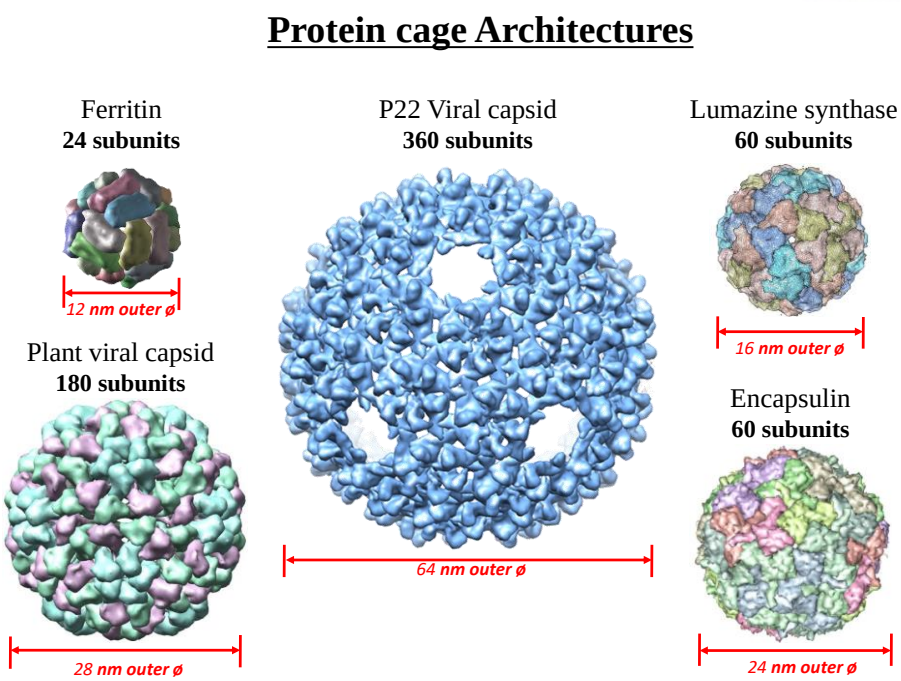

Figure 1.3 A schematic illustration of various types of protein cage architectures as multi-functional nanoplatforms.

Ferritin is one of the most commonly used nanoparticle which is originally an iron storage protein and has been utilized successfully in biomedical fields because ferritin is stable at higher temperature and wide range of pH. Ferritin is composed of 24 subunits, with a size of 12 nm exterior and 8 nm inner diameter, respectively[66] (Figure 1.3). Ferritin has been manipulated to encapsulate various inorganic particles inside ferritin cavity which is capable for storing iron, through biomineralization, and has been used for in vitro or MRI.[66-71] Since the inside of ferritin is not enough large size, it is not easy to encapsulate other guest molecules besides small sized inorganic particles. Thus, the exterior surface was modified and used for applications such as drug delivery or targeted cell imaging.

A relatively short amino acid sequence, RGD-4C (DCDRGDCFC)[72], was genetically presented on the exterior surface of ferritin and manipulated to target it to cells in which integrin $\alpha_{\gamma}\beta_3$ over expressed cells.[8, 73-74] In addition, chemotherapeutic agent, doxorubicin was labeled and used in a targeted drug delivery system. EGF-human heavy chain ferritin (HFn) nanoparticles were also used to target epidermal growth factor receptor (EGFR) expressed in many breast cancer cells.[75-76]

In another group, the Fc binding peptide (FcBP) was genetically introduced into the loop region which exposed to the exterior surface of pyrococcus furiosus ferritin (PfFn), bound to IgG, and then targeted to folate receptor overexpressed breast cancer cells.[77]

Ferritin was also exploited through chemical conjugation such as click chemistry. The reactive cysteine residue on the exterior surface and 24 β-cyclodextrins were conjugated and converted to β-CD-HFn complexes through thiol-maleimide addition.[43, 78] After inclusion complexes form, the encapsulated guest molecules were gradually released into the buffer solution. This study has potential as a system to deliver hydrophobic drugs.

Heat shock protein (Hsp) are expressed in response to other types of stress such as high temperature, and composed of small heat shock protein and *Methanocuccus jannaschii* heat shock protein (MjHsp). MjHsp cage is self-assembled into 24 subunits, and 12 nm of outer and 6.5 nm inner diameter, respectively. The major difference between ferritin and MjHsp is that there are 3 nm pores allowing small molecules to diffuse in or out of the cage. This cage is also extremely robust because very stable up to 70°C and pH 5-11.[79-81]

Heat shock protein, like other protein cages, has been applied in the biomedical field with various functions through interior and/or exterior modifications. Specific amino acid residues were genetically replaced for presenting thiol and amine groups to encapsulate and release the doxorubicin. The encapsulate doxorubicin was quantified by mass spectrometry and the dox was released through a hydrazine linker that causing cleavage at a low pH such as endosome. This MjHsp nanocontainer could have multi-functions like cell targeting peptides or antibodies that are enable to target specific cells. Like ferritin, RGD peptide was used for targeted cell imaging.[7, 82] In addition, LyP-1 peptide which targets a tumor-associated lymphatic vessels and macrophages was attached to the C-terminus of Hsp as a targeting moiety.[83-84]

In another group, they used the SP94 peptide to target the hepatocellular carcinoma (HCC) cells. The amine group on the exterior surface of MjHsp was linked to the SP94 peptides using a bifunctional PEG linker.[46, 48, 85] Targeting efficacy was confirmed using a confocal microscope, and SP94 inserted Hsp was proved to have specificity to Huh-7 cells not to target other cells. This group also demonstrated that the linker length of the N-term of SP94 in Hsp decided cell binding efficacy. This result indicated that the length of the linker controls the density of the SP94 peptides. Furthermore, preS1 peptide that is derived from hepatitis B virus and specifically target the liver cells was introduced to MjHsp indicating high affinity for liver tissue and low cytotoxicity.[86]

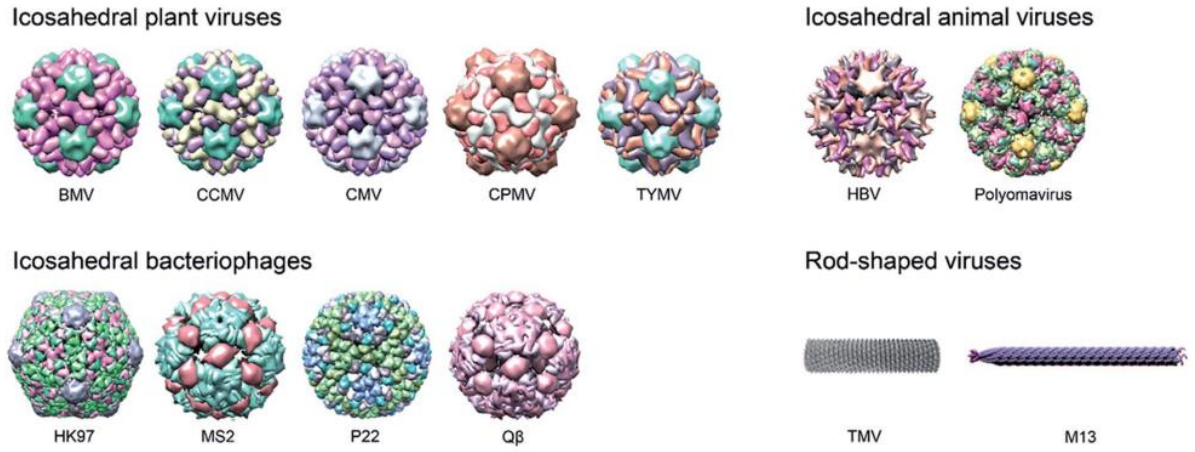

Figure 1.4 Virus (-like) particles used in biomedicine. Icosahedral plant viruses: brome mosaic virus (BMV), cowpea chlorotic mottle virus (CCMV), cucumber mosaic virus (CMV), cowpea mosaic virus (CPMV), turnip yellow mosaic virus (TYMV). Icosahedral animal viruses: human hepatitis B (HBV), murine polyomavirus. Icosahedral bacteriophages: HK97 (tail not shown), MS2, P22 (tail not shown), Qb. Rod-shaped viruses: tobacco mosaic virus (TMV), bacteriophage M13.[87]

Plant and bacterial virus-like particles (VLPs) are another common type of protein cages architectures. Viruses consist of protein capsids that store and protect viral nucleic acids such as DNA and RNA. Virus capsids have properties that are suitable for use in nanotechnology. Especially, it has been sued as a unique nanocontainer due to its various sizes, shapes and strong symmetry. Many studies have shown that most of the viruses can become self-stabilizing into virus-like particles even in absence of genetic materials. Such virus-like particles include plant viruses (CCMV, CMV, CPMV, BMV and TYMV), bacteriophage (HK97, MS2, P22 and Qβ), an animal viruses (HBV, polyomavirus). These virus-like particles have icosahedral architecture, and there are rod-shaped TMV, M13 which are applied in the biotechnology fields[87-88] (Figure 1.4).

The cowpea chlorotic mottle virus (CCMV) capsid consist of 180 identical 20kDa subunits self-assembled to form *T=3* symmetry, with 28 nm of outer and 18 nm of inner diameter, respectively.[89] The coat protein of CCMV can be obtained using *E. coli*-based expression system. The N-terminus of the capsid protein is primarily positively charged and encapsulate negatively charged guest molecules because N-terminus located inside the capsids. An attractive feature of CCMV is capable of reversible expansion depends on pH and has 60 pores of 2 nm in diameter. A group reported that fluorescent dyes could be labeled to existing amines or carboxylic acids exposed on the surface of CCMV without any disrupting the cage structure. Moreover, genetically engineered a mutant with two surface exposed thiols per capsid protein since wild-type virus do not have reactive cysteine residues.[90] Subsequently,

two thiols were chemically linked to 24 amino acids of anti-tumor peptide. In addition, CCMV has also been applied to the treatment of bacterial infections through photodynamic therapy (PDT).[91] Specific wavelengths were used to excite the photosensitizer to generate active oxygen species and kill the target cells. In this study, the ruthenium complexes were chemically attached to the external cysteine residues as a photosensitizer. To enhance the cytotoxic efficacy of PTD, specific antibody which targets *S.aureus* cells was used and compared to untargeted ruthenium complexes. It results that 100-fold increase in the activity. Another group described the encapsulation of zinc phthalocyanine (ZnPc) as a therapeutic agent depends on pH and salt concentration. Depending on the pH and ionic strength, 180 subunits are able to disassemble and reassemble *in vitro* (figure 1.5).[92]

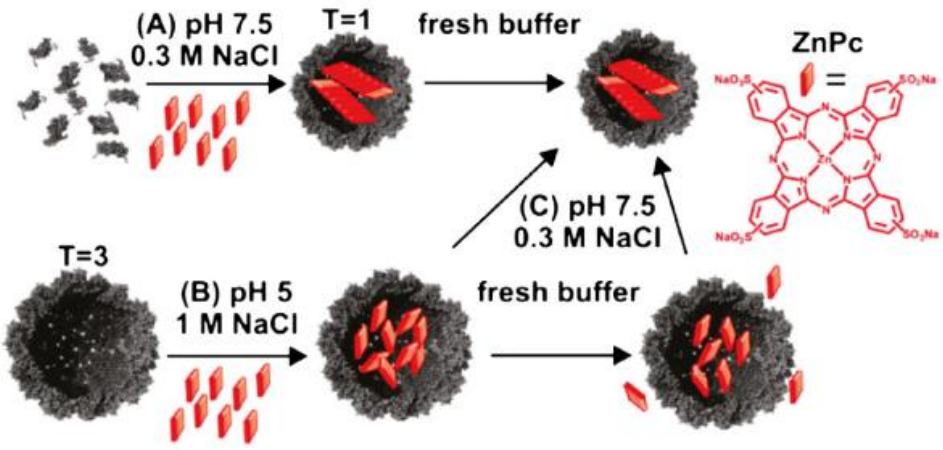

Figure 1.5 Schematic representation of the routes for the encapsulation of ZnPc stacks into CCMV VLPs.[92]

The inside hollow of the CCMV was utilized as well as the outer surfaces. N-terminus of the capsid protein was modified into a positively charge leucine zipper and attached with negatively charged the green fluorescent protein (EGFP). The amount of encapsulated EGFP can be precisely controlled by changing the ratio between wild-type and the capsid protein, and up to 15 EGFP molecules could be encapsulated. CCMV has also been extensively studied for encapsulation of various therapeutic agents and contrast agents for using in a wide variety of applications.

Previous studies have demonstrated that CCMV can encapsulate toxic cargoes or organic and inorganic molecules inside the capsid and it can target the specific cells. It will be useful to continue to be applied in biotechnology and biomedicine fields.

Bacteriophage Qβ is 180 copies of assembled icosahedral virus with a diameter of approximately 30 nm and MG. Finn group have functionalized Qβ in first time. Unlike other virus-like particles, Qβ is characterized in that RNA is packaged inside the Qβ. Some fluorescent proteins were encapsulated inside engineered Qβ via RNA-protein interaction. RNA hairpin aptamer linked between coat protein monomers and tagged fluorescent protein (Figure 1.6).[93] The molecules inside the Qβ were stable at high temperature and pH, with identical photochemical properties, and also protected from proteolytic cleavage. The outer capsid surface was able to be modified through azide-alkyne cycloaddtion without any affecting the packaged fluorescent protein. Carbohydrate-based ligands which has high affinity to the CD22 receptor were attached and targeted cells. The efficacy of targeting was confirmed by confocal microscopy and flow cytometry.

In the same group, two plasmids which were wild-type Qβ and EGF-modified Qβ were co-assembled. Human epidermal growth factor (EGF) was displayed on the exterior surface of Qβ and used for targeted cell imaging. Epidermal carcinoma the A431 cell line is known to be EGFR overexpressed cell. EGF presented Qβ targeted with high affinity to A431 cells and its efficacy was confirmed by confocal microscope. The Qβ-EGF nanoparticles were demonstrated they can be utilized as a targeted delivery imaging and therapeutic agent as a useful tool by killing cells depends on their concentrations different from wild-type Qβ.[52]

In a recently published paper, a method has been proposed to more efficiently utilize the interior cavity of Qβ through the hydrolytic removal of packaged RNAs inside Qβ. The RNAs were removed and fluorescein was loaded inside the Qβ via the atom transfer radical polymerization (ATRP) technique, and the polymerized Qβ expanded a little in size. Qβ VLPs filled with cationic polymer appeared to be more cellular internalized than polymer-free Qβ.[94-95] Mutant which has enhanced cell binding and uptake ability indicated the possibility of being used in cellular delivery.

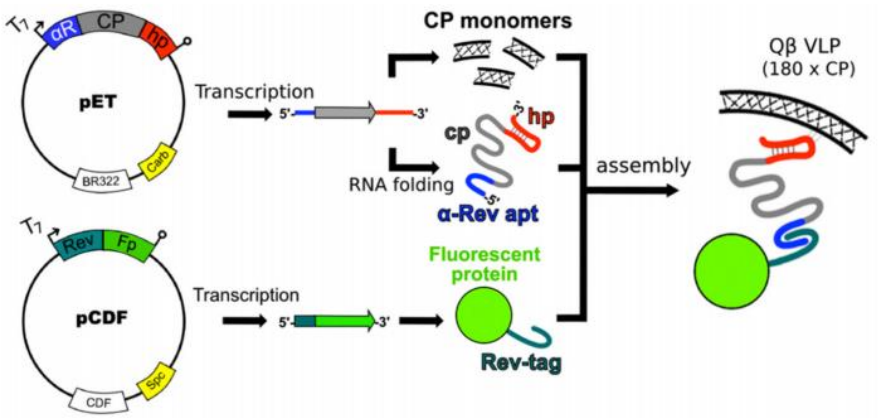

Figure 1.6 Schematic representation of the technique used to package protein inside Qβ VLPs.[93]

There is another bacteriophage nanoparticle as well. The *Salmonella* bacteriophage P22 is now regarded as a robust nanoparticle and have been applied to biotechnology and biomedical fields. The assembly pathway of P22 is well understood and initially assembled into 58 nm icosahedral procapsid structure with approximately 300 copies of identical scaffolding proteins. Heat treatment of P22 procapsid at 75°C for 15 min transformed to 64 nm waffle-ball (WB) capsid with twelve 10 nm pores, creating a hollow nanocomposite (Figure 1.7).[96]

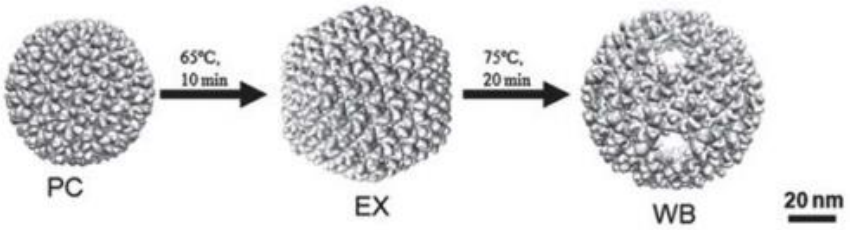

Figure 1.7 P22 VLP morphology and packaging assembly (Cryo-EM reconstructions images).[96]

P22 is mainly used for encapsulation because it is relatively large compared to other nanoparticles and the interior space is also suitable for incorporating other guest molecules. The P22 studies were mainly activated by T. Douglas group. The exact structure of virus-like particles such as P22 has been proven to be advantageous in synthetic material applications. These properties can be used not only as nanocontainers but also to find local intermolecular communication between encapsulated proteins.[96-

[100] In FRET technique, the length between two molecules plays an important role, thus limited space such as inside space of P22 particles is required.

In co-encapsulation system, P22 was used as a promising platform for studying dense, forced proximity and restriction effect on communication between active proteins.[101] Considering the size of P22, three enzymes were packed for enzyme cascade. In the meaning of a spatially separate internal space, P22 particles have been exploited as nanocontainers to produce hydrogen using hydrogenase which in inside of P22, hydrogenase was protected against air, heat or external factors.[98] In addition, P22 was used as a high-density transferring means to make protein polymers by using this limited space via ATRP.[64] This technique was a good tool in the development of a better MRI contrast agent as more molecules were loaded. It has also been used as a template for the limited synthesis of Fe_2O_3, complementing the bottle neck of synthesis of inorganic particles with non-uniform size and shapes.[60, 102] Another group developed the drug loaded targeted cell imaging particles. They conjugated doxorubicin or BTZ drug inside the WB and SP94 peptide was genetically inserted on the exterior surface[55] (Figure 1.8).

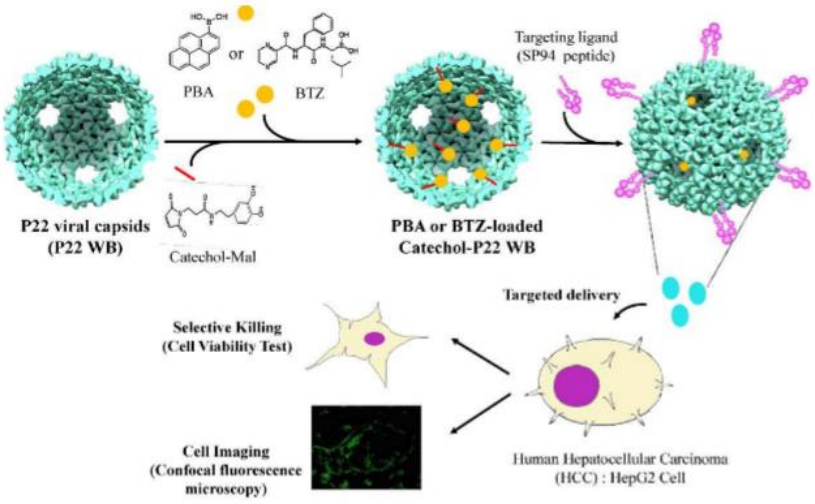

Figure 1.8 Covalent encapsulation of cargo molecules and evaluating the targeted delivery and the efficacy of P22 WB capsid nanocomposites by cell imaging and cell viability test.[55]

Encapsulin protein cage is isolated from *Thermotoga maritima*, recently developed as a multi-functional nanoplatform. Its atomic resolution structure information has been recently resolved by Sutter group (Figure 1.9). Encapsulin is spontaneously composed 60 copies of identical subunit with around 31 kDa to form u uniform icosahedral cage architecture with 18 nm and 24 nm of interior and exterior diameters, respectively. Although the exact function of encapsulin in *Thermotoga maritima* is not clearly understood yet, its function was postulated as a cellular compartment that encapsulates proteins such as DyP (Dye decolorizing peroxidase) and Flp (Ferritin like protein) which are involved in oxidative stress responses.[103] These properties of the protein cages make it possible to insert guest molecules into the interior of the cages, especially molecules that enzymes or require protecting. Guest molecules are encapsulated inside the protein cages using disassembled and reassembled process depends on pH condition, and they have biocompatible, stabilizing and protecting from the external circumstances without any toxic and immunogenic responses.

The number of encapsulin is now increasingly being isolated from 15 kinds of bacteria and encapsulin is a novel protein cage with the potential to developed in a variety of applications. Encapsulin has the ability to encapsulate specific molecules, and using these properties, many research groups have applied other molecules into encapsulin for biotechnology applications.

Several techniques for encapsulating in encapsulin protein cages have been used, one of that is assembly and reassembly system depending on pH value. To pack peroxidase DypB into *R.jostii* RHA1 encapsulin, it is diassembled at acidic pH (pH 3), mixed with peroxidase DypB molecules, and then increased to neutral pH to obtain encapulin having peroxidase DypB inserted therein. Reassembled encapsulin showed no changes in shape but slightly increased in size, indicating that structure extended.[104]

In the case of encapsulin isolated from *Brevibacterium linens*, a docking sequence was inserted at the C-terminus of the teal fluorescent protein (TFP), and then it was recognized with specific amino acids of interior surface in encapsulin. To quantify the number of TFP, native mass spectrometry was used and approximately 12 TFPs were encapsulated.[105] Another group also encapusted guest molecules such as EGFP and firefly luciferase using this specific recognition sequence. In this study, a proteolysis, trypsin was treated to packaged guest molecules to determine of protect function by encapsulin protein cage and whether the molecules inside were active. It demonstrated that packaged molecules were protected by a protein cage, but do not lose activity and they can be exploited in more applications.[106]

Recently, silver was synthesized in encpasulin through mineralization. As silver particles have an antimicrobial activity, silver mineralized encapsulin can be used for killing the bacteria. The silver nanoparticles grew by limited size of encapsulin and absorbed at 420 nm wavelength, indicating that silver ions mineralized well inside the encapsulin protein cages. Encapsulated silver was more stable

than unwrapped silver nanoparticles. In addition, a uniform silver particles could be formed and well-capping silver nanoparticles by encapsuilin could be utilized for antimicrobial tools[107] (Figure 1.10).

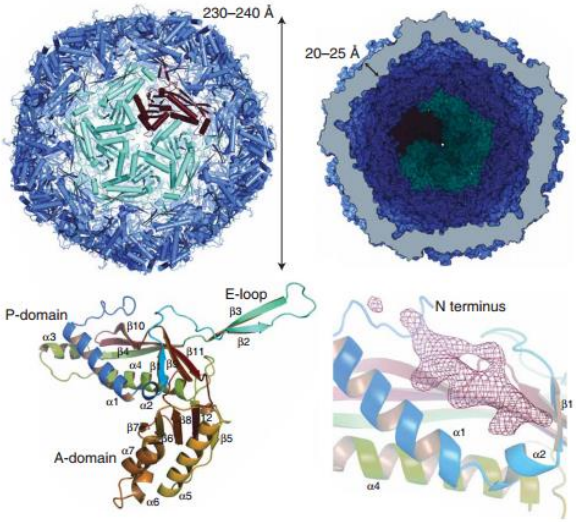

Figure 1.9 Structure of the *T. maritima* encapsulin. View from the outside on the five-fold symmetry axis. (Pentamer is highlighted in cyan, with one monomer in red. Pink mesh indicated docking site.)[103]

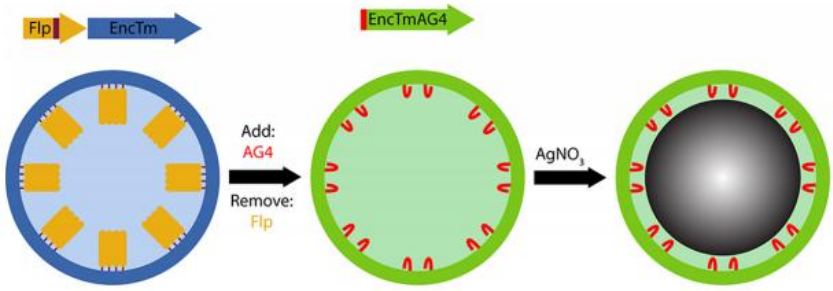

Figure 1.10 Engineering of the *T. maritima* protein compartment. Schematic depiction of capsid engineering. The ferritin-like protein (Flp, orange) was removed from the wild-type encapsulin system and the AG4 peptide (red) was fused to the N-terminus of EncTm yielding EncTmAG4, which would then allow the size-constrained synthesis of silver nanoparticles in its interior when exposed to silver ions.[107]

1.2.2 Fusion Proteins using Monomeric Proteins

Since monomeric proteins are small size and capable of various chemical and genetic modification and have high biocompatibility, they are useful tools to construct fusion proteins for biomedical fields.

Cancer cell targeting using Affibody molecules

The specific binding moiety of cancer cells that have been studied so far include antibodies, peptides, affibodies, chemical ligands, aptamers, and the like. These moieties can target to highly overexpressed receptors on specific cancer cell surfaces. Targeting moieties conjugated with cytotoxic drugs, pro-apoptosis agents, therapeutic oligonucleotides can be utilized as complexes that act to diagnosis and treatment, simultaneously.

Currently, antibodies are the most successful and widely used affinity proteins in the life sciences. The advantages of varied antibodies are strong affinity, specificity and readily available. Antibodies exhibit strong binding and may be selected for high selectivity, but they have limitations in terms of molecular properties. IgG molecules, the most commonly used antibody types, are multi-domain proteins and have relatively poor thermal stability and are subject to expensive manufacturing processes. In addition, antibodies use only a small portion of the molecule to recognize the antigen, while large domains with antibodies add structural complexity. Therefore, alternative scaffold proteins are capable of expressing small size, high yield in bacteria system with high affinity, which is an advantage of antibodies.

These days, as lots of technologies have been advanced and developed, *in vitro* generation of large pools of candidates for non-antibody affinity proteins is much more convenience (Figure 1.11). One of the alternatives to the antibodies is affibody molecule. Affibody molecules are originally derived from the B-domain in the immunoglobulin-binding region of staphylococcal protein A. The B-domain consists of 58 amino acids, a relatively short, cysteine-free peptide, folded into three-helical bundle structures. The kinetics of the folding reaction rate is the fastest that has been reported.[108] Affibody molecules showing specific binding to a variety of different proteins (e.g. IL-2, gp120, insulin, fibronectin, tumor necrosis factor-α, human serum albumin, HER2 and EGFR) have been generated, demonstrating affinities (Kd) in the μM to pM range. According to the fact that the reports focusing on studies about possible use of the affibody have been significantly increased recently, engineering and developing a small affinity protein have a tremendous potential to be used in theranostics as an alternative form of the conventional antibodies.

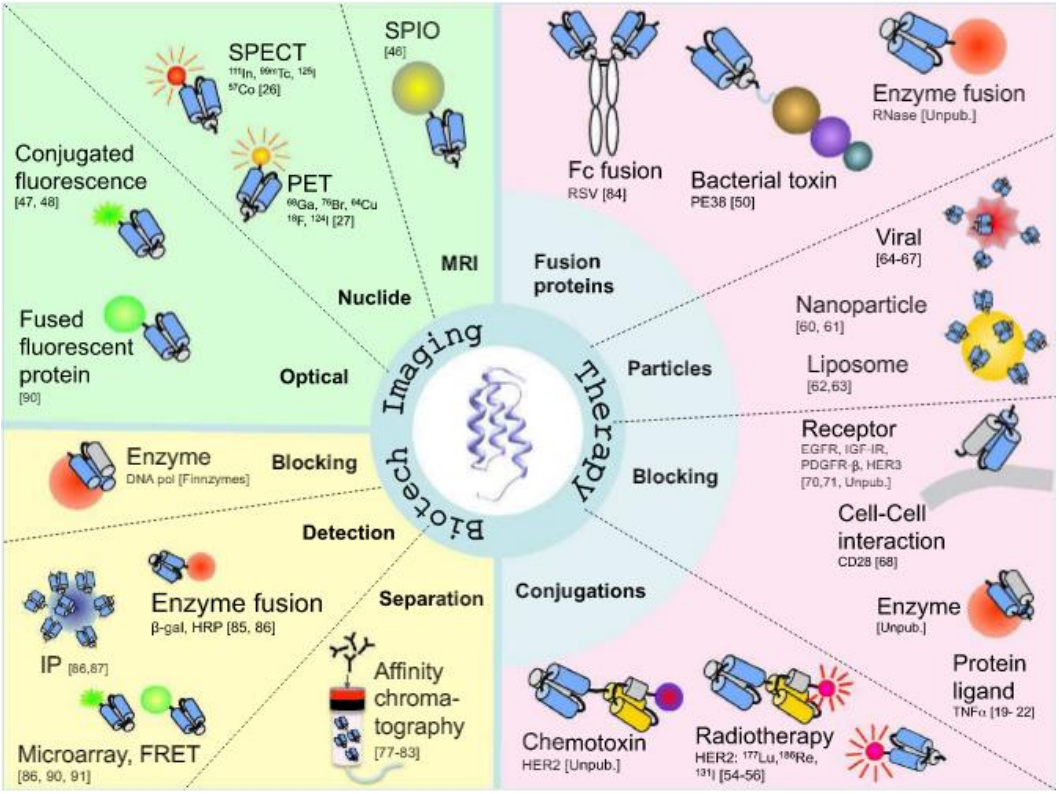

Figure 1.11 Overview of applications of affibody molecules. Applications are divided into three research area, Biotechnology, imaging and therapy.[108]

Fluorescent proteins for cancer cell imaging

With the advent of fluorescent protein technology, the ability to visualize, track, and quantify of molecules in living cells with high spatial and temporal resolution is essential for understanding biological systems.[109-110] Fluorescent proteins are basically used as markers to see what they want in biological research. In addition to fluorescent proteins, there are many tools that can function as markers, but they are most useful because of the many advantages of fluorescent protein alone. One of them is a short-length protein fragment of a fluorescent protein that can function as a unit. Also, there is no additional factor required for fluorescence and not toxic to cells because living cells express genes and produce proteins by themselves. Therefore, unlike many previous dyeing methods, there is an excellent advantage that a cell can be observed in a living state (Figure 1.12).

Monomeric fusion proteins

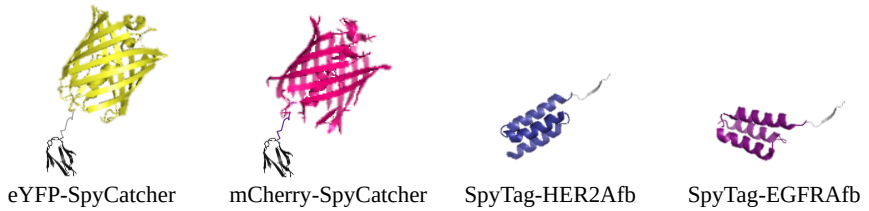

Figure 1.12 Schematic illustrations of various types of monomeric fusion protein as multi-functional nanoplatforms.

Protein ligation system for fusion proteins

SpyCatcher and SpyTag protein ligation system allows individual functional protein modules to be independently expressed and then combined together post-translationally to have multi-function. SpyCatcher/SpyTag protein ligation system, the 15 kDa SpyCatcher protein recognize the 13-amino acid SpyTag (AHIVMVDATKPTK), and they spontaneously form an irreversible isopeptide covalent bond. SpyCatcher and SpyTag could be genetically fused to any type of protein individually both *in vitro* and *in vivo*, and they do not significantly alter the functions of the fused proteins (Figure 1.13).

Ligation reaction is very rapid and effective and can be used in a lot of applications since the reaction is complete in most 5 minutes, condition of buffer pH (pH 5-8), temperature (4-40°C) range, regardless of detergents.[111-114]

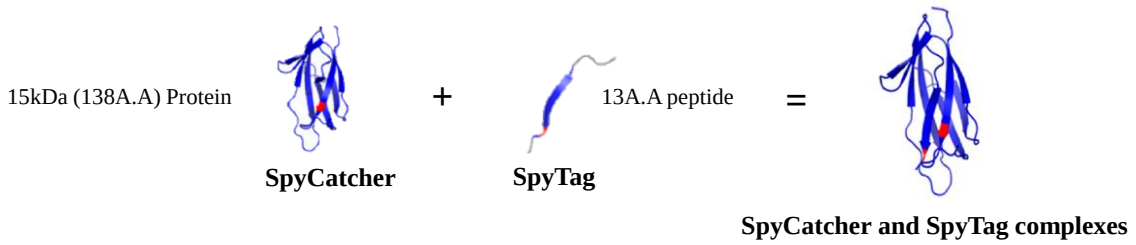

Figure 1.13 Cartoon of SpyTag and SpyCatcher construction.

Chapter 2. Encapsulin Protein Cage as a Targeted Delivery Nanoplatform

2.1 Introduction

A fundamental issue for biomedical application is early detection and localized treatment of diseases to minimize the undesired side-effect. To achieve this, a wide kind of nanometer-size delivery particles has been developed for the past few decades. Surface engineering of nanoparticles and nanometer-range size particles usually tends to allow carry therapeutics and diagnostics for a long circulation time, and spread readily inside the cancer tissue.[40-41] To diagnose the symptoms target-specifically and localized treatment of diseases, a lot of targeting ligands, like chemicals, antibodies, peptides have been used.[115]

The delivery nanoplatforms such as inorganic and polymeric particles have typically heterogeneity and chemical complexity often results in nonuniform size, irregular shape, and mixed composition. However, protein cage nanoparticles were built by nature, thus have well-defined architectures.[65, 88] They constitute multiple identical proteins subunits or biomaterials having symmetric form and a highly uniform structure.[65] In addition, many protein cages have been solved the atomic structure of crystal and control the number and location of molecular encapsulation of diagnostic probes or/and drugs. Thus, protein cage nanoparticles are regarded as excellent candidates to carry various functions to cells or tissues.

Protein cage nanoparticles have been widely utilized to apply for biomedical fields. Ferritin is one of the commonly used protein nanoparticles for biomedical applications. The cavity of ferritin is utilized not only for sequestration of irons and have been used as nanoreactors[8, 116] but also carrying therapeutic and/or diagnostic cargo molecules as nanocontainers.[42-45] Contrast agents encapsulated ferritin has been studied for MRI and applied for targeted delivery of cargoes.[8, 42, 116] Protein nanoparticles have been extensively studied in another group are typically derived from viral capsids, especially bacterial viruses. VLPs have been utilized not only as vaccine development as an antigen delivery platform, but also as a target delivery vehicle for imaging probes and therapeutic drugs.[51-52]

The crystal structure of encapsulin protein cage has been recently solved. A newly studied encapsulin was derived from the thermophilic bacteria, *Thermotoga maritima*. Encapsulin is composed of 60 same subunits of 31 kDa monomers and icosahedral capsid architecture (T=1 state) having an outer diameter of 23-24 nm.[103] Encapsulin have been recently reported that serves as a cellular compartment that encapsulates proteins although the exact function of *T. maritima* encapsulin is not clearly elucidated up to date. This research implied that encapsulin protein cage nanoparticle has

potential as robust cargo delivery nanoplatforms with a cavity to pack of diagnostic reagents and/or therapeutics.[103, 105]

In here, we demonstrated encapsulin can be exploited as a targeted delivery platform through genetic engineering (Figure 2.1). SP94 targeting ligand, hepatocellular carcinoma peptide[46-47], was decorated on the exterior surface of encapsulin via both genetic and chemical modifications. In addition, fluorescent detecting probe and prodrugs (AlDox) were chemically introduced and target to HepG2 cells. Doxorubicin was release from conjugated encapsulin depends on pH in acidic condition of tumor cells and killing effect of AlDox-encapsulin was confirmed with cell viability test. The effective delivery of encapsulin to the HepG2 cells was estimated through *in vitro* confocal cell imaging. A novel protein cage, encapsulin demonstrated that they were robust and genome-free unlike virus like particles. The plasticity of the encapsulin allows us to target the specific cells by using detecting probes and/or therapeutic agents, simultaneously.

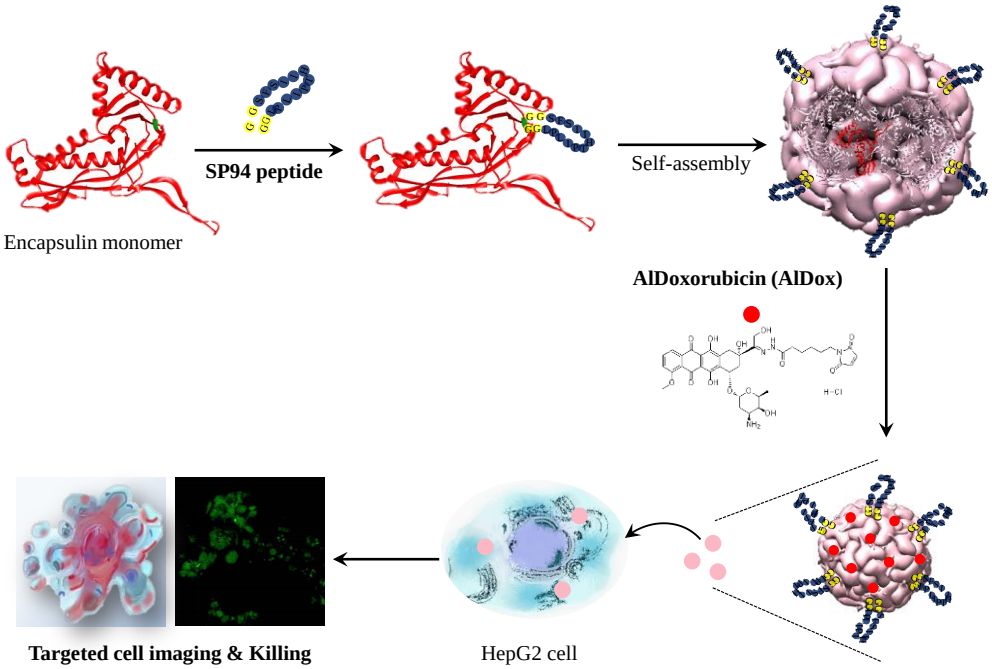

Figure 2.1 Schematic representation of encapsulin utilized as a versatile modular nanoplatform for the targeted delivery of drugs and fluorescent probes.[a]

[a] The position to introduce the SP94-peptide is indicated in green. SP94-peptide (blue) with linker (yellow) was genetically or chemically introduced onto the exterior surface of the assembled encapsulin to target surface markers of HCC cells. The corresponding anticancer drug Aldoxorubicin (AlDox) was chemically attached to E_LH42C123 and delivered to the target cells.

2.2 Materials and Methods

Genetic modification of wt encapsulin and protein cage purification

Hexa histidines with linker ($G_5His_6G_5$) were inserted into residues between 42 and 43 of wt encapsulin (E_LH42) by an established PCR protocol using primers containing extra nucleotides and pET-30b based plasmids containing genes encoding wt encapsulin. The cysteine residue at position 197 of E_LH42 was substituted with serine (E_LH42C123). The SP94-peptide (SFSIIHTPTLPL) was inserted residue between 138 and 139 of E_LH42C123 by an established PCR protocol (SP94-E_LH42C123). Peptide insertion and site mutagenesis were confirmed by DNA sequencing. E_LH42C123 and SP94-E_LH42C123 DNAs were transformed into the competent *E.coli* strain BL21 (DE3) and the protein cages were over-expressed in *E.coli*. The pelleted *E.coli* cells from 1.0 L of culture were resuspended in 35 mL of phosphate buffer (50 mM sodium phosphate and 100 mM sodium chloride, pH 6.5). Lysozyme was added and the solution was incubated for 30 min at 4°C. The suspension was sonicated for 10 min in 30 s intervals, and subsequently centrifuged at 12000 g for 1 hr at 4°C. SP94-E_LH42C123 protein cage was purified by size exclusion chromatography (SEC) after heat precipitation for 10 min at 65°C.

Chemical modifications of E_LH42C123 and SP94-E_LH42C123

E_LH42C123 and SP94-LH42C123 were incubated with 5 mol equivalent of fluorescein-5-maleimide (F5M) at room temperature with vigorous shaking overnight. Reactions were dialyzed against phosphate buffer (50 mM sodium phosphate, 100 mM sodium chloride, pH 7.5) overnight to remove unreacted F5M. For SP94-peptide conjugation, E_LH42C123 was incubated with 10 mol equivalent of SMCC chemical cross-linker at room temperature with vigorous shaking for 3 hr, and the reaction was dialyzed against phosphate buffer (50 mM sodium phosphate, 100 mM sodium chloride, pH 6.5) overnight. Subsequently, 10 mol equivalent of SP94-peptide was incubated with E_LH42C123-SMCC with vigorous shaking overnight and dialyzed against same buffer (50 mM sodium phosphate, 100 mM sodium chloride, pH 6.5) another overnight.

To conjugate Aldoxorubicin (AlDox, INNO-206, CytRx) with SP94-E_LH42C123, SP94-E_LH42C123 was dialyzed against HEPES buffer (50 mM HEPES, pH 9.0) overnight to exchange the buffer and incubated with 5 mol equivalent of AlDox for 3 hr at room temperature with vigorous shaking. Unreacted AlDox was removed using spin column (BIO-RAD).

Mass Spectrometry of modified encapsulin protein cage

For ESI-TOF analysis, wt encapsulin, E_LH42, and SP94-E_LH42 protein cages were loaded onto the MassPREP Micro-desalting column (Waters) and eluted with a gradient of 5-95% (v/v) acetonitrile containing 0.1% formic acid at a flow rate of 500 μL/min. The molecular masses of each species can be determined from the charges and the observed mass-to-charge (m/z) ratio values. Mass spectra were acquired in the range of m/z 500-3000 and deconvoluted using MaxEnt1 from MassLynx version 4.1 to obtain the average mass from multiple charge state distributions.[117]

Cell culture and confocal fluorescence microscopy

HepG2 cells were incubated in RPMI 1640 medium with 10% fetal bovine serum (FBS), 1% streptomycin in a humidified atmosphere of 5% CO_2 and 95% air at 37°C. Cells were grown on microscope cover glasses (18 mm Ø) in 12-well culture plate (SPL, 30012). The cells were fixed with 4% paraformaldehyde in PBS and washed 2 times with PBS containing 0.1% Tween 20. The fixed cells were blocked with 5% BSA, 5% FBS, and 0.5% Tween 20 in PBS at 4°C for 12 hr and blocking buffer was aspirated. SP94-fE_LH42C123 and fE_LH42C123-SMCC-SP94 were treated for 18 hr at 4°C. In the same way, fE_LH42C123 was treated as a negative control (final concentration 200 nM). Before sealing, the cells on the cover glasses were washed 3 times (15 min) and nuclei were stained with DAPI. Images of stained substrates were collected using Olympus Fluoview FV1000 confocal microscope (Olympus, UOBC).

MTT assay

The cytotoxicity of SP94-E_LH42C123, AlDox-SP94-E_LH42C123 and free AlDox was evaluated with HepG2 cells using the 3-(4,5-dimethylthiazol-2-yl)-2,5-diphenyltetrazolium bromide (MTT) cell viability. Cells were seeded into 96-well plates with an initial cell density of 2.5×10^4 cells/well and grown in medium (10% FBS and 1% streptomycin in RPMI 1640) for 2 days at 37°C. After adding SP94-E_LH42C123, AlDox-SP94-E_LH42C123 and free AlDox to cells, the cells were incubated at 37°C for 5 hr and washed with 200 μL of fresh medium for 36 hr and the cells were treated for 4 hr in 200 μL of medium containing 0.5 mg/ml of MTT. Then the medium was replaced by 200 μL of dimethylsulfoxide (DMSO) to dissolve the formazan crystals formed by viable cells. Absorbance was measured at 595 nm using a multiscanner (TECAN). SP94-E_LH42C123 was treated as a negative control.

2.3 Results and Discussion

Wild-type encapsulin (wt encapsulin) in pET-30b was over-expressed and purified using ultracentrifugation and size exclusion chromatography protocol. The subunit molecular mass of wt encapsulin were estimated using mass spectrometry (ESI-TOF MS), and it is corresponded with the calculated value (Figure 2.5 A, bottom). Their size intactness of wt encapsulin was confirmed by transmission electron microscopy (TEM) with outer diameter of 23-24 nm. (Figure 2.5 B, bottom). However, wt encapsulin was eluted much earlier than was expected and the ratio of absorbance of 260nm to 280nm was higher in size exclusion chromatography (SEC) (Figure 2.5 C, bottom). In addition, wt encapsulin have significantly large hydrodynamic diameter of 182 nm in dynamic light scattering (DLS) measurement (Figure 2.5 D, bottom). These results demonstrate that wt encapsulin may randomly associated with nucleic acids causing in a larger hydrodynamic diameter. Moreover, wt encapsulin was not stable at high temperatures although encapsulin was isolated from thermophilic microorganism, *Thermotoga maritima* (Figure 2.2 A).

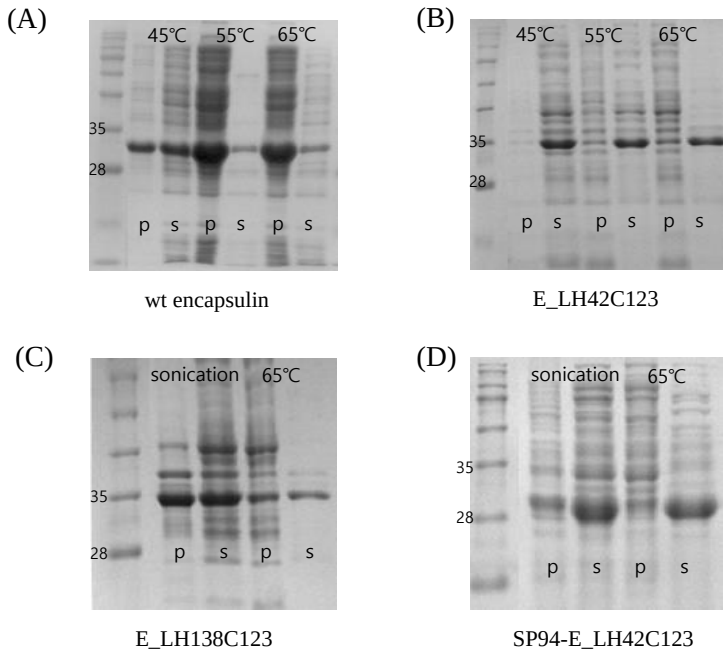

Figure 2.2 Solubility and heat stability test of encapsulins using SDS-PAGE at 45, 55, 65ºC. E_LH42C123 (B), E_LH138C123(C) and SP94-E_LH42C123 (D) have heat stability unlike wt (D). (P and S stand for precipitation and supernatant, respectively.)

Nucleic acids attached on encapsulin could not be removed even a variety of purification methods, such as protamine sulfate treatment and ion exchange chromatography were carried out. Alternatively,

we tried an immobilized metal chromatography, to obtain purified encapsulin without nucleic acids. Six consecutive histidine residues (His_6) were genetically inserted to several loop regions and the C-termini of wt encapsulin which are exposed to outer surface. However, the C-terminal his-tags introduced into encapsulin did not be purified using Ni-NTA column indicating that C-termini of encapuslin are not fully exposed to outer surface. As alternative candidates, loop 42 (E_LH42) or 138 (E_LH138) in encapsulin, six consecutive histidine with linker were introduced into wt encapsulin resulting unusual heat-stability (Figure 2.2 B and C). This result indicated that residue 42 and 138 loop regions were exposed outer surface or inner surface (Figure 2.3 A and B). The E_LH42 became stable at 90°C (Figure 2.4). The thermal stability of E_LH42 allow us to easily increase purity as well as to use it for functional nanomaterials synthesis as metal-binding template like other heat-stable protein cages.[8, 116]

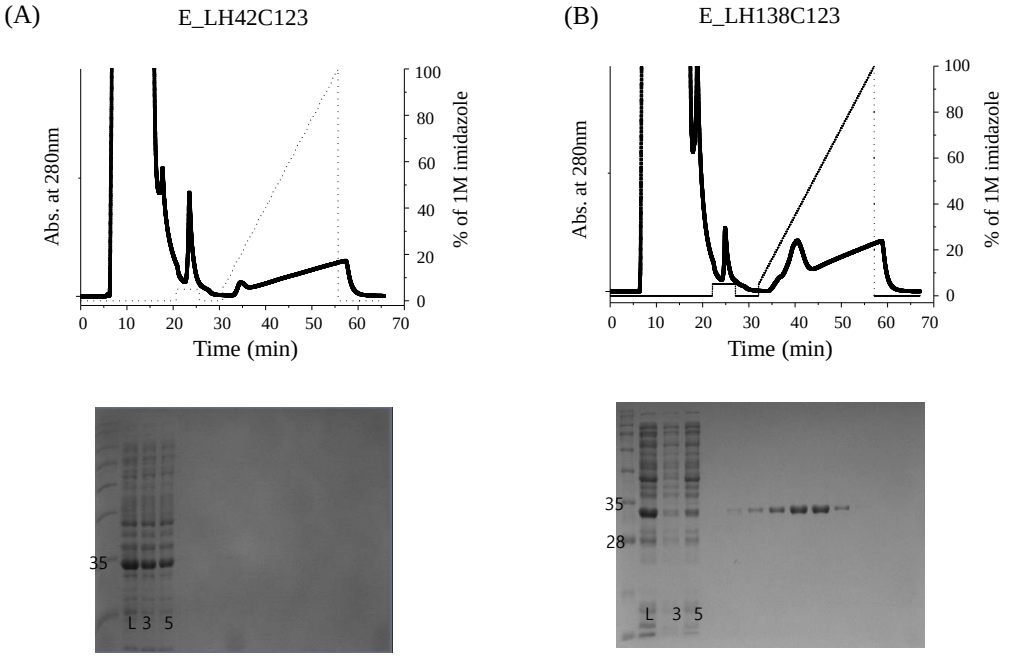

Figure 2.3 IMAC of E_LH42C123 (A) and E_LH138C123 (B). E_LH138C123 was captured with a Ni-ion-carged Histrap column and eluted with a linear gradient of a 5-100% elution buffer (1M imidazole in 20 mM sodium phosphate and 500 mM sodium chloride), while E_LH42C123 was not. Absorption trace at 280 nm.

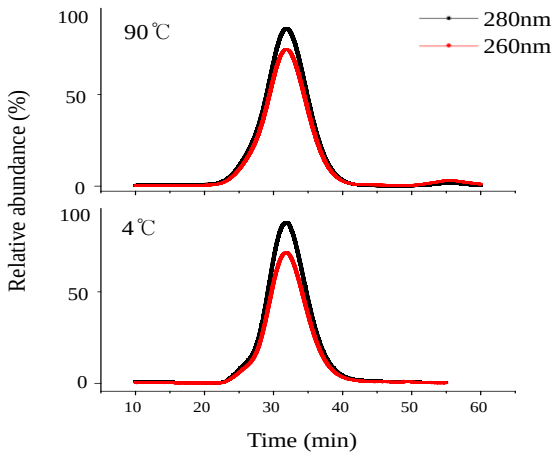

Figure 2.4 Size exclusion elution profiles of E_LH42C123 at 4ºC (bottom), and after heating at 90ºC (top). It demonstrates E_LH42C123 is heat stable at 90ºC.

Two intrinsic cysteines in encapulsin subunit, at position 123 and 197, the cysteine residue at position 197 in the interface was genetically replaced by serine residue because interfacial cysteine residue could cause the cage structure unstable upon chemical modifications (C197S, E_LH42C123). The molecular weight of the dissociated subunit was measured to confirm amino acid substitution (Figure 2.5 A, middle).

E_LH42C123 has the same heat stability after having one cysteine residue per subunit. While there was no size change such as dissociation or aggregation observed under the TEM (Figure 2.5 B, middle), purified E_LH42C123 eluted much later than wt encapsulinin in SEC (Figure 2.5 C, middle and bottom) indicating that the hydrodynamic diameter becomes smaller than wt encapsulin. The increase of ratio at 280/260 nm was observed, indicating that there was no apparent nucleic acid association with cage (Figure 2.5 C, middle). In DLS data, the hydrodynamic size with 22 nm consistent with crystallographic studies and SEC was observed (Figure 2.5 D, middle).[103] These data demonstrated that hexa histidine residue insertion and heat procedure are effective methods to remove randomly associated nucleic acid from encapsulin and it changed the hydrodynamic properties of wt encapsulin (Figure 2.5 C and D, middle).

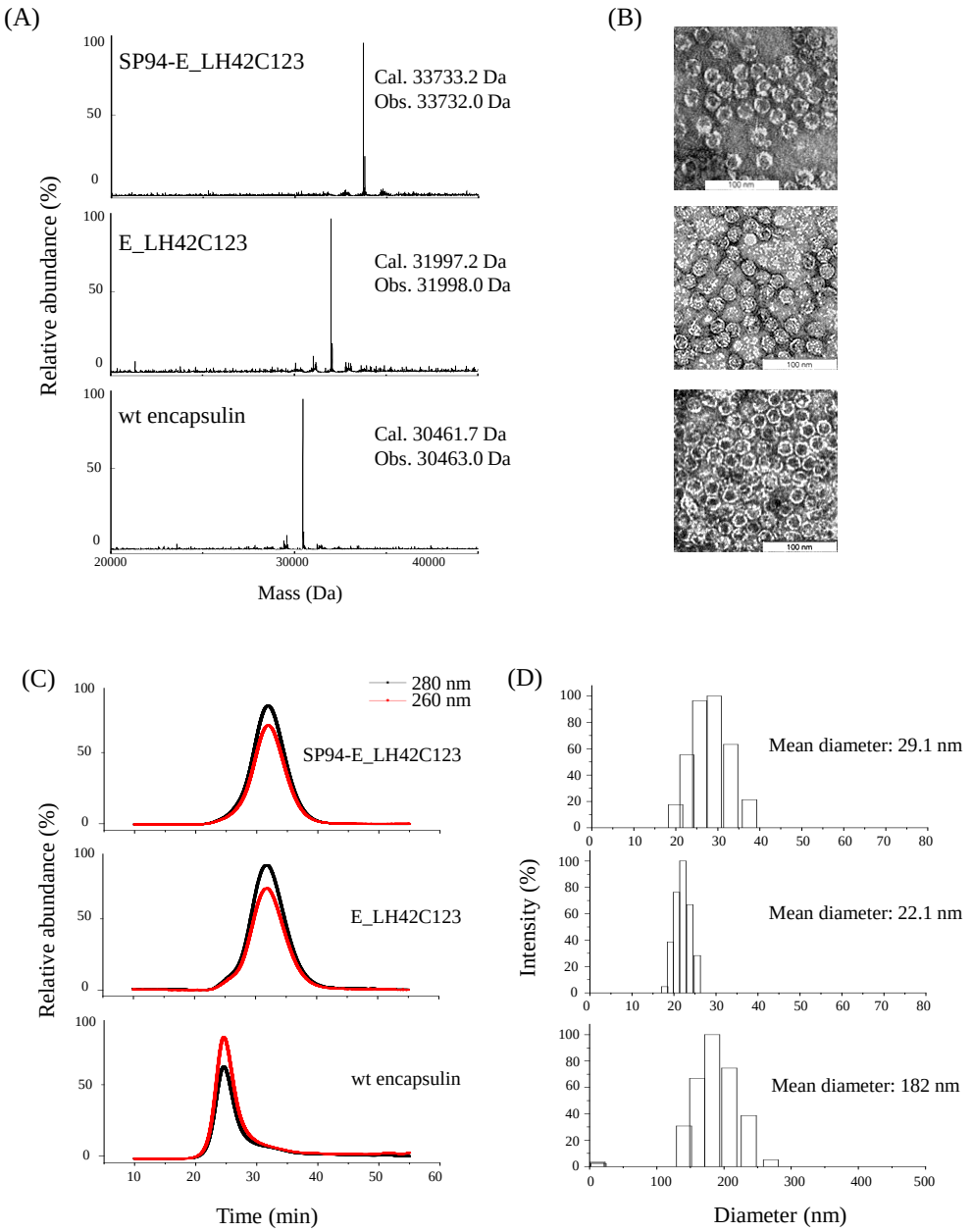

Figure 2.5 Characterization of WT encapsulin, E_LH42C123, and SP94-E_LH42C123. (A) Molecular mass measurement of dissociated subunits of WT encapsulin (bottom), E_LH42_C123 (middle), and SP94-E_LH42C123 (top). Calculated and observed molecular masses are indicated. (B) TEM images of negatively stained WT encapsulin (bottom), E_LH42C123 (middle), and SP94-E_LH42C123 (top) with 1.5% uranyl acetate. (C) SEC profiles of WT encapuslin (bottom), E_LH42C123 (middle), and SP94-E_LH42C123 (top). (D) DLS measurements of WT encapsulin (bottom), Encap_loohis42C123 (middle), and SP94-E_LH42C123 (top)

To utilize encapsulin as targeted delivery nanoplatforms, N-terminal cysteine synthesized SP94-peptide (CGGSFSIIHTPTLPL) was covalently conjugated to the exposure surface of E_LH42C123 through a chemical cross-linker, SMCC. SMCC is a heterobifunctional cross-linker that comprise maleimide moiety at one end and *N*-hydroxysuccinimide (NHS) ester at the other end. Once E_LH42C123 were conjugated with NHS ester in SMCC first and then maleimide functional group in SMCC and cysteine residue in SP94-peptide ligands were subsequently conjugated through thiol-maleimide Michael-type addition (E_LH42C123-SMCC-SP94) because SP94-peptide could not bind directly with E_LH42C123. Prior to SMCC conjugation, E_LH42C123 were labeled with fluorescein-5-maleimide (F5M) or prodrug, Aldoxorubicin (AlDox), to block thiols of E_LH42C123 (C123).

Engineered cysteine residue of E_LH42 (E-LH42C123) was attached with F5M as a detect reagent for confocal microscopic imaging and used for labeling prodrugs (AlDox) later (see below). After all chemical conjugation, its shell integrity of the chemically modified E_LH42C123 were estimated with ESI-TO MS, SEC and TEM images. The dissociated subunit of fluorescein labeled E_LH42C123 (fE_LH42C123) was observed to be 32426.0 Da (Figure 2.6 A), having an additional mass of F5M molecular mass (427.4 Da) to the subunit mass of E_LH42C123 (31998.0 Da, Figure 2.5 A, middle). In SEC, fE_LH42C123-SMCC-SP94 eluted at the same position as E_LH42C123 (Figure 2.6 B). It suggested that no changes in their structures were observed after chemical conjugating SP94 peptide and F5M and not induced the dissociation or aggregation of encapuslin. The TEM images of fE_LH42C123-SMCC-SP94 also estimated the uniform size distribution and their intactness with their exact size as we expected (Figure 2.6 C).

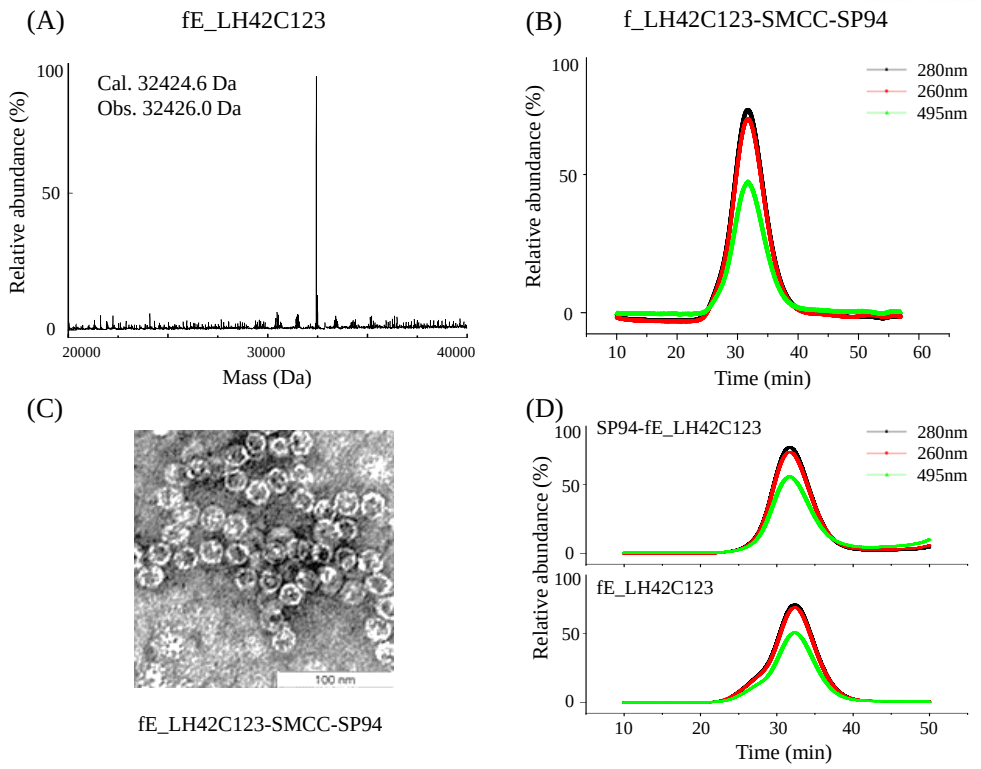

Figure 2.6 Characterization of fE_LH42C123, fE_LH42-SMCC-SP94 and SP94-fE_LH42C123. (A) Molecular mass measurements of dissociated subunits of fE_LH42C123. Calculated and observed molecular masses were indicated. (B) Size exclusion elution profiles of fE_LH42C123-SMCC-SP94. (C) Transmission electron microscopic images of negatively stained fE_LH42C123-SMCC-SP94. (D) Size exclusion elution profiles of fE_LH42C123 (bottom) and SP94-fE_LH42C123 (top).

To evaluate the target efficacy of fE_LH42C123-SMCC-SP94, they were treated to HepG2 cells and confirmed them using confocal microscopy.[46-47] Although fE_LH42C123-SMCC-SP94 effectively bound to HepG2 cells, fE_LH42C123 without SP94-pepeide little bind to HepG2 cell (Figure 2.7). This data implied that the SP94-peptide displayed on fE_LH42C123-SMCC-SP94 surface well and effectively recognize to the target cells. These results that a series of chemical conjugation allows us to utilize encapuslin protein cages as target-specific diagnostic probes.

While the chemical conjugation can give the function of targeting to encapsulin and have potential usage of cargo delivery platforms, it is difficult to control and determine the number of SP94-peptide conjugation due to multi-step chemical reactions. To overcome this drawback, we tried to genetically insert SP94-peptide with extra linker (GGTSSFSIIHTPILPLGG) at residue between 138 and 139 loop position of E_LH42C123. This loop 138 was already confirmed by inserting his-tag and it did not alter

their architectures after introduced targeting peptide and also, they were located at the exterior as we expected (Figure 2.3 B). This construct was also confirmed their heat stability (Figure 2.2 D).

The subunit mass of genetically inserted SP94-peptide into E_LH42C123 template (SP94-E_LH42C123) was estimated to be 33732.0 Da (Figure 2.5 A, top). The SEC data of SP94-E_LH42C123 was same as that of E_LH42C123 (Figure 2.5 C, middle and top). Their intactness with a uniform size of approximately 23 nm in diameter was confirmed using TEM (Figure 2.5 B, top). In DLS measurement, SP94-E_LH42C123 verified a hydrodynamic diameter of 29.1 nm, slightly larger than that of E_LH42C123 (22.1 nm) probably because of the inserted surface SP94-peptide (Figure 2.5 D, top). Even after F5M conjugation, the same elution profile was observed (Figure 2.6 D). The efficacy of targeted delivery of SP94-fE_LH42C123 was evaluated using same methods. While SP94-fE_LH42C123 bound to HepG2 cells well, fE_LH42C123 without SP94-peptide bound little (Figure 2.7) indicating that the genetically introduced SP94-peptide is successfully presented on the surface of encapsulin and allowed them to bind to the target cells specifically. This result indicated that encapsulin has potential as a nanoplatform acquiring specific targeting and imaging simultaneously.

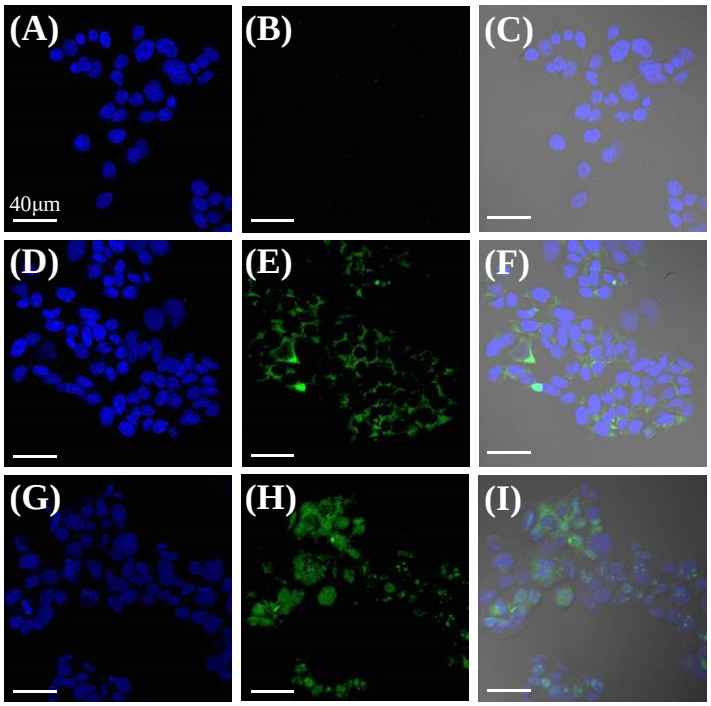

Figure 2.7 Fluorescent microscopy images of HepG2 cells treated with fE_LH42C123 (A-C), fE_LH42C123-SMCC-SP94 (D-F), and SP94-fE_LH42C123 (G-I). DAPI (left rows), fluorescein (middle rows), and merged (right rows) images are presented. fE_LH42C123, fEcnap_loophis42C123-SMCC-SP94, and SP94-fE_LH42C123 are visualized as green, and nuclei are shown in blue.

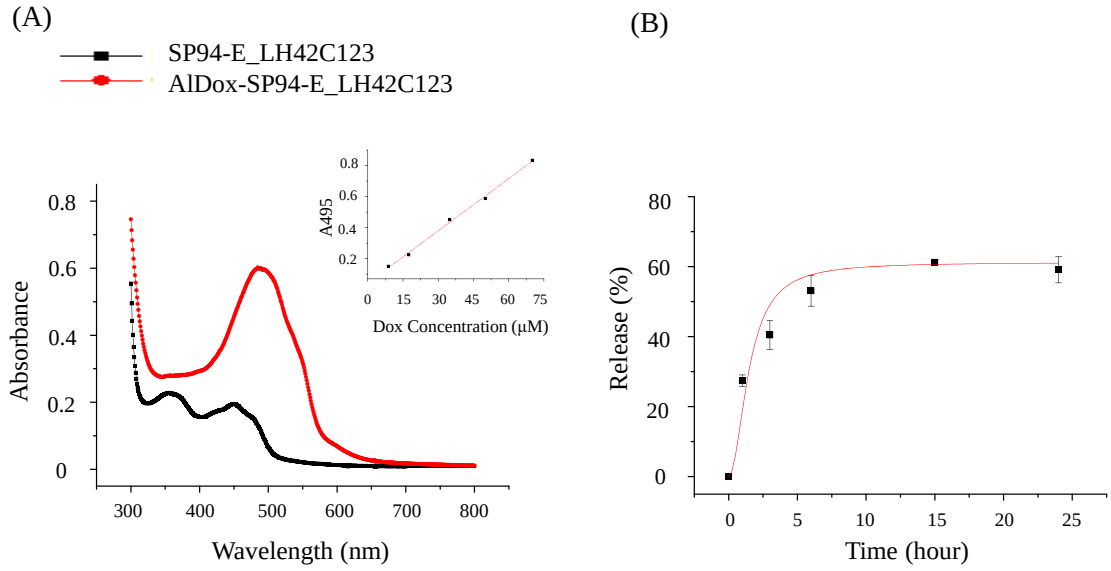

Figure 2.8 *In vitro* assay for the binding and release of drug molecules. (A) UV/vis absorption spectra of AlDox-SP94-E_LH42 (red, circles) and SP94-E_LH42C123 only (black, squares) at pH 9.0. A standard absorption curve of concentration-dependent AlDox is plotted (inset). (B) Time-dependent release profile of AlDox from SP94-E_LH42C123 at pH 5.5.

To investigate the killing effect of genetically engineered AlDox-SP94-E_LH42C123. The 3-(4,5-dimethylthiazol-2-yl)-2,5-diphenyltetrazolium bromide (MTT) assay was performed. Although chemical and genetic modifications for targeting ligand presentations exhibited similar level of targeting capability, the genetic modified encapsulin was simpler for further applications and it is easy to control exact number of SP94-peptide. 6-maleimidocaproyl hydrazone prodrug of doxorubicin (AlDox)[118] were chemically loaded onto the cysteine residues at C123 of SP94-E_LH42C123 (AlDox-SP94-E_LH42C123) through thiol-maleimide Michael-type addition and treated HepG2 cells. By measuring the absorbance at 495 nm using UV/Vis, the amount of AlDox was quantified per SP94-LH42C123 subunit and compared to that of a standard curve of free AlDox (Figure 2.8 A). The AlDox contents were estimated one per encapsulin subunit via UV/Vis analysis. It means that all cysteines in encapsulin were conjugated with AlDox. As AlDox is anchored through hydrazine linker which is sensitive at acidic condition like tumors environment, doxorubicin could be released from delivered encapsulin under the acidic environment of cancer cells. Doxorubicin release profile show that 60% of doxorubicin was released form AlDox-SP94-E_LH42 at pH 5.5 within 8 hr (Figure 2.8 B).[118]

For 5 hr, SP94-E_LH42C123-AlDox treated to HepG2 cells, and washed several times with fresh medium for 36 hr. The cytotoxic effect of HepG2 cells treated with SP94-E_LH42C123-AlDox

increased in a dose-dependent manner, as was also observed with free AlDox (Figure 2.9). In contrast, there was no significant effect on cell viability in only SP94-E_LH42C123 without AlDox. This result indicated that the encapsulin do not have killing effect themselves, but they effectively deliver loaded AlDox and releases drugs into target cells resulting in the severe cytotoxicity toward their target cells. Although SP94-E_LH42C123-AlDox showed similar cytotoxicity to that of free doxorubicin in *in vitro* cell viability test, SP94-E_LH42C123 may improve the solubility of the AlDox and allow target specific delivery of drugs reducing the side-effects which are critical for *in vivo* applications. Thus, combined incorporations of target SP94-peptide and anti-cancer prodrug, AlDox, on encapsulin may show clinical potential to improve the systemic treatment of a hepatocellular carcinoma.

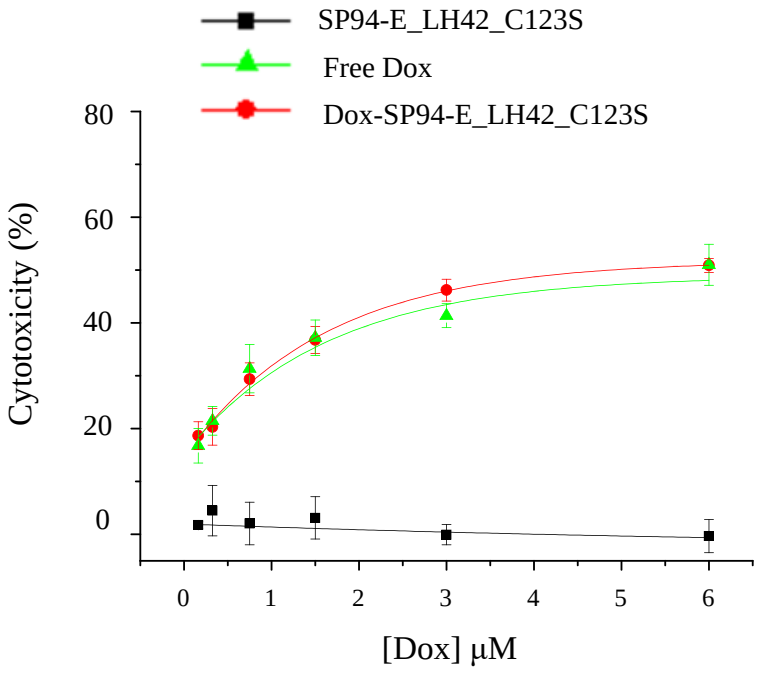

Figure 2.9 MTT cell viability assay. Dose-dependent cytotoxicity profiles of AlDox-SP94-E_LH42 (red, circles), free AlDox (green, triagles), and SP94-E_LH42 (black, squares) toward HepG2 cells. Three independent experiments were performed.

2.4 Conclusions

In this research, we designed and engineered modular and multifunctional delivery platforms using a novel protein cage, encapsulin, through both genetic and chemical modifications. E_LH42C123 have unusual heat stability after insertion of hexa histidines with extra linker at residue 42 of wt encapsulin and allowed us to readily produce them high yield. SP94-peptide, HepG2 targeting peptide, was displayed onto the outer surface of E_LH42C123 through either chemical conjugation or genetic insertion. Engineered encapsulin have stability after genetic and chemical modification. SP94-peptide presenting E_LH42C123 have specific binding efficacy to hepatocellular carcinoma cell, HepG2 and confirmed the cytotoxic effect of doxorubicin released from SP94-E-LH42C123-AlDox. Only SP94-E-LH42C123 had no severe effect on cell viability. We were certain that the engineered encapsulin can be used for targeting specific cancer cell and delivering therapeutic reagents simultaneously as a multifunctional nanoplatform.

Chapter 3. Cell Imaging Modular Toolkits using SpyTag/SpyCatcher

3.1 Introduction

Cancers remains one of the main reasons of human death in the world because of a late diagnosis and low effectiveness of treatment. Rapid, simple and target-specific diagnosis to reduce the side effect is still necessary for effective cancer diagnosis and treatment. One of the most commonly used cancer detection methods is optical imaging analysis. Optical cancer diagnosis techniques such as microscopy, photography, fluorescence tomography, bioluminescence and photoacoustic imaging can be successfully developed *in vitro* and *in vivo*. Although these diagnosis techniques require time-consuming and costly procedures and have some limitation for applications and utilizations, they still have been used up to date for *in vitro* or *in vivo* imaging. Especially fluorescent microscope is a powerful tool for biomedical and clinical applications because it is easy to detect various specimens of cells and tissues with conjugation of fluorescent probes.[119-121]

There are various methods to use detection of cancer cells and to give some functions for diagnosis tools. Although genetic or chemical engineering is the most ordinary technique to give functions, it is not easy to have multiple functions at the same time.[122-124] Biological sample, protein units can be engineered genetically into one long open reading frame, but errors in protein synthesis and misfolding soon become limiting. Chemical modifications have possibilities to misgauge the exact number of conjugates and some need specific amino acid like cysteines to react. Therefore, we chose post-translational modification method to ligase detecting and probing proteins. To overcome these challenges, individually modules expressing and then linking the modules together and also feasible to add the functions after expression of each proteins. Protein-peptide or protein-protein interaction such as epitope and FLAG tags have been widely used for diagnostic or detecting tools for cancer cells, but is often limited by stability and weak interactions. However, posttranslational ligation methods allow us to add other functions by a minimal risk of disrupting the function of the attached proteins and are easy, simple reaction without specific amino acids like cysteines.

Particularly SpyTag peptide of 13 amino acids that spontaneously and irreversibly formed a covalent bond with its protein partner, SpyCatcher (138 amino acids, 15 kDa)[111-114]. SpyTag/Catcher are feasible to be fused genetically to any types of proteins because they have many advantages which are quiet stable in general biophysical condition and able to reduce risk of disrupting the function of target to apply *in vitro* and *in vivo* applications.

In this study, mCherry/eYFP and HER2/EGFR affibodies which are usually used in target-specific imaging method however we established a simpler, easier and more rapid imaging toolkit to target specifically cancer cells while we minimally engineered fluorescent proteins and affibodies using conventional fluorescent microscope and post-translational ligation method. Affibodies are genetically engineered small proteins which bind their receptors, target peptides or proteins with high affinity and are therefore a member of antibody mimetics, imitating monoclonal antibodies. Among them, we used HER2/EGFR affibodies, to target HER2 (Human epidermal growth factor 2) or EGFR (Epidermal growth factor receptor) which are members of the EGFR family of cell-surface receptors. HER2-positive breast cancer has a more aggressive disease, greater likelihood of recurrence, pooper prognosis, and decreased survival rate, compare to HER2-negative cases.[9, 125-127] Therefore, affibodies conjugated imaging tool is important for designing affibody target therapies and determination of its role in cells. Imaging modular toolkits have not only specific targeting ability but also functionality of cargo carrying using scaffolding protein, GST.[124] Fluorescent imaging modular toolkits aim to overcome some limitations of current tools to provide functions of peptide-protein interaction technique and mix and match strategy (Figure 3.1).

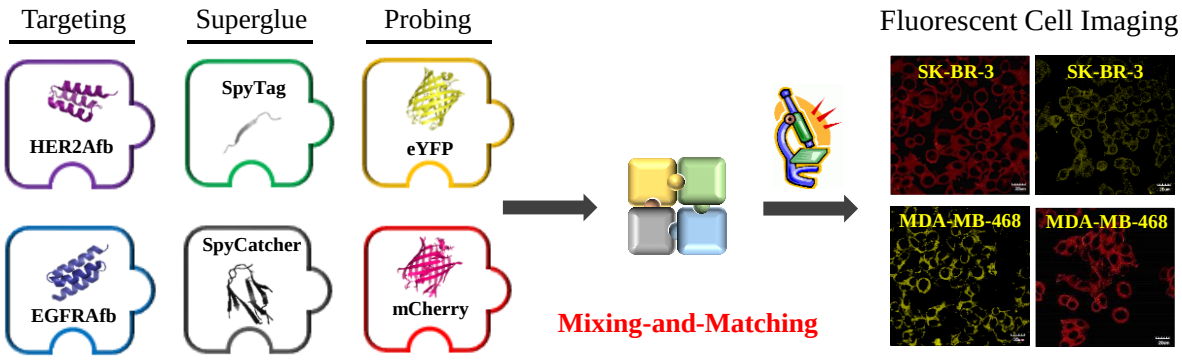

Figure 3.1 Schematic representation of constructing plug-and-playable fluorescent cell imaging modular toolkits using the bacterial superglue, SpyTag/SpyCatcher protein ligation system, and applying them to fluorescent cell imaging using a mix-and-match strategy.

3.2 Materials and Methods

Genetic modification and Protein purification of monomeric proteins

SpyTag peptide (AHIVMVDAYKPTK) with extra amino acids was genetically added to the N-termini of affibodies (HER2 and EGFR affibodies (Afb)) and fluorescent proteins (mCherry and eYFP) by an established polymerase chain reaction (PCR). SpyCatcher protein with extra amino acids also was genetically fused to the C-termini of fluorescent protein and N-termini of affibodies by PCR. SpyTag Peptide or SpyCatcher protein insertion was confirmed by DNA sequencing. Eight types of proteins (ST-HER2Afb/ST-EGFRAfb, mCherry-SC/eYFP-SC, SC-HER2Afb/SC-EGFRAfb and ST-mCherry/ST-EGFRAfb) are transformed into competent *Escherichia coli* strain BL21 (DE3), and the proteins were overexpressed and induced by 0.5 mM isopropyl-β-D-thiogalactopyfanoside (IPTG). Cell growth continued 30°C (except ST-HER2Afb/ST-EGFRAfb, 37°C) for 12-15 hr after IPTG induction and cells were harvested by centrifugation at 5000 rpm for 10min at 4°C. The pelleted cells were resuspended in 35 mL pH 6.5 phosphate buffer (50 mM sodium phosphate and 100 mM sodium chloride) and sonicated for 10 min in 30 s intervals after lysozyme was added in the resuspended solution. All types of proteins were subsequently centrifuged at 12000 g for 1 hr at 4°C and purified by IMAC (1 mL HisTrap FF column / GE HealthCare).

Characterization and ligation of AFPC (affibody:fluorescent protein conjugates)

Concentration of purified ST-affibodies (or ST-fluorescent protein) and fluorescent-SC (or SC-affibodies) were examined by BCA assay and mixed them at 5min to overnight at room temperature, and then analyzed reaction products with SDS-PAGE and MS. Reaction was stopped at indicated time by adding SDS loading buffer and boiling at 110°C. Each monomeric proteins or reaction products was loaded onto a MassPREP microdesalting column (Waters) with aqueous acetonitrile solvents (buffer A: 5% acetonitrile, 1% formic acid in water) and eluted with buffer B (5% water, 1% formic acid in acetonitrile) at a flow rate of 0.5 mL/min. The molecular masses of each species can be determined from the charges and the observed m/z ratio values. Mass spectra were acquired in the range of m/z 500-3000 and deconvoluted using MaxEnt1 from MassLynx program to obtain the average mass from multiple charge state distributions.

Cell culture and confocal microscopy imaging

SK-BR-3 cells were cultured in DMEM medium with 10% fetal bovine serum (FBS) and 1%

antibiotic-antimycotic, MCF-10A cells were grown in DMEM/F12 with 5% horse serum, 1% penicillin/streptomycin, EGF, hydrocortisone, insulin and 25 mM sodium bicarbonate. MDA-MB-468 cells were grown in Leibovitz's L-15 medium with 10% FBS, 1% antibiotic-antimycotic, 25 mM HEPES and sodium bicarbonate. MCF-7 cells were cultured in RPMI-1640 with 10% FBS and 1% antibiotic-antimycotic. SK-BR-3, MCF-10A, MDA-MB-468 and MCF-7 cells were incubated in humidified atmosphere of 5% CO_2 and 95% air at 37°C. The cells were grown on microscope cover glass in 12-well plate. AFPC (affibody:fluorescent protein conjugates) samples were treated for 1hr at 37°C and cells were fixed with 4% paraformaldehyde in PBS in case of live cell imaging. Negative control (only fluorescent protein) also were treated in cells same methods. Before sealing, the cells were washed two times with PBS, and nuclei were stained with DAPI. Images of AFPC samples were collected using Olympus Fluoview FV1000 confocal microscope (Olympus, UOBC).

Cytotoxicity assay

The *in vitro* cytotoxicity was measured using thiazolyl blue tetrazolium bromide (MTT, sigma-Aldrich) assay. SK-BR-3 and MCF10A cells were seeded into 96-well cell culture plate at 1×10^4 cells/well and then incubated in grow medium for 24 hr at 37°C under 5% CO_2. After treated AFPC, AlDox loaded AFPC, free AlDox and PBS in cells for 1 hr and then washed with fresh medium for 7 days. The cells were treated 200 μL of medium containing of 0.5 mg/mL of MTT for 4 hr and then, removed medium and resuspended with 200 μL of dimethyl sulfoxide (DMSO) to dissolve the formazan crystals formed by viable cells. Absorbance of 96-well plate were measured at 595 nm using multiscanner (TECAN).

3.3 Results and Discussion

For effective cancer treatment, target-specific and simple diagnosis should be achieved. Conjugation of target-specific affibodies and sensitive fluorescent proteins may allow us to effectively detect various types of cancer cells depending on targeting affibodies. HER2 and EGFR have been known to be over-expressed in numerous cancer cells such as breast, ovarian, stomach, kidney, prostate and lung cancer cells and they are good candidates as cancer biomarkers. Therefore, we chose HER2 and EGFR affibodies, which selectively recognize HER2 and EGFR and tightly bind to them respectively, as targeting affibodies and eYFP and mCherry as fluorescent proteins. Genetic fusion may be the most commonly used approach to combine two or more functional proteins together. However, genetic fusion of two different proteins often causes misfolding or the loss of function. Furthermore,

each targeting moiety and fluorescent protein should be individually fused in the molecular level. To avoid this issue and establish a new cell imaging modular toolkit, we applied protein ligation system, SpyTag/SpyCatcher, which covalently conjugates two functional proteins post-translationally. SpyTag (ST) peptide (AHIVMVDAYKPTK) with extra amino acids was genetically added to the N-termini of affibodies (ST-HER2Afb and ST-EGFRAfb), whereas SpyCatcher (SC) protein with extra amino acids was genetically fused to the C-termini of fluorescent proteins (eYFP-SC and mCherry-SC). Each construct was efficiently over-expressed in *E. coli,* simply purified with IMAC as previously described (refs), and confirmed with molecular mass measurements with electrospray ionization-time of flight mass spectrometry (ESI-TOF MS) (Figure 3.2).

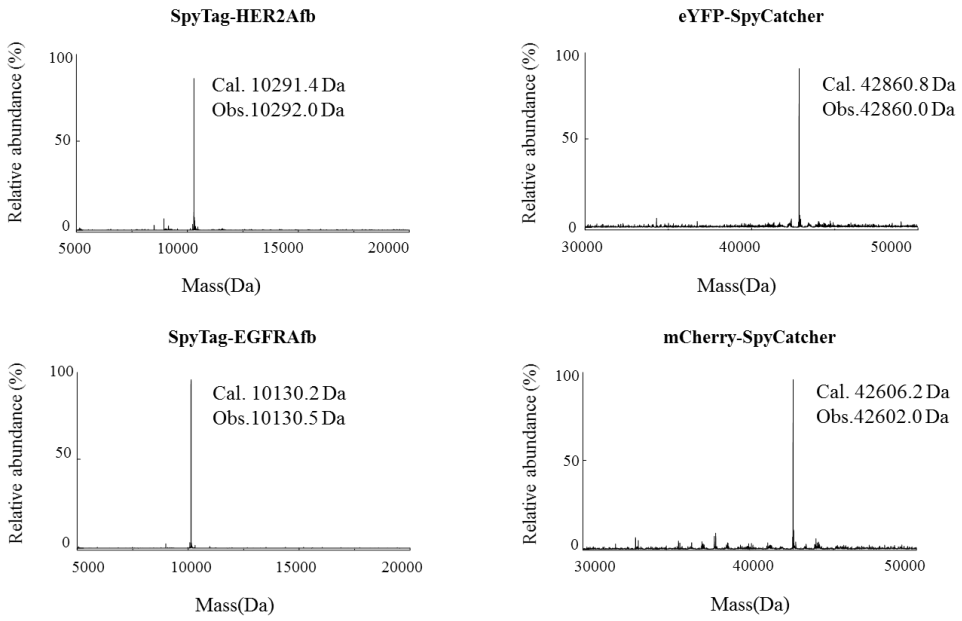

Figure 3.2 Molecular mass measurements of SpyTag-affibodies and fluorescent protein-SpyCatcher.

To investigate whether genetically engineered ST-affibodies (ST-HER2Afb and ST-EGFRAfb) and fluorescent protein-SC (eYFP-SC and mCherry-SC) can form isopeptide bond to covalently conjugate to each other as previously described[112], we mixed them, sampled them at indicated times, and analyzed reaction products with SDS-PAGE and MS. SDS-PAGE analyses showed that the covalent ligation between ST-affibodies and fluorescent protein-SC were almost completed within 5 min regardless of species of affibodies or fluorescent proteins (Figure 3.3 A-D) consistent with previous reports.[111-114] Molecular mass measurements of reaction products showed the sum of the individual masses minus 18 Da due to loss of water confirming isopeptide bond formation between ST-affibodies and fluorescent protein-SC (Figure 3.3 E-H) as proposed in the previous reports.[111-114]

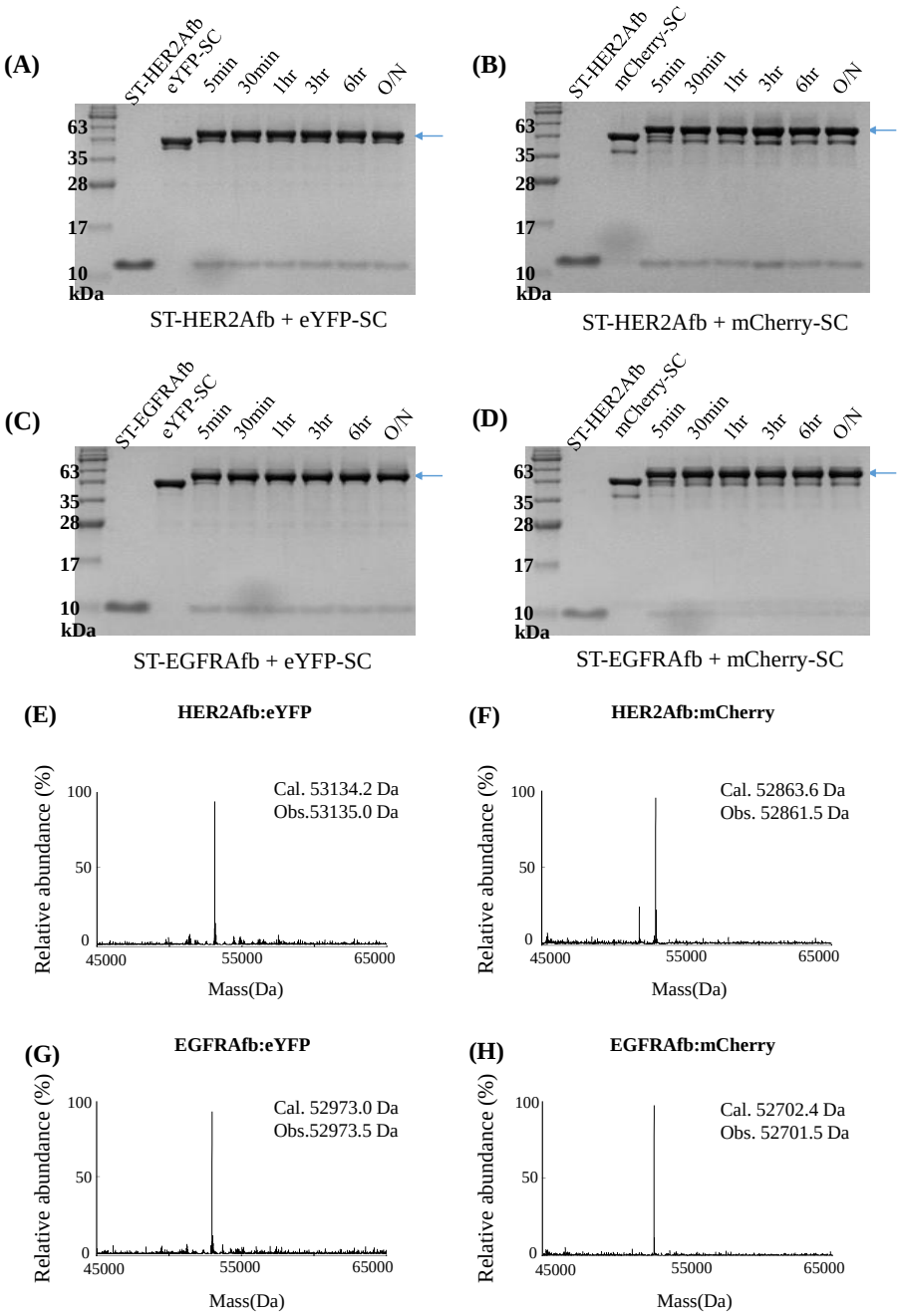

Figure 3.3 Characterization of AFPCs as results of the isopeptide bond formation between ST-affibody and fluorescent protein-SC. Reaction products of ST-HER2Afb and eYFP-SC (A and E), ST-HERAfb and mCherry-SC (B and F), ST-EGFRAfb and eYFP-SC (C and G), and ST-EGFRAfb and mCherry-SC (D and H) were analyzed using SDS-PAGE (A-D) and ESI-TOF MS (E-H). Reaction times and molecular weight markers are indicated and proteins are indicated and proteins are stained with Coomassie blue (A-D). Calculated and observed molecular masses are indicated (E-H) (blue arrow: conjugated product of AFPCs).

As expected, covalent conjugation of two distinct any proteins of interest can be easily achieved by SpyTag-SpyCatcher ligation method, because isopeptide bond formation between fused ST and SC is simple, rapid, and effective and fusion proteins would be used for modular toolkits using mixing-and-matching strategy through simple protein ligation pairs as Howarth group demonstrated.[111-114]

To assess the dual functionalities, targeting and detecting capabilities, of AFPCs, we prepared SK-BR-3 and MDA-MB-468 cells which are known to overexpress HER2 and EGFR on their surface, respectively, treated them with HER2Afb:fluorescent protein (HER2Afb:eYFP or HER2Afb:mCherry) or EGFRAfb: fluorescent protein (EGFRAfb:eYFP or EGFRAfb:mCherry), and monitored them with confocal fluorescence microscope. Each AFPC efficiently bound to their corresponding SK-BR-3 or MDA-MB-468 cells, whereas fluorescent protein-SC without ST-affibodies did not bind to SK-BR-3 or MDA-MB-468 cells (Figure 3.4). However, AFPC did not bind to MCF10A or MCF7 cells because they are known not to express HER2 or EGFR on their surface (Figure 3.4). These data suggest that AFPC effectively recognize their target cells and bind to them selectively with minimum non-specific binding allowing us to visualize specific cancer cells with selective colors on demands. One advantage of utilizing modular toolkits is universality (or versatility) and SpyTag/SpyCathcer system should be daptively applicable to various system.

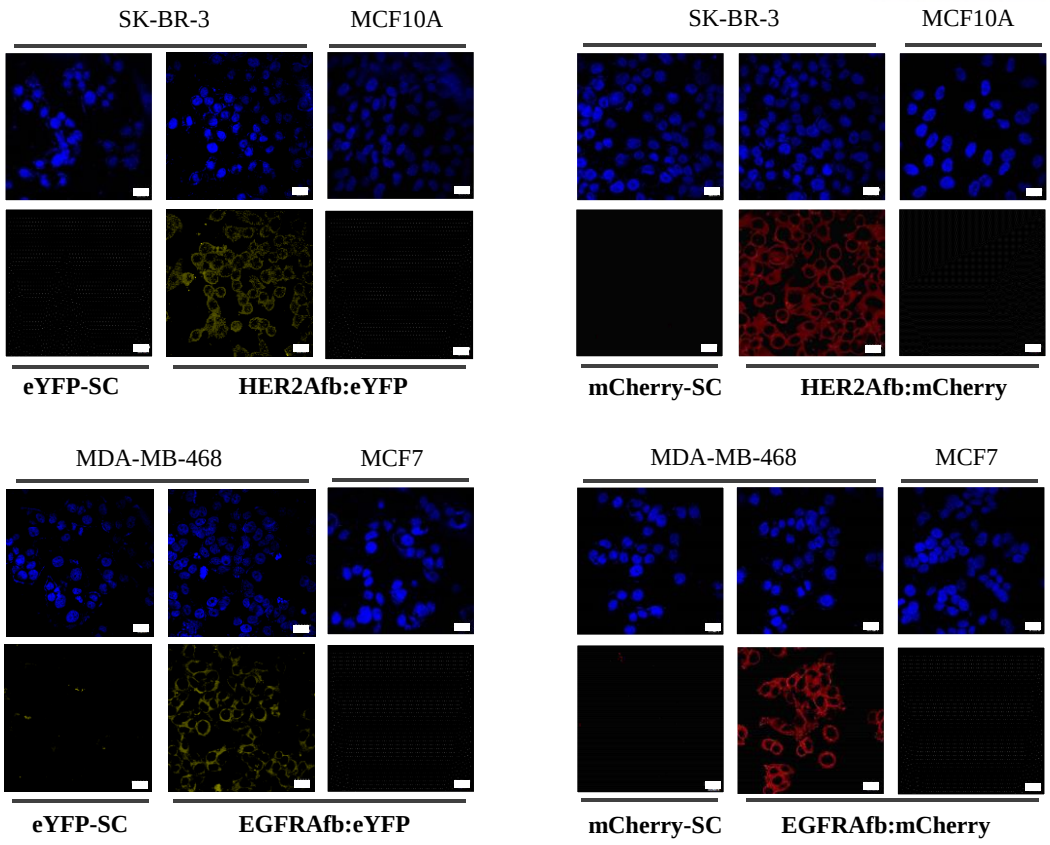

Figure 3.4 Fluorescent microscopic images of various cells treated with AFPCs and fluorescent protein-SC. Cells and AFPCs are indicated on the top and bottom of image panels, respectively. Nuclei are stained with DAPI (blue, top panels), and eYFP and Cherry are visualized in yellow and red, respectively (bottom panels) (scale bar: 20 μM).

We examined whether SpyTag and SpyCatcher can be alternatively introduced to affibodies and fluorescent proteins, respectively. We genetically fused SC with affibodies to form SC-HER2Afb or SC-EGFRAfb and independently introduced ST to fluorescent proteins to produce ST-eYFP or ST-mCherry (Figure 3.5).

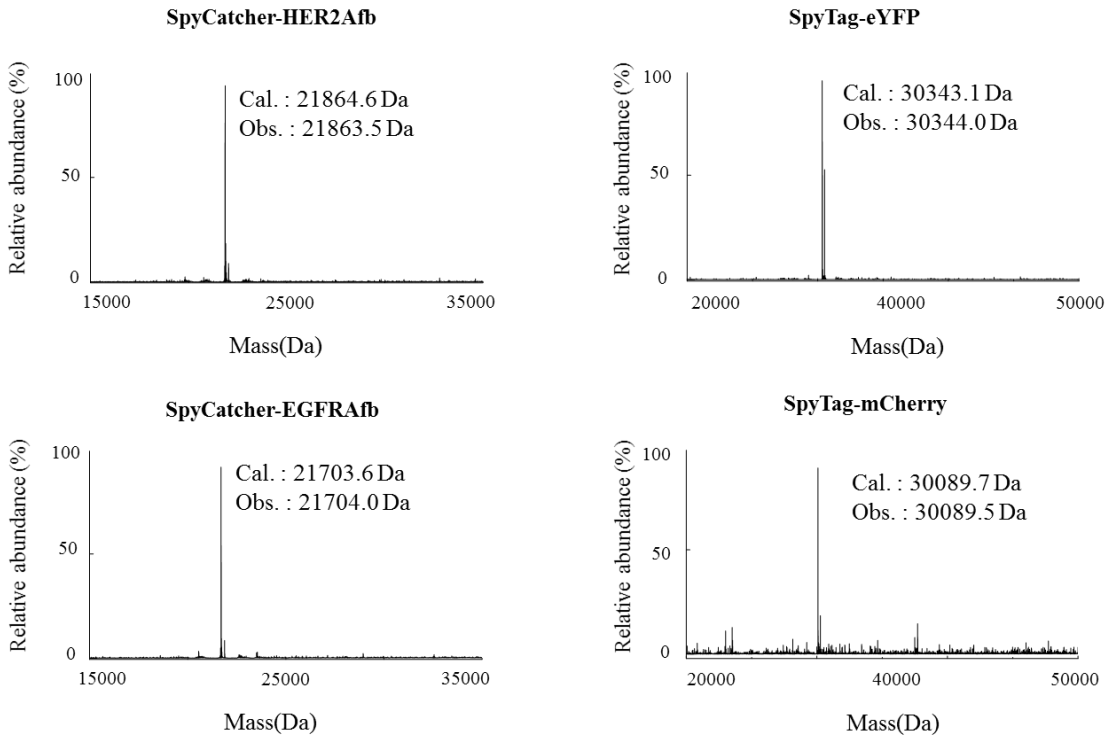

Figure 3.5 Molecular mass measurements of SpyCatcher-affibodies and SpyTag-fluorescent proteins.

We prepared them with same purification methods without any significant trouble and confirmed their proper covalent ligation with almost identical efficiency with SDS-PAGE and MS analyses (Figure 3.6). Resulting conjugates also showed almost identical targeting and detecting efficacy regardless of fused proteins to ST or SC suggesting that switching of ST or SC did not influence on the efficiency of isopeptide formation nor to dual functions, targeting and detecting efficacy, at all (Figure 3.7).

These fluorescence cell image data imply that targeting and probing functionalities can be easily implanted simultaneously by protein ligation system depending on user's choice and this approach can be extended to various other functional combinations in addition to targeted cell imaging systems we discussed here.

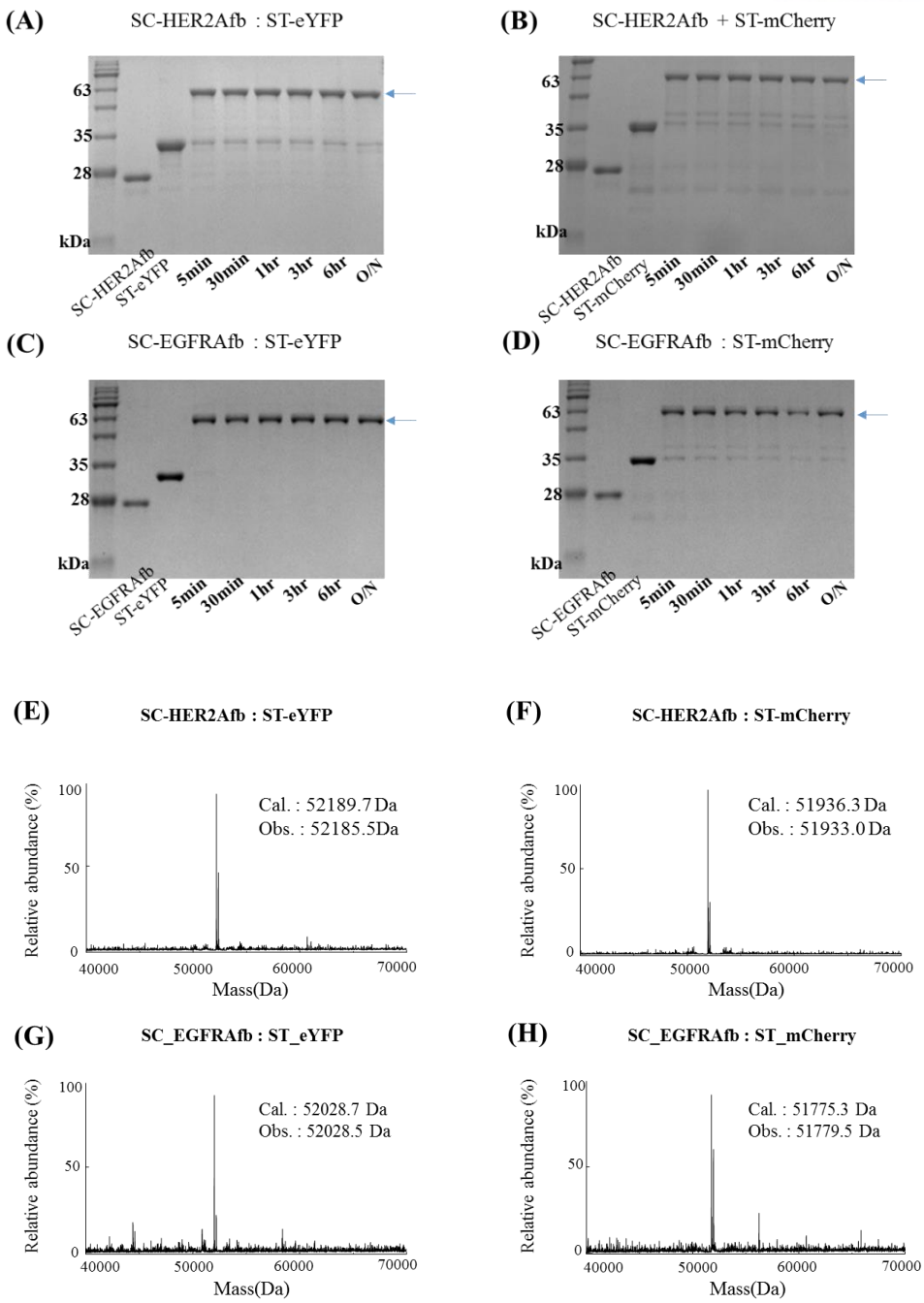

Figure 3.6 Characterization of AFPC. Products of SC-HER2Afb and ST-eYFP (A, E), SC-HER2Afb and ST-mCherry (B, F), SC-EGFRAfb and ST-eYFP (C, G), and SC-EGFRAfb and ST-mCherry (D, H) are analyzed with SDS-PAGE (A-D) and ESI-TOF MS (E-H). Reaction times and molecular weight markers are indicated (A-D). Calculated and observed molecular masses are indicated (E-H). (Blue arrow: conjugated product of AFPCs)

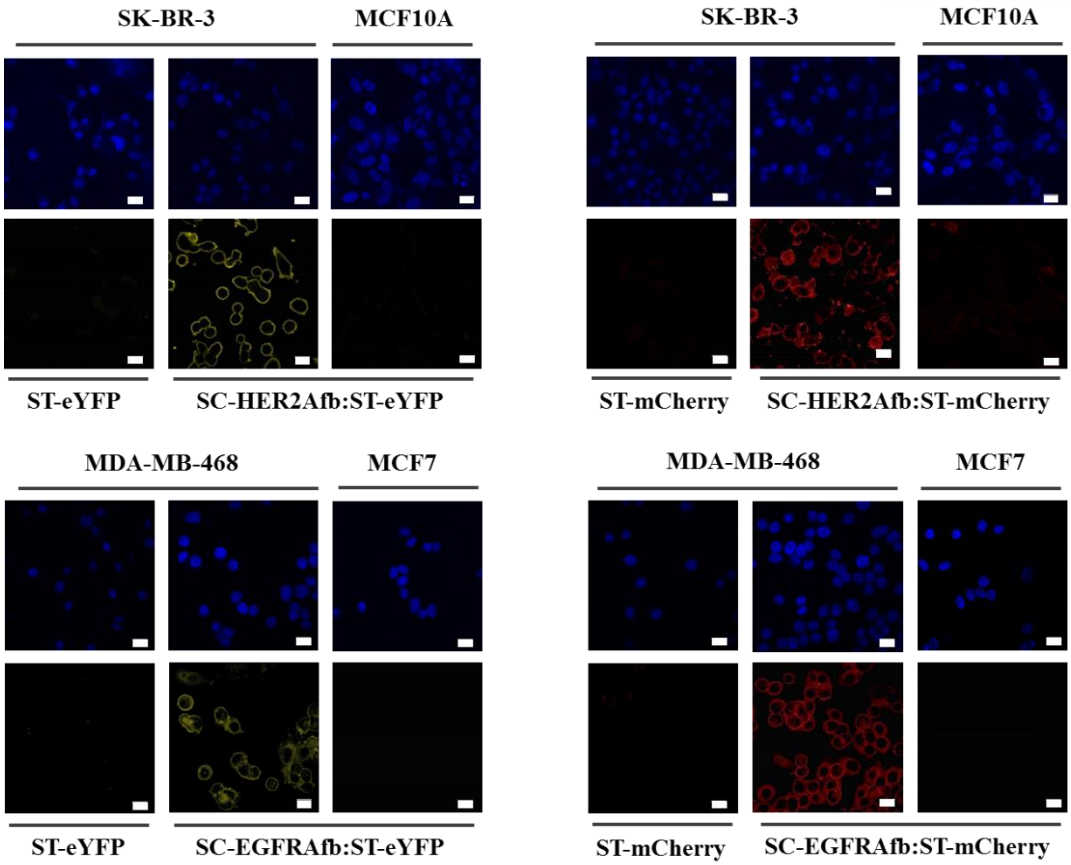

Figure 3.7 Fluorescent microscopic images of various cells treated with AFPCs and ST-fluorescent proteins. Cells and AFPCs are indicated on top and the bottom of image panels, respectively. Nuclei are stained with DAPI (blue, top panels), and eYFP and mCherry are visualized with yellow and red, respectively (bottom panels).

In addition to targeting and detecting dual functionalities implanted by SC-ST mediated ligation, additional functionality can be incorporated using genetic fusion prior to protein ligation. We genetically introduced glutathione-*S*-transferase (GST) between ST and HER2 affibody to form ST-GST-HER2Afb fusion protein. ST-GST-HER2Afb was purified with same methods as those of ST-HER2Afb. Molecular mass of ST-GST-HER2Afb was measured as 37782.0 Da which is well matched with theoretically calculated value (Figure 3.8) and stability and solubility of ST-GST-HER2Afb did not significantly altered. ST-GST-HER2Afb was also successfully conjugated with both mCherry-SC and eYFP-SC through same isopeptide bond formation with almost identical efficiency as previously described (Figure 3.8).

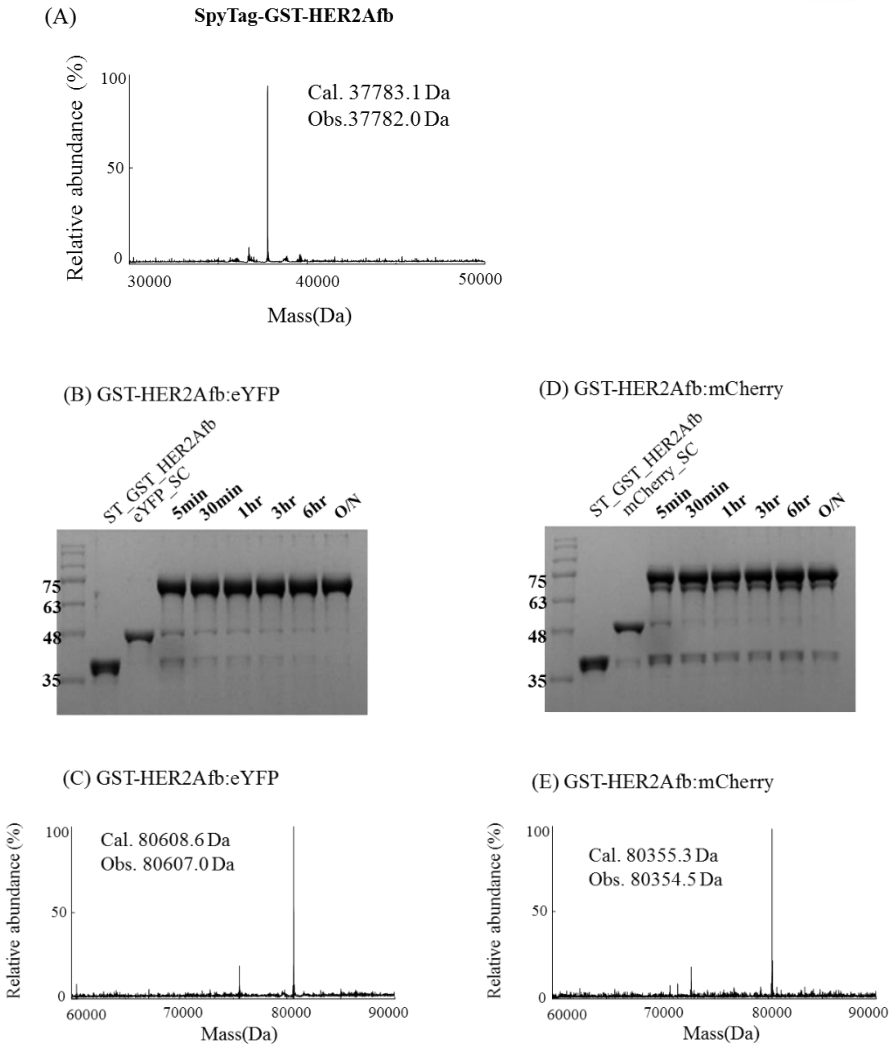

Figure 3.8 Characterization of ST-GST-HER2 (A) and conjugates between ST-GST-HER2Afb and fluorescent protein-SC. Reaction products are analyzed via SDS-PAGE (B, D) and ESI-TOF MS (C, E).

Fluorescent confocal images of SK-BR-3 cells treated with GST-HER2Afb:eYFP (ST-GST-HER2Afb and eYFP-SC) and GST-HER2Afb:mCherry (ST-GST-HER2Afb and mCherry-SC) suggested that GST insertion did not alter the targeting and imaging capability of complexes and thus complexes could be also utilized as an imaging toolkit and cargo carrier concurrently (Figure 3.9).

Since GST and extra linkers have four cysteines, any cargoes which have cysteine-reactive moieties can be easily conjugated.[124] We chose 6-maleimidocaproyl hydrazine prodrug of doxorubicin (AlDox) as a cargo because it has cysteine-reactive maleimide moiety and doxorubicin (Dox)[118] is a popular anti-cancer reagent when it is released. Contents of conjugated AlDox were evaluated by

UV/Vis spectrophotometer, since AlDox specifically absorbs 495 nm. UV/Vis analysis showed that approximately two AlDox were conjugated to a ST-GST-HER2Afb molecule on average.

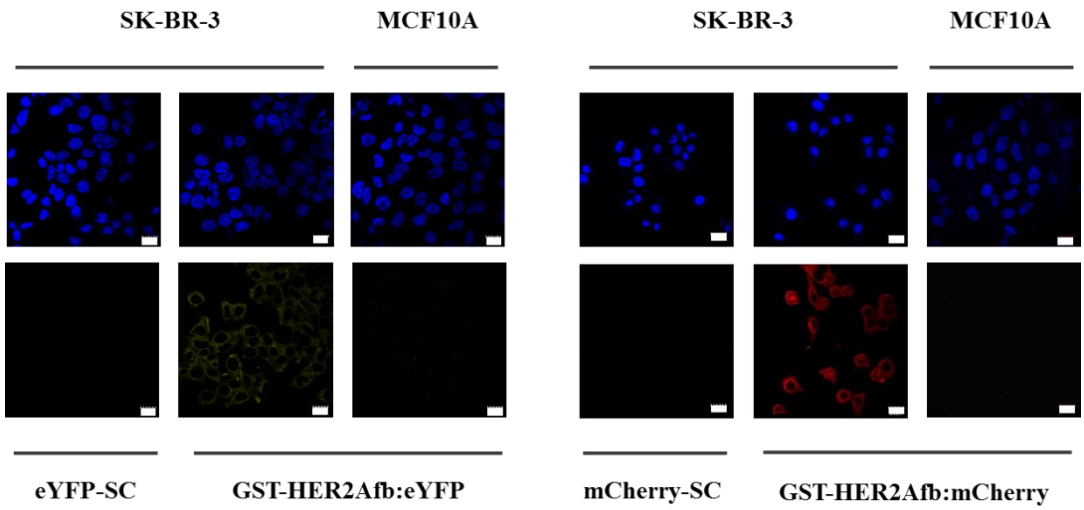

Figure 3.9 Fluorescent microscopic images of SK-BR-3 and MCF 10A cells treated with fluorescent proteins-SC, GST-HER2Afb:fluorescent proteins (GST-HER2Afb:eYFP or GST-HER2Afb:mCherry). Cells and AFPCs are indicated on top and the bottom of image panels, respectively. Nuclei are stained with DAPI (blue, top panels), and eYFP and mCherry are visualized with yellow and red, respectively(bottom panels). (Scale bar: 20 μM)

Two proposed mechanisms which by doxorubicin acts in cancer cells are well-known. One is damaging to cellular membrane, DNA and protein due to generation of free radicals and the other is interaction into DNA and disruption of topoisomerase-II-mediated DNA repair.[128-129] To confirm how to doxorubicin loaded ST-GST-HER2Afb works and effect cytotoxicity in SK-BR-3 cells by these proposed mechanisms, we performed live confocal microscope cell imaging. Live fluorescence cell images of SK-BR-3 cells showed the positions of the free AlDox (red), eYFP-SC (yellow) and AlDox loaded GST-HER2Afb:eYFP (AlDox-GST-HER2Afb:eYFP), respectively (Figure 3.10). Although red fluorescent signal of AlDox-GST-HER2Afb:eYFP appeared strongly in both nucleus and cytosol (Figure 3.10 middle), yellow fluorescent signal of GST-HER2Afb:eYFP complex was found only in cytosol (Figure 3.10 bottom). These data suggested that AlDox-GST-HER2Afb:eYFP bound to surface HER2 receptors of SK-BR-3 cells and were endocytosed into the cytosol and subsequently some Dox were released from AlDox-GST-HER2Afb:eYFP and got into the nucleus.[128-129]

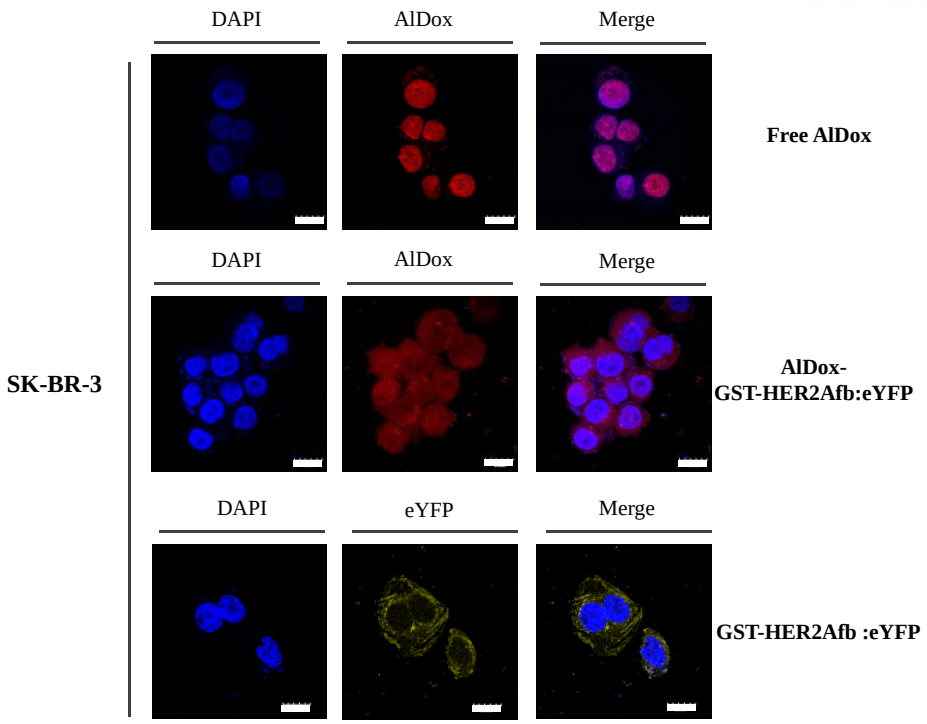

Figure 3.10 Fluorescent microscopic images of SK-BR-3 treated with free AlDox, AlDox-GST-HER2Afb:eYFP, or GST-HER2Afb:eYFP. Nuclei are stained with DAPI and shown in blue (left columns). eYFP and Dox are visualized with yellow and red, respectively (middle columns) and merged images (right columns) are presented. (Scale bar: 20 μM)

To follow post-target binding event, we treated SK-BR-3 cells with GST-HER2Afb:eYFP and visualized their positions according to incubation times (Figure 3.11). We additionally used lysotracker, which stains acidic subcellular organelles in living cells, to prove that GST-HER2Afb:eYFP are endocytosed and stayed mainly within acidic subcellular organelles in cytosol. GST-HER2Afb:eYFP were excluded from nucleus and localized together with lysotracker (Figure 3.11).

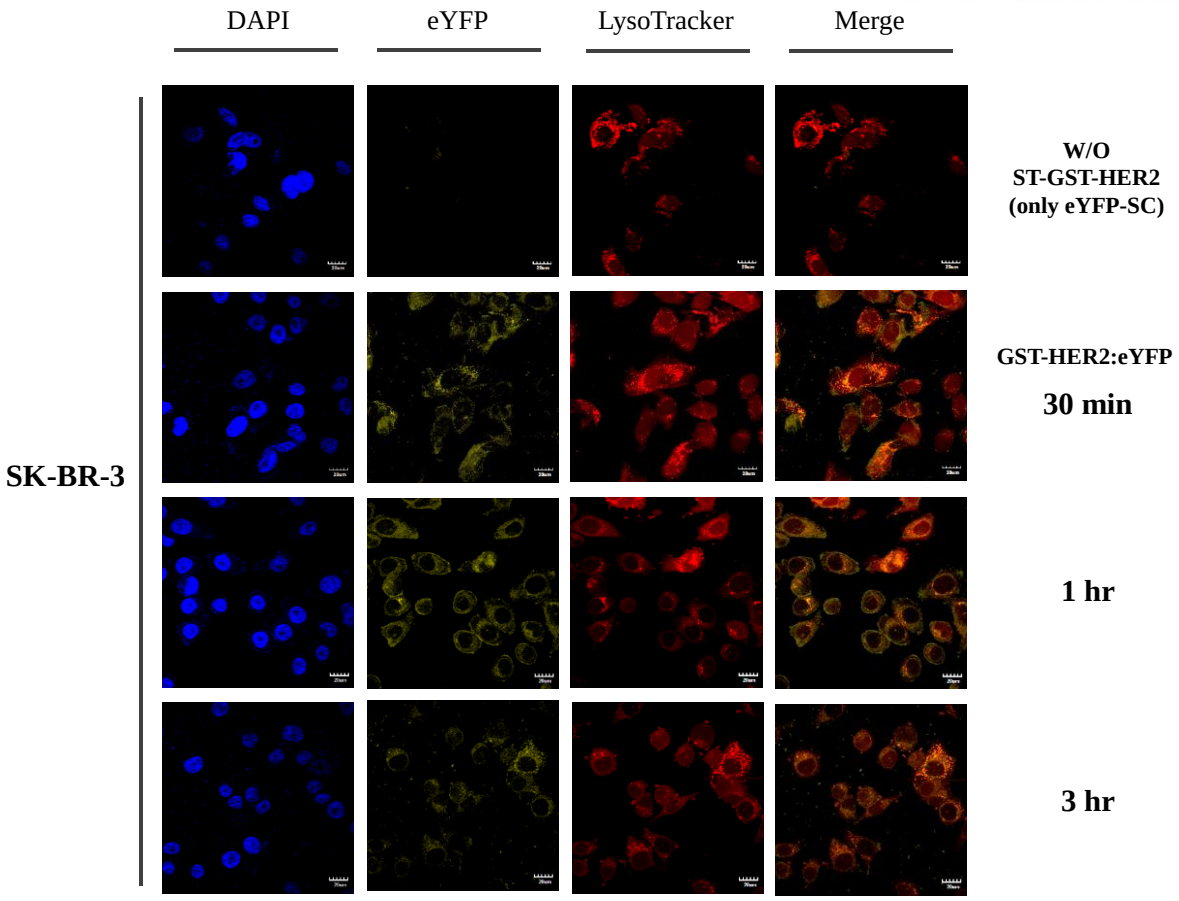

Figure 3.11 Subcellular localization of GST–HER2Afb:eYFP in SK-BR-3 cells are visualized according to incubation times. Nuclei are stained with DAPI (blue, left column), and eYFP and lysotracker are visualized with yellow and red, respectively (middle two columns). Merged images of eYFP and lysotracker are presented in right column. (Scale bar: 20 μM)

Hydrazine linkage is well known to be relatively stable at neutral pH, but effectively cleaved at low pH (pH 4.5-5.5). A time-dependent release study of Dox from AlDox conjugated ST-GST-HER2Afb at pH5.5 showed that approximately 50% of Dox was released within 15 hr (Figure 3.12). These data supported the idea that acid-sensitive hydrazine linkages were cleaved resulting in the release of Dox from AlDox-GST-HER2Afb:eYFP in acidic endosomes and the released Dox only went into nucleus to kill the cells.[118]

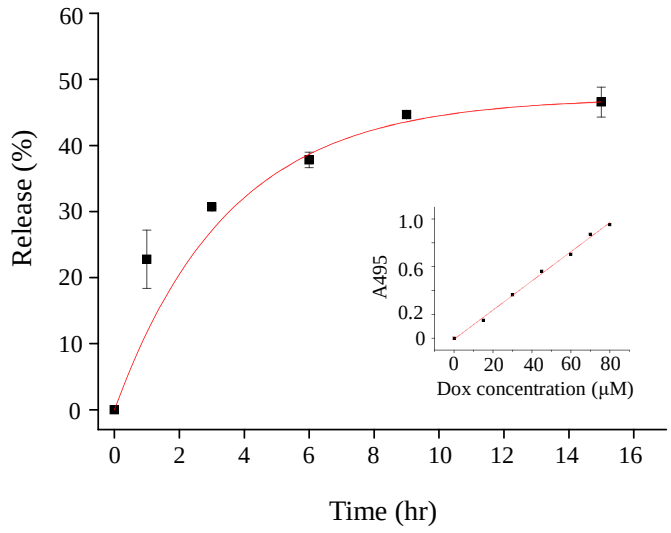

Figure 3.12 Time-dependent release profile of AlDox from ST-GST-HER2Afb at pH 5.5.

To further confirm that the released Dox moves to the nucleus upon low pH-induced cleavage, we conjugated fluorescein-5-maleimide (F5M), which is not acid-cleavable, to the cysteine residues of ST-GST-HER2Afb through thiol-maleimide Michael-type addition. SK-BR-3 (high HRE2 receptor expression), MDAMB231 (low expression) or MCF10A (no expression) cells were treated with F5M-GST-HER2Afb:mCherry and we observed high (SK-BR-3), low (MDAMB231) or no (MCF10A) fluorescent signals in cytosol depending on the levels of HER2 expression (Figure 3.13). In addition, green and red fluorescent signals were overlapped to each other suggesting that non-cleavable fluorescein stayed with GST-HER2Afb:mCherry in cytosol (Figure 3.13). These fluorescent cell image data verified that only released Dox triggered by low pH get into nucleus inducing effective cell death.

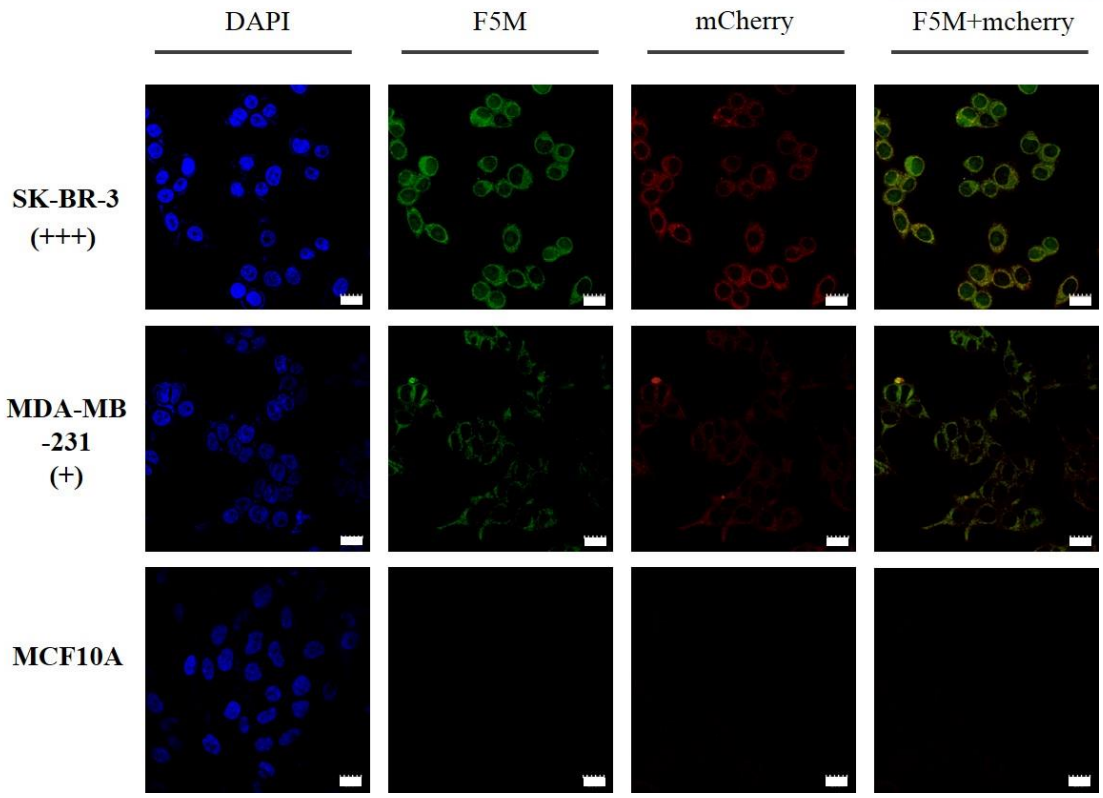

Figure 3.13 Fluorescent microscopic images of various cells treated with F5M-GST-HER2Afb:mCherry. High (SK-BR-3, top panels), low (MDA-MB-231, middle panels), or no (MCF10A, bottom panels) fluorescent signals are observed in the cytosol, depending on the levels of HER2 expression and green and red fluorescent signals overlap to each other. Nuclei are stained with DAPI (blue, left columns), and F5M and mCherry are visualized with green and red, respectively (second and third columns). Merged images of F5M and mCherry channels are presented in right columns. (Scale bar: 20 μM)

To further support action mechanism of AlDox-GST-HER2Afb:eYFP, we collected fluorescent live cell images in a time course upon treatments of AlDox-GST-HER2Afb:eYFP (Figure 3.14). ST-GST-HER2Afb only without AlDox did not show any red fluorescence signal, whereas AlDox-GST-HER2Afb:eYFP exhibited strong red fluorescence signals (Dox) through all time courses (Figure 3.14). We could observe red fluorescence signals in not only nucleus but also cytosol and the morphology of SK-BR-3 cells treated with AlDox-GST-HER2Afb:eYFP was significantly altered even in early time (30 min) (Figure 3.14). Live cell imaging results suggested that Dox was effectively released from GST-HER2Afb:eYFP, got into nucleus, and killed the SK-BR-3 cells efficiently.

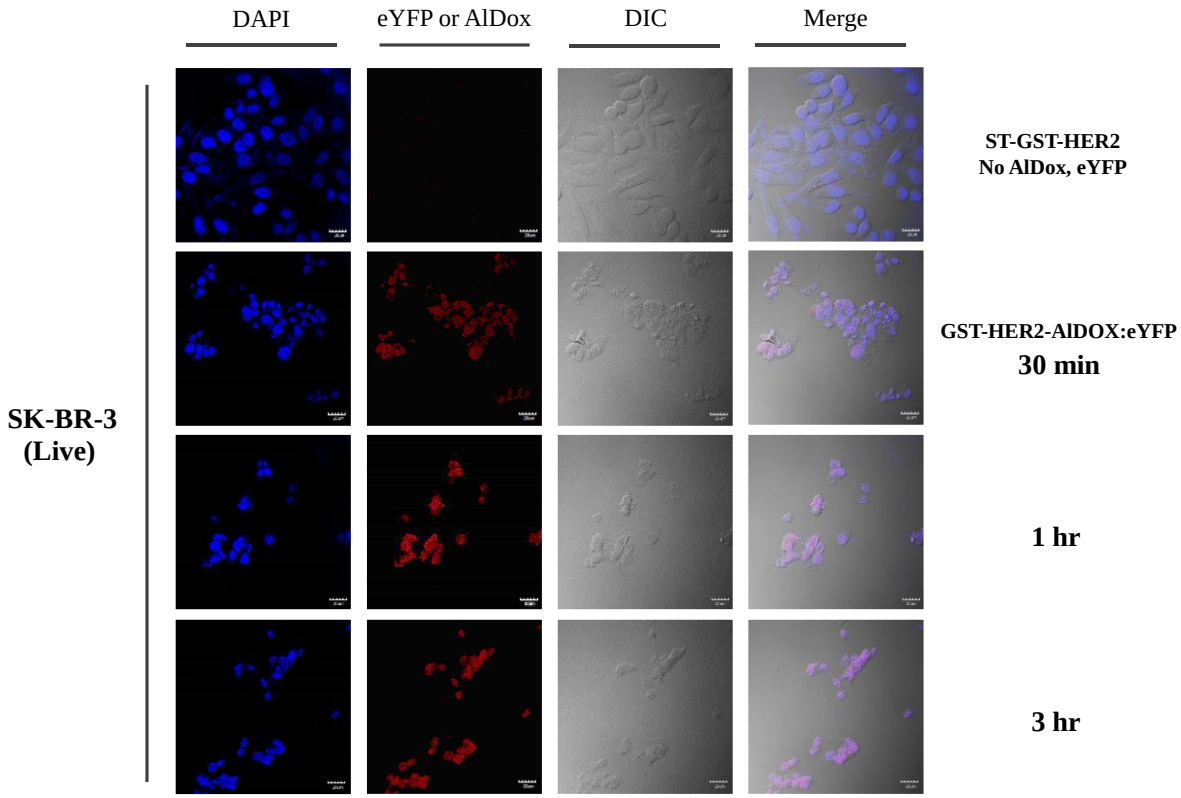

Figure 3.14 Confocal images of AlDox-GST-HER2Afb:eYFP to confirm action mechanism depend on time. Nuclei are stained with DAPI and shown in blue (left columns). Dox and DIC are visualized with red and gray, respectively (middle columns) and merged images (right columns) are presented. (Scale bar: 20 μM)

The cytotoxicity of AlDox-GST-HER2Afb:eYFP was examined using 3-(4,5-dimethylthiazol-2-yl)-2,5-diphenylatetrazolium bromide (MTT) cell viability assay and the results are given Figure 3.16. While viabilities of SK-BR-3 cells treated with AlDox-GST-HER2Afb:eYFP or free AlDox decreased significantly as the concentrations of AlDox increased, those of GST-HERAfb:eYFP were not influenced. These results implied that GST-HER2Afb:eYFP itself does not alter cell viability but effectively delivers conjugated Dox resulting in almost identical cytotoxic efficacy to that of free Dox. Although AlDox-GST-HER2Afb:eYFP has a targeting capability, it did not show any superior cytotoxicity to free Dox in cell viability tests probably because free Dox can easily diffuse in almost any types of cells. One major advantage of targeting strategy would be minimizing side-effect of drugs. To test whether AlDox-GST-HER2Afb:eYFP indeed minimizes off-target effects, we treated MCF10A cells, which do not overexpress HER2 receptors, with GST-HER2Afb:eYFP, AlDox-GST-

HER2Afb:eYFP, or free Dox. While free Dox effectively killed MCF10A cells almost identical levels to those of SK-BR-3, only approximately 20% of MCF10A cells were killed upon AlDox-GST-HER2Afb:eYFP treatment (Figure 3.15). These data indicated that AlDox-GST-HER2Afb:eYFP has a targeting ability to specific cancer cells avoiding significant side effects on normal cells.

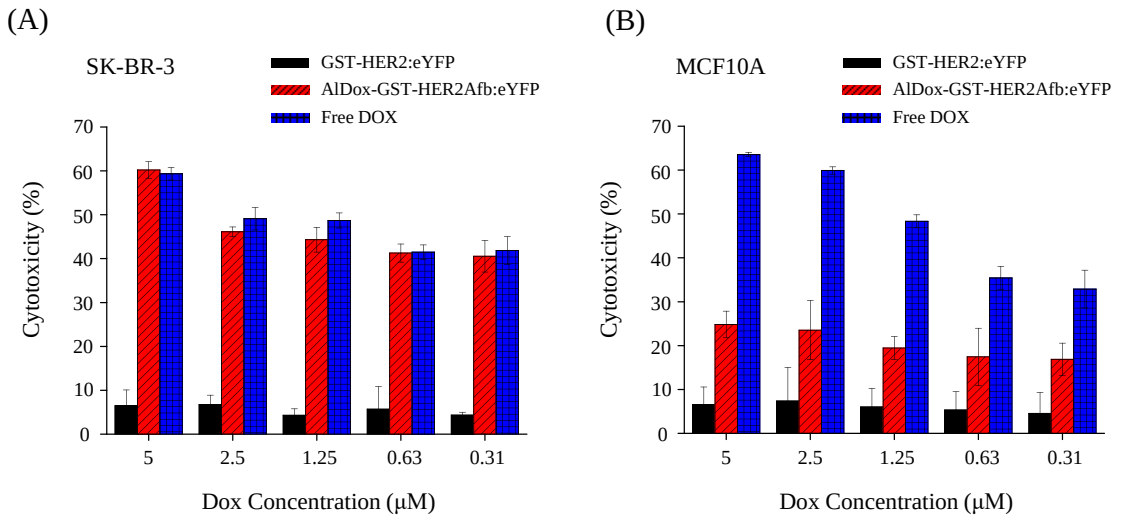

Figure 3.15 MTT cell viability assay. Dose dependent cytotoxicity profiles of AlDox-GST-HER2Afb:eYFP, GST-HER2Afb:eYFP, and free Dox toward SK-BR-3 (A) and MCF10A (B). Five independent experiments were performed and the error bars are indicated.

3.4 Conclusions

Simple plug-and-playable fluorescent cell imaging modular toolkits are established using the bacterial superglue SpyTag/SpyCatcher protein ligation system. A variety of affibody-fluorescent protein conjugates (AFPCs) are post-translationally generated *via* the isopeptide bond formation, and each AFPC effectively recognizes and binds to its targeting cells, visualizing them with selective colors on demand.

Chapter 4. Layer-by-layer Assemblies with Protein Cage via His-tag/metal Recognition

4.1 Introduction

The development of uniform nanostructures containing biomolecules is important in the area of biomaterial science and technology. Multilayered arrays of functional biomolecules provide a high specificity and/or activity on a smaller scale. Their spontaneous or directed assembly is accomplished by cooperative interactions–covalent or noncovalent–of one or more small components that assemble in a predefined way to produce a larger structure from the bottom-up. Thus molecular nanostructures with well-defined particle size and shape is used for many applications such as imaging agents, multilayer films, nanoelectronic devices[29, 130-133] and layer-by-layer (LbL) assemblies.

During recently years, nanoparticles such as viral nanoparticles (VNP), inorganic nanoparticles, polymers and protein cages have become popular building blocks for nanostructures. Protein cages such as ferritins, heat shock proteins (Hsp), viral capsids and DNA-binding proteins have been widely used as nano-scale building blocks to LbL assembly[32-38] since protein cage architectures are biocompatible, endogenously self-assembled from a limited number of protein subunits into higher order structures with uniform size distribution as they are gene products, and easy to be modified either by genetically or chemically, indicating that both structural and functional components can be integrated. Also, atomic resolution structural information of the cage is identified, allowing us rationally to design and control at the molecular level. LbL assemblies can be used to make semi-permeable membranes, sensors, solid-state electrolytic films for fuel-cell components and nanomechanical films. The versatility of LbL assembly is due to the fact that multiple functionalities can be readily incorporated into the films, even on irregular or flexible supports.

One of the main strategies to construct nanostructures is the ability to have immobilized biomolecules with preserved activity, and lots of research groups have incorporated mediators that significantly improve sensing ability such as specific interaction between biotin and streptavidins. However, such binding mediators have formation often causing size-mismatching and huge gap between two building blocks. To overcome this, we made a novel nanostructure using the binding affinity of histidine and Ni-NTA within one template without mediators. The hexahistidine were genetically inserted and Maleimido-NTA-Ni was chemically introduced into the protein cage template that can recognize and bind each other. Polyhistidine and other metal-binding motifs have proven highly advantageous to protein identification of fusion proteins and to speed up the purification process as well can be used to immobilize proteins on a surface, as required for certain assays. Nevertheless we used

metal affinity tags in order to build a uniform nanostructure and indicate expand the possibilities for fabricating functional materials and developing new devices.[134-135]

Herein, we used a previously redesigned natural capsid-forming enzyme, lumazine synthase protein cage nanoparticles (PCN) from *Aquifex aeolicus* (AaLS) for building blocks (Figure 4.1). AaLS is an enzyme which catalyses the penultimate step in the synthesis of riboflavin and forms icosahedral capsids consisting of 60 identical subunits with exterior diameter is 15.4nm and an 8nm interior cavity. AaLS have been used as template for crystallization of inorganic nanoparticles such as iron oxide and for encapsulation of guest molecules such as green fluorescent proteins (GFP) by using engineered electrostatic interactions between host and guest to drive binding. However, it has not been tried to use AaLS as one of the building blocks to construct a nanostructure before.[136-138]

To build a uniform nanostructure, novel protein cage, genetically modified AaLS-His$_6$ and chemically modified Maleimido-NTA-Ni labeled AaLS L153C PCN were utilized. By using direct interaction between AaLS-His$_6$ and Maleimido-NTA-Ni labeled AaLS L153C PCN, LbL assembly was developed on the single protein cage without mediators.

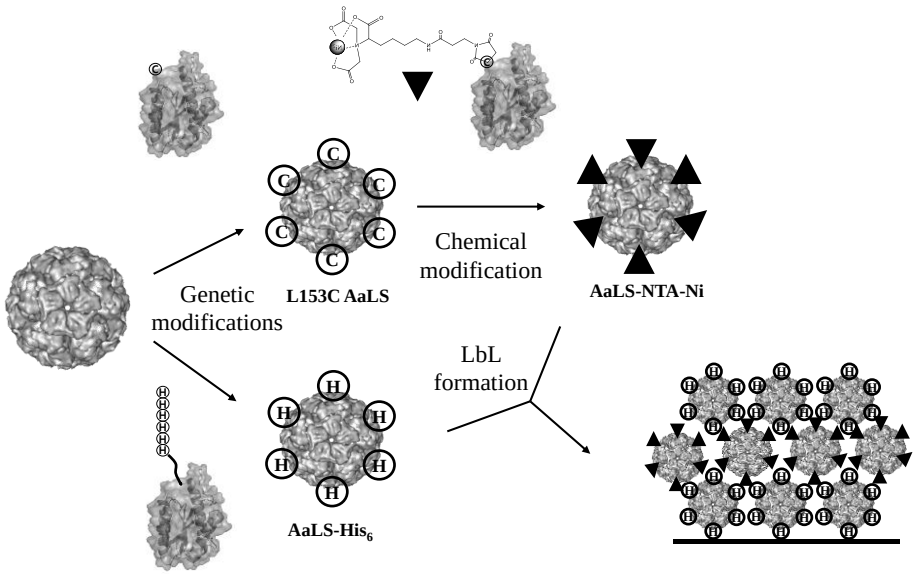

Figure 4.1 Uniform LbL assemblies were constructed by using two genetically and/or chemically modified complementary AaLS PCN derivatives.

4.2 Materials and methods

AaLS PCN mutagenesis, expression and purification

The optimized AaLS gene was synthesized and subcloned into the IPTG-inducible pET-30b expression vector (Invitrogen) containing hexa-histidine tags at the C-terminus with extra linker residues (ADPGGLVPRGSGPNSSSVDKLAAALE). Cysteine substitution of leucine 153 was conducted by using established quick change mutagenesis protocol using pET-30b based plasmids encoding genes for AaLS PCN. The amplified DNAs were used to transform the competent *Escherichia coli* strain BL21 (DE), which resulted in the over-expression of the AaLS PCN containing either the C-terminal histag (AaLS-His_6) or cysteine instead of leucine at residue 153 (L153C AaLS), respectively. The resultant AaLS-His_6 PCNs and L153C AaLS PCNs were purified by immobilized ion-metal affinity chromatography (IMAC) and heat precipitation followed by size exclusion chromatography as previously described.[34]

Synthesis of N^{α},N^{α}-bis(carboxylmethyl)-N^{ε}-(3-maleimidopropionyl)-L-lysine (Maleimido-NTA)

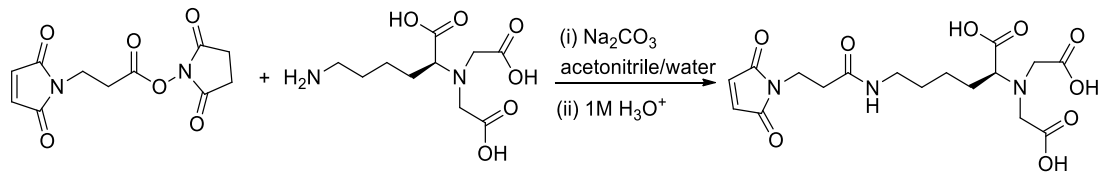

Maleimido-NTA was prepared via the slight modification of the reported procedure.[43] *N*-Succinimidyl 3-maleimidopropionate (61.2 mg, 0.23 mmol)[139] in acetonitrile (50 mL) was added to the 10mM aqueous sodium carbonate solution (60 mL) with N^{α},N^{α}-bis(carboxylmethyl)-L-lysine hydrate (50 mg, 0.19 mmol: anhydrous base) at pH 8.5. After stirring overnight at room temperature, the reaction mixture was neutralized with 1 M hydrochloric acid, and then concentrated *in vacuo.* The reaction mixture was purified by rinsing with acetonitrile to afford the title compound as a white solid.

Chemical modifications of L153C AaLS PCN

Complexes of Ni ion and maleimido-NTA were formed via mixing $NiSO_4$ and maleimide-NTA with 1:1 ratio at room temperature for an hr. Subsequently, L153C AaLS PCNs were incubated with 10 mol equivalents of maleimido-NTA-Ni ion complexes at room temperature with vigorous shaking overnight. Unreacted maleimido-NTA-Ni ion complexes were removed by extensive dialysis at 4°C.[140]

Immobilized metal affinity chromatography (IMAC)

Chromatography was performed using Histrap HP 1 mL columns (GE Healthcare) under the control of a Duoflow FPLC system (Bio-Rad). Solutions for chromatography were pH 7.4 with 5 mM imidazole in 20 mM sodium phosphate, 500 mM NaCl (A, Binding buffer) and pH 7.4 with 1 M imidazole in 20 mM sodium phosphate, 500 mM NaCl (B, Elution buffer). After injection of the sample, column was equilibrated with binding buffer A and AaLS-His_6 PCNs were eluted with a linear gradient of 5-100% elution buffer B with a flow rate of 1 mL/min. Protein elution was monitored by UV detector at 280 nm.

Mass spectrometry

The subunit masses of genetically and chemically modified AaLS PCNs were analyzed using an ESI-TOF mass spectrometer (Xevo G2 TOF, Waters) interfaced to a Waters UPLC and an autosampler. Samples were loaded onto the MassPREP Micro desalting column (Waters) and eluted with a gradient of 5-95% (v/v) acetonitrile containing 0.1% formic acid with a flow rate of 500 μL/min. ESI generally produces a series of multiply charged ions and the charges are typically distributed as a continuous series with a Gaussian intensity distribution and the molecular masses of each species can be determined from the charges and the observed mass-to-charge (m/z) ratio values. Mass spectra were acquired in the range of m/z 500-3000 and deconvoluted using MaxEnt1 from MassLynx version 4.1 to obtain the average mass from multiple charge state distributions. For clarity, only deconvoluted masses were presented.

Surface plasmon resonance (SPR) analysis

SPR experiments were performed with NTA immobilized sensor chip (GE Healthcare) on a Biacore 3000 device at 25°C. Running buffer (10 mM HEPES, 150 mM NaCl and 50 μM EDTA at pH 7.4), nickel ion solution, and regeneration solution (10mM HEPES, 150mM NaCl and 350mM EDTA at pH 7.4) were prepared for binding analysis. 500 μM $NiSO_4$ solution was injected to NTA immobilized sensor chips at a flow rate of 10 μL/min for 4 mins for Ni (II)/NTA chelation and unbound Ni ions were removed with running buffer. Various amounts of AaLS-His_6 PCNs (0.1, 0.2, 0.4, 0.8 and 1.6 μg/mL) were loaded to the activated Ni (II)/NTA sensor chips at a flow rate of 5 μL/min for 8 mins.

Quartz crystal microbalance (QCM) measurements

QCM experiments were performed using Q-Sense E4 and standard gold QCM sensors (Q-sense, Sweden) as described previously, with slight modifications (ref). The system was operated in flow mode with a pump and temperature was maintained at room temperature (25.0±0.1°C). Each sample solution was introduced to the measurement chamber with a pump and continuously measured for 3 min prior to the subsequent introductions. AaLS-His_6 and AaLS-NTA-Ni PCNs were introduced at concentrations of approximately 100 μg/mL, respectively, in HEPES buffer (10 mM HEPES, 100 mM NaCl, pH 7.4. Resonance frequencies were measured simultaneously at seven harmonics (5, 15, 25, 35, 45, 55 and 65 MHz). For clarity, only the normalized frequency of the third overtone is shown.

Atomic force microscopy (AFM) analysis

For the layer-by-layer coating of protein cages on Au surfaces, Au thin films (~13 nm) were thermally deposited on Si substrates. Prior to thermal deposition, a Si wafer was washed in an ultrasonic bath with isopropanol, and blow dried with nitrogen gas. Protein cages were coated on Au/Si substrate by dip coating method. In this process, Au/Si substrates were dipped into AaLS-His_6 PCN solution for 25 min, slowly taken out of the solution with vertical direction, blow-dried with nitrogen gas, and then rinsed with DI water, resulting in the monolayer coating of AaLS-His_6 PCN on Au/Si substrates. By alternatively repeating these procedures with AaLS-NTA-Ni PCN and AaLS-His_6 PCN solution, bilayer and trilayer coated samples were obtained. The root mean square or RMS roughness (R_q) of these layers was compared by using AFM analysis (DI-3000, Veeco).

4.3 Results and discussion

To construct highly ordered nanostructures, AaLS PCNs were utilized for constructing the nano-building blocks. Six consecutive histidine residues (His_6) is known to be an affinity tag which binds tightly to nitrilotriacetic (NTA)-chelated Ni ions, and this approach has been widely used for protein purification.[134-135, 141] By manipulating wild-type AaLS PCNs (wt AaLS) so that one type had His_6 tag and the other had Ni ion-chelating agent, these two types of AaLS PCNs can form clusters through specific and simple recognition each other (Figure 4.1). The His_6 affinity tag was genetically introduced to the C-terminus of the wt AaLS PCNs. As C-termini of the wt AaLS exposed to exterior surface, it is feasible to anchor the functional moieties.[142] Alternatively, leucine residue at position 153 of the wt AaLS was substituted to cysteine (L153C) for selective chemical modifications (Figure 4.1).

The AaLS-His$_6$ PCNs were over-expressed and purified by IMAC. Bound AaLS-His$_6$ PCNs were eluted from the column with an elution buffer containing approximately 600 mM imidazole (Figure 4.2 A). The AaLS-His$_6$ PCNs was confirmed by ESI-TOF MS. Whereas the subunit mass of the wt AaLS was 16,705.2 Da (Figure 4.4), the subunit mass of AaLS-His$_6$ PCN was determined to be 19,098.5 Da, which good agreement with the calculated value (Figure 4.2 B). To investigate the cage integrity of AaLS-His$_6$ PCNs, size-exclusion chromatography (SEC) and transmission electron microscopy (TEM) were used. AaLS-His$_6$ PCNs eluted at the same position as did wt AaLS PCNs on the SEC (Figure 4.2 C). The intact cage architecture of AaLS-His$_6$ PCNs confirmed using negatively stained TEM images with a uniform size distribution of 15-16 nm in diameter (Figure 4.2 D), indicating that the hexa histidine do not alter their own architecture of the AaLS PCNs or induce the dissociation or aggregation of AaLS PCNs.

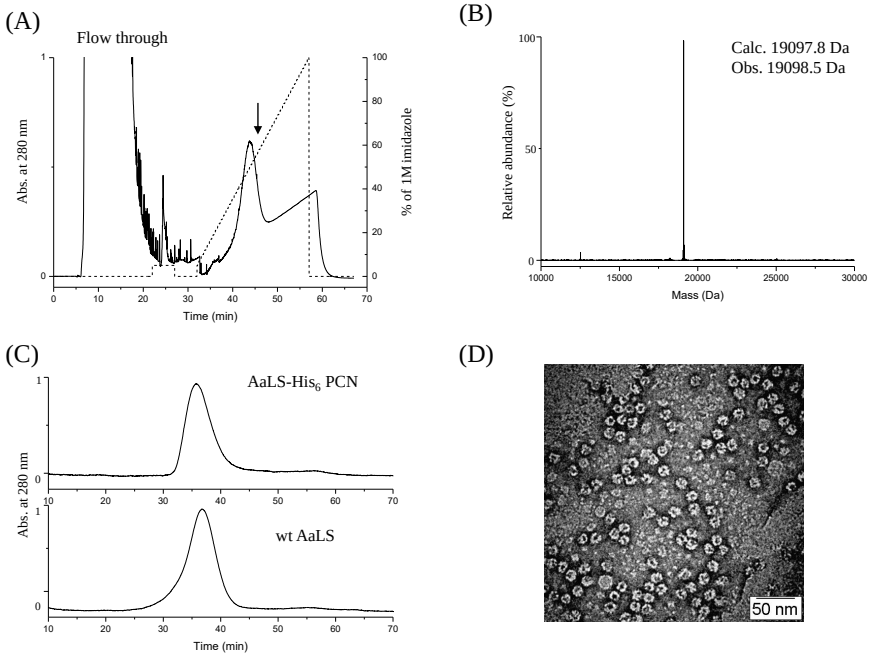

Figure 4.2 Characterization of AaLS PCN containing His-tags at the C-termini (AaLS-His$_6$ PCNs). (A) IMAC of AaLS-His$_6$ PCNs. AaLS-His$_6$ PCNs were captured with a Ni ion-charged Histrap column and eluted with linear gradient of 5-100% elution buffer (1 M imidazole in 20 mM sodium phosphate and 500 mM NaCl). Absorption traces at 280nm. (B) Molecular mass measurement of dissociated subunits of AaLS-His$_6$ PCNs (calculated, 19097.8 Da; observed, 19098.5 Da). (C) SEC profiles (280nm) of AaLS-His$_6$ PCNs (top) and wt AaLS PCNs (bottom). The samples were loaded onto a 10 x 300 mm superpose 6 (GE healthcare) size exclusion column which is pre-equilibrated with 50 mM phosphate, 100 mM NaCl (pH 6.5) and eluted with same buffer at a rate of 0.5 mL/min. (D) TEM image of 2% uranyl acetate stained AaLS-His$_6$ PCNs.

The binding affinity between AaLS-His$_6$ PCNs and Ni ion chelates were further examined using surface plasmon resonance (SPR). NTA immobilized SPR sensor chip was first activated with the Ni ion solution to form Ni-NTA chelating complexes on the surface of SPR sensor chip. Before proceeding with each experiment, removing AaLS-His$_6$ PCNs bound to Ni ions on the sensor chip using 350mM EDTA, subsequently reactivating the surface with the Ni ions solution. Although gradual increases in SPR response units (RU) were observed upon AaLS-His$_6$ PCNs, with RU values reaching a plateau at each concentration (Figure 4.3 A), no RU change was observed with wt AaLS PCNs (Figure 4.3 B). No apparent dissociation of AaLS-His$_6$ PCNs from the immobilized Ni was observed even after buffer washing, suggesting that the multiple His-tags on the surface of the AaLS-His$_6$ PCN cooperatively interacted with the chelated Ni ions.[80, 134, 143]

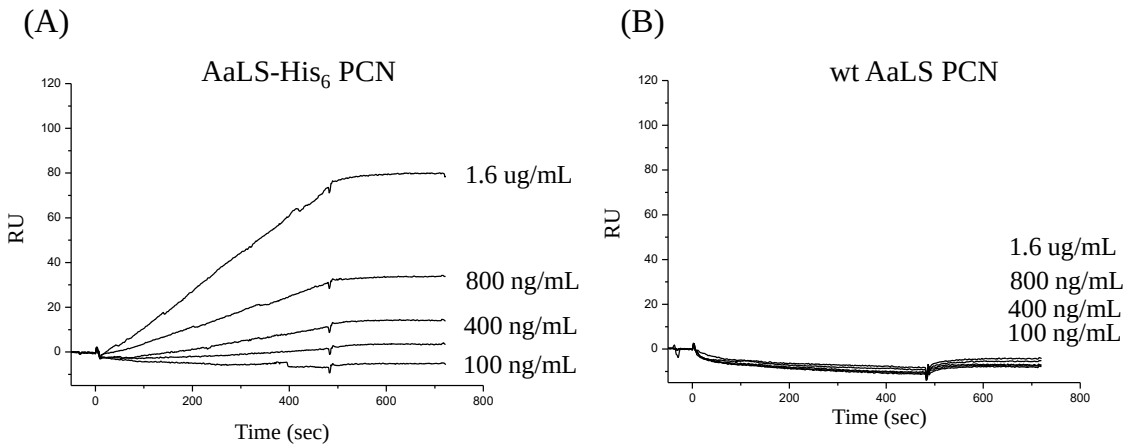

Figure 4.3 SPR analyses of AaLS PCNs binding to Ni-NTA immobilized SPR sensor chip. Various amounts of AaLS- His$_6$ PCNs and wt AaLS PCNs (0.1, 0.2, 0.4, 0.8 and 1.6 μg/mL) were loaded to the activated Ni-NTA sensor chips at a flow rate of 5 μL/min for 8 mins. (A) Gradual increases in SPR responses (RU) were observed upon the introduction of AaLS-His$_6$ PCNs, with RU values reaching a plateau at each concentration. (B) No RU change was observed with wt AaLS PCNs.

AaLS L153C PCNs were chemically modified with N^{α},N^{α}-bis(carboxylmethyl)-N^{ε}-(3-maleimidopropionyl)-L-lysine (maleimido-NTA) complexed with Ni ions (maleimido-NTA-Ni) for counterpart building blocks. Maleimido-NTA was prepared via a slight modification of the reported procedure. The crystal structure of AaLS demonstrates position 153 leucine residue is exposed to the exterior and cysteine residue at 37 is in interface, that is not appropriate for labeling ligands. This being

so, leucine residue 153 was substituted to cysteine and attached functional moieties for being exposed. The chemical attachment of AaLS L153C PCN with maleimido-NTA-Ni(II) was measured by ESI-TOF MS (Figure 4.5 A) and 470 Da difference between AaLS L153C PCN and that of AaLS L153C PCN labeled with maleimido-NTA-Ni(II) is observed. However, two distinct molecular masses, 17166.0 Da and 17636.0 Da, were observed in mass spectrometric analyses (Figure 4.5 A, top). The observed molecular masses matched well to the calculated molecular masses of of AaLS L153C PCN labeled with one or two maleimido-NTA-Ni(II) moieties. This result indicated that some interfacial cysteines at 37 residue were also conjugated with maleimido-NTA-Ni(II) in addition to the introduced cysteine at C153. Maleimido-NTA-Ni(II)-treated AaLS L153C PCN and wt or untreated AaLS L153C PCN eluted at the same position (Figure 4.5 B) suggesting that chemical modification does not significantly change the cage construct of AaLS PCN. Maleimido-NTA-Ni(II)-labeled AaLS L153C PCN (AaLS-NTA-Ni PCN) also confirmed the intactness implied an average diameter of 15-16 nm using TEM (Figure 4.5 C and D).

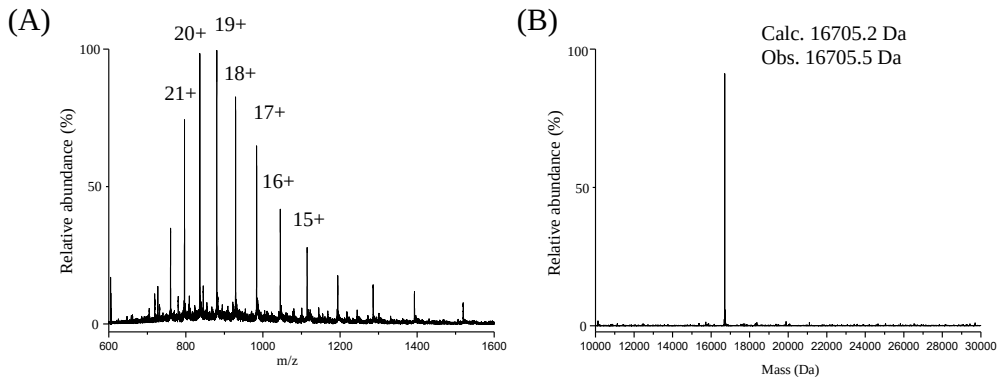

Figure 4.4 ESI-TOF mass spectrum of the dissociated subunits of wt AaLS PCN. (A) Gaussian charge state distribution is shown and a series of charged peaks is indicated (15+ to 21+). (B) Deconvoluted molecular mass of the dissociated subunits of wt AaLS PCN (Calculated, 16705.2 Da; observed 16705.5 Da)

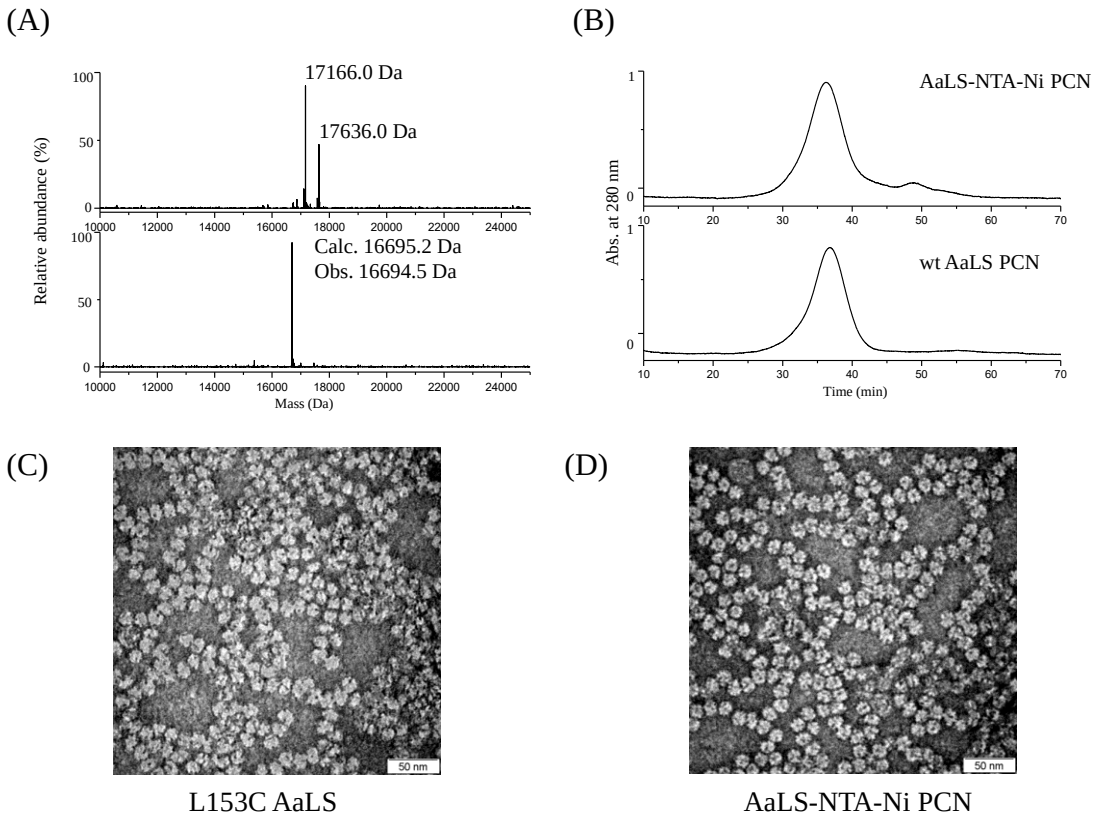

Figure 4.5 Characterization of AaLS-NTA-Ni PCNs. (A) Molecular mass measurement of the dissociated subunits of AaLS L153C treated with maleimido-NTA-Ni(II) (top) and untreated AaLS L153C (bottom). (B) Size exclustion elution profiles (280nm) of AaLS-NTA-Ni PCNs (top) and wt AaLS PCNs (bottom). (C) TEM image of 2% uranyl acetate stained AaLS L153C. (D) AaLS-NTA-Ni PCNs.

QCM is a useful tool to study the processes of protein adsorption and monitor the deposition of molecules. The binding affinity between AaLS-His_6 and AaLS-NTA-Ni was investigated using quartz-crystal microbalance (QCM) measurements. To form regular nanostructures, biomacromolecules chemically modified with biotin and streptavidin have been carried out as a universal mediator in most previous studies. Biotin-Streptavidin interaction often inducing huge functionality gaps due to size mismatching between two molecules although the interactions are highly specific and strong interaction under harsh conditions.[144-145] Typically, the masses of deposited molecules on the chips, the QCM sensor results in a decrease in the resonance frequency ($-\Delta F$). Wt and AaLS-His_6 bound individually to the gold QCM sensor no modification (Figure 4.6). The resonance frequency ($-\Delta F$) decrease for wt AaLS

was lower than that of AaLS-His$_6$, probably because of the approximately 15% higher mass of AaLS-His$_6$ PCN resulting from the presence of the C-terminal His$_6$ tags with extra residues. The resonance frequency decreased and plateaued at a certain value (Figure 4.6). We flowed excess amount of sample buffer until the frequency reached to plateau to remove the unbound materials. It was indicated that AaLS-His$_6$ had formed a strong uniformed monolayer on the gold sensor surface.

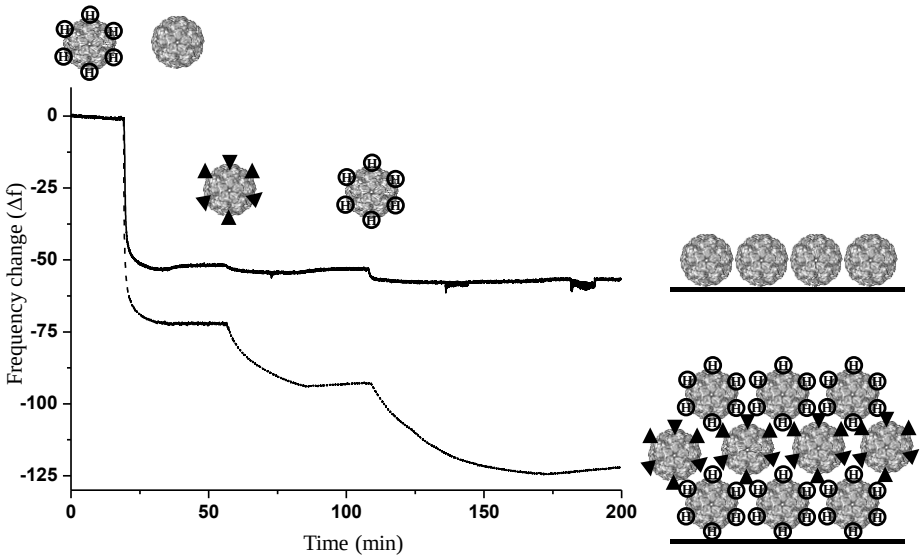

Figure 4.6 QCM resonance frequency change (-Δ*F*) profiles of either wt AaLS (solid line) or AaLS-His$_6$ (dashed line) PCNs on the QCM sensors and subsequent deposition of AaLS-NTA-Ni on the monolayer of AaLS-His$_6$. While the frequency of AaLS-His$_6$ PCN monolayered QCM sensor decreased dramatically upon introduction of AaLS-NTA-Ni PCNs (dashed line), the frequency of wt AaLS PCN monolayered QCM sensor remained unchanged (solid line).

After monolayers of wt AaLS and AaLS-His$_6$ were individually adsorbed, we infused the solution containing AaLS-NTA-Ni over the monolayered QCM sensor chips and monitored real-time changes in the frequencies. While AaLS NTA-Ni bound to monolayer of AaLS-His$_6$, QCM sensor frequency decreased dramatically until a certain value, the frequency of wt AaLS was not changed. (Figure 4.6). These data suggest that wt AaLS monolayer did not recognize to the AaLS-His$_6$ monolayer but AaLS-NTA-Ni strongly bind and form a second layer through specific metal (Ni) ion/His-tag interactions. After that buffer was flowed for removing loosely and unbound materials and then AaLS-His$_6$ solution was flowed over the QCM sensor. (Figure 4.6). The resonance frequency of double-layer of AaLS-His$_6$

and AaLS-NTA-Ni was significantly decrease in the QCM sensor, whereas no noticeable change of wt AaLS monolayer was observed in the QCM sensor. These data indicated that Ni ions on the surface of AaLS-NTA-Ni and His-tags on the surface of AaLS-His_6 PCNs interact directly each other and allow the formation of regular LbL assemblies and stabilize a multi-layered nanostructure.

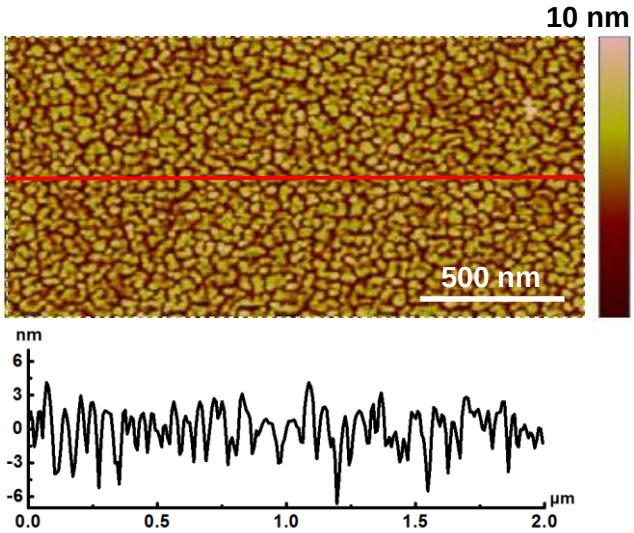

Figure 4.7 Atomic force microscopic image of basic gold film for the LbL assemblies. Surface roughness is 1.94 nm.

To confirm uniform LbL formation by AaLS PCN derivatives, the surface roughness of each layer formed on flat gold surfaces was estimated using atomic force microscopy (AFM). Since the surface of the QCM sensor chip itself is quite rough at the atomic level (Figure 4.7) but has the same properties as the ACM gold sensor chip, the LbL assemblies of AaLS PCN derivatives was measured through AFM. The root mean square (RMS) roughness (Rq) value showed 1.45 nm indicated that deposition of AaLS-His_6 PCNs resulted in a uniform monolayer (Figure 4.8 A) without significant clumping. Successive layer formations were achieved by the alternate deposition of AaLS-NTA-Ni PCNs and AaLS-His_6 PCNs, identical to the QCM experiments. Notably, the surfaces were similarly uniform with no significant clumping, and exhibited Rq values of 2.17 nm and 2.66 nm for double-layer and triple-layer coatings, respectively (Figure 4.8 B and C). The slight progressive increases in surface roughness observed for double- and triple-layer assemblies most likely resulted from slight spatial mismatch between the two different AaLS PCN derivatives.

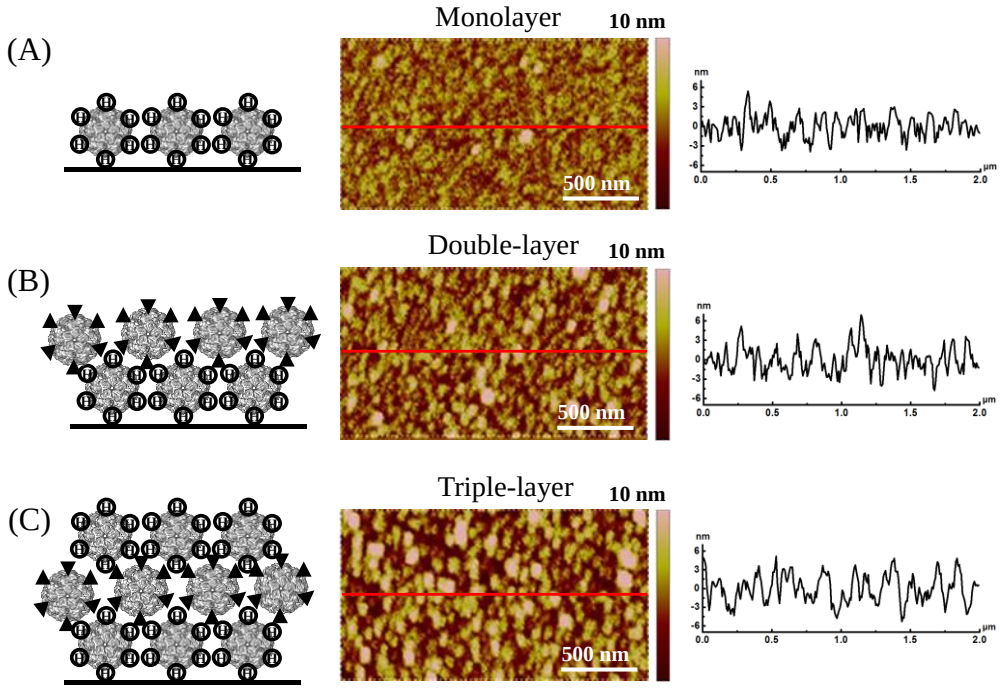

Figure 4.8 Surface roughness of LbL assemblies. Atomic force microscopic (AFM) images of (A) monolayer (AaLS-His$_6$ PCN) with a Rq value of 1.45 nm, (b) bilayer (AaLS-His$_6$ PCN/AaLS-NTA-Ni PCN) with a Rq value of 2.17 nm, and (C) trilayer (AaLS-His$_6$ PCN/AaLS-NTA-Ni PCN/AaLS-His$_6$ PCN) LbL assemblies with a Rq value of 2.66 nm, respectively.

4.4 Conclusion

Two complementary AaLS PCN nanobuilding blocks were modified for constructing nano structures. AaLS L153C and AaLS-His$_6$ were genetically modified and L153C was chemically conjugated with maleimido-NTA-Ni. These two nanobuilding blocks were characterized by TEM and SEC for their intactness and formed LbL assemblies through recognition each other without mediators. In order to build a uniform nanostructure, we used AaLS PCNs which are highly symmetric and multivalent. LbL formation of AaLS PCN derivatives were characterized by QCM and AFM for confirming binding affinities and surface roughness. Similar approaches are able to use for other functional nanomaterials and will expand the possibilities for fabricating uniform and functional materials and developing new advices.

Chapter 5. Concluding Remarks

5.1 Summary and Conclusions

As stated in Chapter 1, the applications of multi-functional nanoplatform were described. Nanoparticles commonly defined in this thesis were protein cages and fusion monomeric proteins. Nanoparticles are derived from nature and have uniform shape, nano-meter size, stability and they are robust being engineered, these characteristics are the reasons to utilize them for developing multi-functional nanoplatforms for decades. Although I focused only targeted cell imaging, delivery cargoes and high-ordered structures, protein-based nanoparticles can be exploited a wide range of applications.

First, in Chapter 2, derivatives of encapsulin protein cages were utilized as multifunctional nanoplatforms through genetic or/and chemical manipulations. It was first trial to use encapsulin nanoparticles as targeted drug delivery nanoplatforms. Hexa histidine inserted in residue 42 of encapsulin nanoparticles were heat stable and allowed us to purify encapsulin readily. Genetically introduced SP94-E_LH42 and chemically conjugated E_LH42-SMCC-SP94 were both able to specifically bind to hepatocellular carcinoma cell, HepG2 via confocal microscope indicating that SP94 peptides were well displayed on the exterior surfaces of encapsulin and SP94 introduced encapsulin had potential as targeted delivery platforms. The MTT assay demonstrated that drug loaded encapsulin had cytotoxicity although encapsulin without drugs did not have any toxicity. These studies clearly suggest that engineered encapsulin can be one of the specific targeting therapeutic delivery platform.

Secondly, in Chapter 3, I demonstrated that monomeric protein could be utilized as a cellular imaging toolkit. In this study, simple and easy fluorescent cell imaging toolkits were established using post translational ligation system, SpyTag and SpyCatcher. Recently developed SpyTag and SpyCatcher ligation system is rapid, simple, and allow us detect cancer cells easily with selective colors on demand. We utilized affibody molecules and fluorescent proteins with ligation systems in the versatility, which can be applied to various specific cell detect tools. In addition, GST scaffold protein inserted monomeric protein can load more cargoes such as doxorubicin via chemical conjugation, we confirmed the cell viability depends on doxorubicin concentration and their localization in cells.

Finally, in Chapter 4, we focused on developing nano-building blocks using two complementary AaLS, his-tags presented AaLS and AaLS-NTA-Ni particles. The streptavidin-biotin interactions used in the previous studies could affect the high-ordered structures despite the strong binding affinity. However, histidine tagged AaLS and Ni-NTA conjugated AaLS can overcome these drawbacks. Each genetically or chemically manipulated AaLS were characterized mass spectrometry and size exclusion

chromatography, and the well-defined LbL assembly was confirmed by QCM and AFM. We only utilized the exterior surface of AaLS protein cages which can have more functions in interior cavity, it will be applied in various biomaterial fields.

References

1. Chudakov, D. M.; Lukyanov, S.; Lukyanov, K. A., Fluorescent proteins as a toolkit for in vivo imaging. *Trends in Biotechnology* **2005,** *23* (12), 605-613.

2. Weissleder, R., Molecular Imaging in Cancer. *Science* **2006,** *312* (5777), 1168-1171.

3. Choi, K. Y.; Liu, G.; Lee, S.; Chen, X., Theranostic nanoplatforms for simultaneous cancer imaging and therapy: current approaches and future perspectives. *Nanoscale* **2012,** *4* (2), 330-342.

4. Byrne, J. D.; Betancourt, T.; Brannon-Peppas, L., Active targeting schemes for nanoparticle systems in cancer therapeutics. *Advanced Drug Delivery Reviews* **2008,** *60* (15), 1615-1626.

5. Murelli, R. P.; Zhang, A. X.; Michel, J.; Jorgensen, W. L.; Spiegel, D. A., Chemical Control Over Immune Recognition: A Class of Antibody-Recruiting Small Molecules (ARMs) that Target Prostate Cancer. *Journal of the American Chemical Society* **2009,** *131* (47), 17090-17092.

6. Alkilany, A. M.; Boulos, S. P.; Lohse, S. E.; Thompson, L. B.; Murphy, C. J., Homing Peptide-Conjugated Gold Nanorods: The Effect of Amino Acid Sequence Display on Nanorod Uptake and Cellular Proliferation. *Bioconjugate Chemistry* **2014,** *25* (6), 1162-1171.

7. Choi, S.-H.; Kwon, I. C.; Hwang, K. Y.; Kim, I.-S.; Ahn, H. J., Small Heat Shock Protein as a Multifunctional Scaffold: Integrated Tumor Targeting and Caspase Imaging within a Single Cage. *Biomacromolecules* **2011,** *12* (8), 3099-3106.

8. Uchida, M.; Flenniken, M. L.; Allen, M.; Willits, D. A.; Crowley, B. E.; Brumfield, S.; Willis, A. F.; Jackiw, L.; Jutila, M.; Young, M. J.; Douglas, T., Targeting of cancer cells with ferrimagnetic ferritin cage nanoparticles. *J Am Chem Soc* **2006,** *128*.

9. Arteaga, C. L.; Sliwkowski, M. X.; Osborne, C. K.; Perez, E. A.; Puglisi, F.; Gianni, L., Treatment of HER2-positive breast cancer: current status and future perspectives. *Nat Rev Clin Oncol* **2012,** *9* (1), 16-32.

10. Tseng, Y.-J.; Chou, S.-W.; Shyue, J.-J.; Lin, S.-Y.; Hsiao, J.-K.; Chou, P.-T., A Versatile Theranostic Delivery Platform Integrating Magnetic Resonance Imaging/Computed Tomography, pH/cis-Diol Controlled Release, and Targeted Therapy. *ACS Nano* **2016,** *10* (6), 5809-5822.

11. Cho, K.; Wang, X.; Nie, S.; Chen, Z.; Shin, D. M., Therapeutic nanoparticles for drug delivery in cancer. *Clin Cancer Res* **2008,** *14*.

12. Kukowska-Latallo, J. F.; Candido, K. A.; Cao, Z.; Nigavekar, S. S.; Majoros, I. J.; Thomas, T. P.; Balogh, L. P.; Khan, M. K.; Baker, J. R., Nanoparticle Targeting of Anticancer Drug Improves Therapeutic Response in Animal Model of Human Epithelial Cancer. *Cancer Research* **2005,** *65* (12), 5317-5324.

13. Pandya, N. M.; Dhalla, N. S.; Santani, D. D., Angiogenesis—a new target for future therapy. *Vascular Pharmacology* **2006,** *44* (5), 265-274.

14. Jones, A.; Harris, A. L., New developments in angiogenesis: a major mechanism for tumor growth and target for therapy. *Cancer J Sci Am* **1998,** *4* (4), 209-217.

15. Kirpotin, D. B.; Drummond, D. C.; Shao, Y.; Shalaby, M. R.; Hong, K.; Nielsen, U. B.; Marks, J. D.; Benz, C. C.; Park, J. W., Antibody Targeting of Long-Circulating Lipidic Nanoparticles Does Not Increase Tumor Localization but Does Increase Internalization in Animal Models. *Cancer Research* **2006,** *66* (13), 6732-6740.

16. Kobayashi, T.; Ishida, T.; Okada, Y.; Ise, S.; Harashima, H.; Kiwada, H., Effect of transferrin receptor-targeted liposomal doxorubicin in P-glycoprotein-mediated drug resistant tumor cells. *International Journal of Pharmaceutics* **2007,** *329* (1–2), 94-102.

17. Iinuma, H.; Maruyama, K.; Okinaga, K.; Sasaki, K.; Sekine, T.; Ishida, O.; Ogiwara, N.; Johkura, K.; Yonemura, Y., Intracellular targeting therapy of cisplatin-encapsulated transferrin-polyethylene glycol liposome on peritoneal dissemination of gastric cancer. *International Journal of Cancer* **2002,** *99* (1), 130-137.

18. Drummond, D. C.; Hong, K.; Park, J. W.; Benz, C. C.; Kirpgtin, D. B., Liposome targeting to tumors using vitamin and growth factor receptors. *Vitamins & Hormones* **2000,** *60*, 285-332.

19. Atobe, K.; Ishida, T.; Ishida, E.; Hashimoto, K.; Kobayashi, H.; Yasuda, J.; Aoki, T.; Obata, K.-i.; Kikuchi, H.; Akita, H.; Asai, T.; Harashima, H.; Oku, N.; Kiwada, H., In Vitro Efficacy of a Sterically Stabilized Immunoliposomes Targeted to Membrane Type 1 Matrix Metalloproteinase (MT1-MMP). *Biological and Pharmaceutical Bulletin* **2007,** *30* (5), 972-978.

20. Chen, H.; Gao, J.; Lu, Y.; Kou, G.; Zhang, H.; Fan, L.; Sun, Z.; Guo, Y.; Zhong, Y., Preparation and characterization of PE38KDEL-loaded anti-HER2 nanoparticles for targeted cancer therapy. *Journal of Controlled Release* **2008,** *128* (3), 209-216.

21. Zhang, Y.; Zhang, J., Surface modification of monodisperse magnetite nanoparticles for improved intracellular uptake to breast cancer cells. *Journal of Colloid and Interface Science* **2005,** *283* (2), 352-357.

22. Leuschner, C.; Kumar, C. S.; Hansel, W.; Soboyejo, W.; Zhou, J.; Hormes, J., LHRH-conjugated Magnetic Iron Oxide Nanoparticles for Detection of Breast Cancer Metastases. *Breast Cancer Research and Treatment* **2006,** *99* (2), 163-176.

23. Adsorption, E. L.-b.-L., Assembly of multicomponent protein films by means of electrostatic layer-by-layer adsorption. *J. Am. Chem. Soc* **1995,** *117* (22), 6117-6123.

24. Ringeisen, B. R.; Callahan, J.; Wu, P. K.; Piqué, A.; Spargo, B.; McGill, R. A.; Bucaro, M.; Kim, H.; Bubb, D. M.; Chrisey, D. B., Novel Laser-Based Deposition of Active Protein Thin Films. *Langmuir*

2001, *17* (11), 3472-3479.

25. Hernandez-Perez, M. A.; Garapon, C.; Champeaux, C.; Shahgaldian, P.; Coleman, A.; Mugnier, J., Pulsed laser deposition of bovine serum albumin protein thin films. *Applied Surface Science* **2003,** *208–209*, 658-662.

26. Huang, Y.; Duan, X.; Wei, Q.; Lieber, C. M., Directed Assembly of One-Dimensional Nanostructures into Functional Networks. *Science* **2001,** *291* (5504), 630-633.

27. Patolsky, F.; Zheng, G.; Hayden, O.; Lakadamyali, M.; Zhuang, X.; Lieber, C. M., Electrical detection of single viruses. *Proceedings of the National Academy of Sciences of the United States of America* **2004,** *101* (39), 14017-14022.

28. Kong, J.; Franklin, N. R.; Zhou, C.; Chapline, M. G.; Peng, S.; Cho, K.; Dai, H., Nanotube Molecular Wires as Chemical Sensors. *Science* **2000,** *287* (5453), 622-625.

29. Yoo, P. J.; Nam, K. T.; Qi, J.; Lee, S.-K.; Park, J.; Belcher, A. M.; Hammond, P. T., Spontaneous assembly of viruses on multilayered polymer surfaces. *Nat Mater* **2006,** *5* (3), 234-240.

30. Nam, K. T.; Kim, D.-W.; Yoo, P. J.; Chiang, C.-Y.; Meethong, N.; Hammond, P. T.; Chiang, Y.-M.; Belcher, A. M., Virus-Enabled Synthesis and Assembly of Nanowires for Lithium Ion Battery Electrodes. *Science* **2006,** *312* (5775), 885-888.

31. Onda, M.; Ariga, K.; Kunitake, T., Activity and stability of glucose oxidase in molecular films assembled alternately with polyions. *Journal of Bioscience and Bioengineering* **1999,** *87* (1), 69-75.

32. Suci, P. A.; Klem, M. T.; Arce, F. T.; Douglas, T.; Young, M., Assembly of Multilayer Films Incorporating a Viral Protein Cage Architecture. *Langmuir* **2006,** *22* (21), 8891-8896.

33. Steinmetz, N. F.; Findlay, K. C.; Noel, T. R.; Parker, R.; Lomonossoff, G. R.; Evans, D. J., Layer-by-layer assembly of viral nanoparticles and polyelectrolytes: The film architecture is different for spheres versus rods. *Chembiochem* **2008,** *9* (10), 1662-1670.

34. Kang, Y. J.; Uchida, M.; Shin, H.-H.; Douglas, T.; Kang, S., Biomimetic FePt nanoparticle synthesis within Pyrococcus furiosus ferritins and their layer-by-layer formation. *Soft Matter* **2011,** *7* (23), 11078-11081.

35. Kang, S.; Suci, P. A.; Broomell, C. C.; Iwahori, K.; Kobayashi, M.; Yamashita, I.; Young, M.; Douglas, T., Janus-like Protein Cages. Spatially Controlled Dual-Functional Surface Modifications of Protein Cages. *Nano Lett.* **2009,** *9* (6), 2360-2366.

36. Steinmetz, N. F.; Bock, E.; Richter, R. P.; Spatz, J. P.; Lomonossoff, G. P.; Evans, D. J., Assembly of Multilayer Arrays of Viral Nanoparticles via Biospecific Recognition: A Quartz Crystal Microbalance with Dissipation Monitoring Study. *Biomacromolecules* **2008,** *9* (2), 456-462.

37. Steinmetz, N. F.; Calder, G.; Lomonossoff, G. P.; Evans, D. J., Plant Viral Capsids as Nanobuilding Blocks: Construction of Arrays on Solid Supports. *Langmuir* **2006,** *22* (24), 10032-10037.

38. Suci, P.; Klem, M. T.; Young, M.; Douglas, T., Signal ampflication using nanoplatform cluster formation. *Soft Matter* **2008,** *4* (12), 2519-2523.

39. Steinmetz, N. F.; Evans, D. J., Utilisation of plant viruses in bionanotechnology. *Organic & Biomolecular Chemistry* **2007,** *5* (18), 2891-2902.

40. Farokhzad, O. C.; Langer, R., Impact of Nanotechnology on Drug Delivery. *ACS Nano* **2009,** *3* (1), 16-20.

41. Brigger, I.; Dubernet, C.; Couvreur, P., Nanoparticles in cancer therapy and diagnosis. *Advanced Drug Delivery Reviews* **2002,** *54* (5), 631-651.

42. Aime, S.; Frullano, L.; Geninatti Crich, S., Compartmentalization of a Gadolinium Complex in the Apoferritin Cavity: A Route To Obtain High Relaxivity Contrast Agents for Magnetic Resonance Imaging. *Angewandte Chemie International Edition* **2002,** *41* (6), 1017-1019.

43. Kwon, C.; Kang, Y. J.; Jeon, S.; Jung, S.; Hong, S. Y.; Kang, S., Development of Protein-Cage-Based Delivery Nanoplatforms by Polyvalently Displaying β-Cyclodextrins on the Surface of Ferritins Through Copper(I)-Catalyzed Azide/Alkyne Cycloaddition. *Macromolecular Bioscience* **2012,** *12* (11), 1452-1458.

44. Han, J.-A.; Kang, Y. J.; Shin, C.; Ra, J.-S.; Shin, H.-H.; Hong, S. Y.; Do, Y.; Kang, S., Ferritin protein cage nanoparticles as versatile antigen delivery nanoplatforms for dendritic cell (DC)-based vaccine development. *Nanomedicine: Nanotechnology, Biology and Medicine* **2014,** *10* (3), 561-569.

45. Kang, Y. J.; Park, D. C.; Shin, H.-H.; Park, J.; Kang, S., Incorporation of Thrombin Cleavage Peptide into a Protein Cage for Constructing a Protease-Responsive Multifunctional Delivery Nanoplatform. *Biomacromolecules* **2012,** *13* (12), 4057-4064.

46. Toita, R.; Murata, M.; Tabata, S.; Abe, K.; Narahara, S.; Piao, J. S.; Kang, J.-H.; Hashizume, M., Development of Human Hepatocellular Carcinoma Cell-Targeted Protein Cages. *Bioconjugate Chemistry* **2012,** *23* (7), 1494-1501.

47. Toita, R.; Murata, M.; Abe, K.; Narahara, S.; Piao, J. S.; Kang, J.-H.; Hashizume, M., A nanocarrier based on a genetically engineered protein cage to deliver doxorubicin to human hepatocellular carcinoma cells. *Chemical Communications* **2013,** *49* (67), 7442-7444.

48. Flenniken, M. L.; Liepold, L. O.; Crowley, B. E.; Willits, D. A.; Young, M. J.; Douglas, T., Selective attachment and release of a chemotherapeutic agent from the interior of a protein cage architecture. *Chemical Communications* **2005,** (4), 447-449.

49. Flenniken, M. L.; Willits, D. A.; Brumfield, S.; Young, M. J.; Douglas, T., The Small Heat Shock Protein Cage from Methanococcus jannaschii Is a Versatile Nanoscale Platform for Genetic and Chemical Modification. *Nano Letters* **2003,** *3* (11), 1573-1576.

50. Yildiz, I.; Shukla, S.; Steinmetz, N. F., Applications of viral nanoparticles in medicine. *Current*

Opinion in Biotechnology **2011,** *22* (6), 901-908.

51. Patterson, D. P.; Rynda-Apple, A.; Harmsen, A. L.; Harmsen, A. G.; Douglas, T., Biomimetic Antigenic Nanoparticles Elicit Controlled Protective Immune Response to Influenza. *ACS nano* **2013,** *7* (4), 3036-3044.

52. Pokorski, J. K.; Hovlid, M. L.; Finn, M. G., Cell Targeting with Hybrid Qβ Virus-Like Particles Displaying Epidermal Growth Factor. *ChemBioChem* **2011,** *12* (16), 2441-2447.

53. Li, K.; Chen, Y.; Li, S.; Nguyen, H. G.; Niu, Z.; You, S.; Mello, C. M.; Lu, X.; Wang, Q., Chemical Modification of M13 Bacteriophage and Its Application in Cancer Cell Imaging. *Bioconjugate Chemistry* **2010,** *21* (7), 1369-1377.

54. Zeng, Q.; Wen, H.; Wen, Q.; Chen, X.; Wang, Y.; Xuan, W.; Liang, J.; Wan, S., Cucumber mosaic virus as drug delivery vehicle for doxorubicin. *Biomaterials* **2013,** *34* (19), 4632-4642.

55. Min, J.; Moon, H.; Yang, H. J.; Shin, H.-H.; Hong, S. Y.; Kang, S., Development of P22 Viral Capsid Nanocomposites as Anti-Cancer Drug, Bortezomib (BTZ), Delivery Nanoplatforms. *Macromolecular Bioscience* **2014,** *14* (4), 557-564.

56. Bruckman, M. A.; Jiang, K.; Simpson, E. J.; Randolph, L. N.; Luyt, L. G.; Yu, X.; Steinmetz, N. F., Dual-Modal Magnetic Resonance and Fluorescence Imaging of Atherosclerotic Plaques in Vivo Using VCAM-1 Targeted Tobacco Mosaic Virus. *Nano Letters* **2014,** *14* (3), 1551-1558.

57. Stephanopoulos, N.; Tong, G. J.; Hsiao, S. C.; Francis, M. B., Dual-Surface Modified Virus Capsids for Targeted Delivery of Photodynamic Agents to Cancer Cells. *ACS Nano* **2010,** *4* (10), 6014-6020.

58. Li, F.; Wang, Q., Fabrication of Nanoarchitectures Templated by Virus-Based Nanoparticles: Strategies and Applications. *Small* **2014,** *10* (2), 230-245.

59. Destito, G.; Yeh, R.; Rae, C. S.; Finn, M. G.; Manchester, M., Folic Acid-Mediated Targeting of Cowpea Mosaic Virus Particles to Tumor Cells. *Chemistry & Biology* **2007,** *14* (10), 1152-1162.

60. Min, J.; Jung, H.; Shin, H.-H.; Cho, G.; Cho, H.; Kang, S., Implementation of P22 Viral Capsids As Intravascular Magnetic Resonance T1 Contrast Conjugates via Site-Selective Attachment of Gd(III)-Chelating Agents. *Biomacromolecules* **2013,** *14* (7), 2332-2339.

61. Banerjee, D.; Liu, A. P.; Voss, N. R.; Schmid, S. L.; Finn, M. G., Multivalent Display and Receptor-Mediated Endocytosis of Transferrin on Virus-Like Particles. *ChemBioChem* **2010,** *11* (9), 1273-1279.

62. Farkas, M. E.; Aanei, I. L.; Behrens, C. R.; Tong, G. J.; Murphy, S. T.; O'Neil, J. P.; Francis, M. B., PET Imaging and Biodistribution of Chemically Modified Bacteriophage MS2. *Molecular Pharmaceutics* **2013,** *10* (1), 69-76.

63. Sumer, B.; Gao, J., Theranostic nanomedicine for cancer. *Nanomedicine* **2008,** *3* (2), 137-140.

64. Lucon, J.; Qazi, S.; Uchida, M.; Bedwell, G. J.; LaFrance, B.; Prevelige, P. E.; Douglas, T., Use of the interior cavity of the P22 capsid for site-specific initiation of atom-transfer radical polymerization

with high-density cargo loading. *Nat Chem* **2012,** *4* (10), 781-788.

65. MaHam, A.; Tang, Z.; Wu, H.; Wang, J.; Lin, Y., Protein-Based Nanomedicine Platforms for Drug Delivery. *Small* **2009,** *5* (15), 1706-1721.

66. Uchida, M.; Kang, S.; Reichhardt, C.; Harlen, K.; Douglas, T., The ferritin superfamily: Supramolecular templates for materials synthesis. *Biochimica et Biophysica Acta (BBA) - General Subjects* **2010,** *1800* (8), 834-845.

67. Campan, M.; Lionetti, V.; Aquaro, G. D.; Forini, F.; Matteucci, M.; Vannucci, L.; Chiuppesi, F.; Di Cristofano, C.; Faggioni, M.; Maioli, M.; Barile, L.; Messina, E.; Lombardi, M.; Pucci, A.; Pistello, M.; Recchia, F. A., Ferritin as a reporter gene for in vivo tracking of stem cells by 1.5-T cardiac MRI in a rat model of myocardial infarction. *American Journal of Physiology - Heart and Circulatory Physiology* **2011,** *300* (6), H2238-H2250.

68. Cohen, B.; Dafni, H.; Meir, G.; Harmelin, A.; Neeman, M., Ferritin as an Endogenous MRI Reporter for Noninvasive Imaging of Gene Expression in C6 Glioma Tumors. *Neoplasia* **2005,** *7* (2), 109-117.

69. Grabill, C.; Silva, A. C.; Smith, S. S.; Koretsky, A. P.; Rouault, T. A., MRI detection of ferritin iron overload and associated neuronal pathology in iron regulatory protein-2 knockout mice. *Brain Research* **2003,** *971* (1), 95-106.

70. Bartzokis, G.; Tishler, T. A., MRI evaluation of basal ganglia ferritin iron and neurotoxicity in Alzheimer's and Huntingon's disease. *Cell Mol Biol (Noisy-le-grand)* **2000,** *46* (4), 821-833.

71. Gossuin, Y.; Muller, R. N.; Gillis, P., Relaxation induced by ferritin: a better understanding for an improved MRI iron quantification. *NMR in Biomedicine* **2004,** *17* (7), 427-432.

72. Arap, W.; Pasqualini, R.; Ruoslahti, E., Cancer Treatment by Targeted Drug Delivery to Tumor Vasculature in a Mouse Model. *Science* **1998,** *279* (5349), 377-380.

73. Uchida, M.; Willits, D. A.; Muller, K.; Willis, A. F.; Jackiw, L.; Jutila, M.; Young, M. J.; Porter, A. E.; Douglas, T., Intracellular Distribution of Macrophage Targeting Ferritin–Iron Oxide Nanocomposite. *Advanced Materials* **2009,** *21* (4), 458-462.

74. Kitagawa, T.; Kosuge, H.; Uchida, M.; Dua, M. M.; Iida, Y.; Dalman, R. L.; Douglas, T.; McConnell, M. V., RGD-Conjugated Human Ferritin Nanoparticles for Imaging Vascular Inflammation and Angiogenesis in Experimental Carotid and Aortic Disease. *Molecular Imaging and Biology* **2012,** *14* (3), 315-324.

75. Normanno, N.; De Luca, A.; Bianco, C.; Strizzi, L.; Mancino, M.; Maiello, M. R.; Carotenuto, A.; De Feo, G.; Caponigro, F.; Salomon, D. S., Epidermal growth factor receptor (EGFR) signaling in cancer. *Gene* **2006,** *366* (1), 2-16.

76. Uchida, M.; Morris, D. S.; Kang, S.; Jolley, C. C.; Lucon, J.; Liepold, L. O.; LaFrance, B.; Prevelige, P. E.; Douglas, T., Site-Directed Coordination Chemistry with P22 Virus-like Particles. *Langmuir* **2012,**

28 (4), 1998-2006.

77. Kang, H. J.; Kang, Y. J.; Lee, Y.-M.; Shin, H.-H.; Chung, S. J.; Kang, S., Developing an antibody-binding protein cage as a molecular recognition drug modular nanoplatform. *Biomaterials* **2012,** *33* (21), 5423-5430.

78. Kobayashi, K.; Ishii, N.; Sasabe, H.; Knoll, W., Monomolecular Layer Formation of Ferritin Molecules on an Amphiphilic Cyclodextrin Derivative at the Air/Water Interface. *Bioscience, Biotechnology, and Biochemistry* **2001,** *65* (1), 176-179.

79. Kim, K. K.; Kim, R.; Kim, S.-H., Crystal structure of a small heat-shock protein. *Nature* **1998,** *394* (6693), 595-599.

80. Kim, K. K.; Yokota, H.; Santoso, S.; Lerner, D.; Kim, R.; Kim, S.-H., Purification, Crystallization, and Preliminary X-Ray Crystallographic Data Analysis of Small Heat Shock Protein Homolog fromMethanococcus jannaschii,a Hyperthermophile. *Journal of Structural Biology* **1998,** *121* (1), 76-80.

81. Kim, R.; Kim, K. K.; Yokota, H.; Kim, S.-H., Small heat shock protein of Methanococcus jannaschii, a hyperthermophile. *Proceedings of the National Academy of Sciences* **1998,** *95* (16), 9129-9133.

82. Flenniken, M. L.; Willits, D. A.; Harmsen, A. L.; Liepold, L. O.; Harmsen, A. G.; Young, M. J.; Douglas, T., Melanoma and Lymphocyte Cell-Specific Targeting Incorporated into a Heat Shock Protein Cage Architecture. *Chemistry & Biology* **2006,** *13* (2), 161-170.

83. Fogal, V.; Zhang, L.; Krajewski, S.; Ruoslahti, E., Mitochondrial/Cell-Surface Protein p32/gC1qR as a Molecular Target in Tumor Cells and Tumor Stroma. *Cancer Research* **2008,** *68* (17), 7210-7218.

84. Laakkonen, P.; Porkka, K.; Hoffman, J.; Ruoslahti, E., A tumor-homing peptide with a lymphatic vessel-related targeting specificity. *Nat Med* **2002,** *8*, 751-755.

85. Lo, A.; Lin, C.-T.; Wu, H.-C., Hepatocellular carcinoma cell-specific peptide ligand for targeted drug delivery. *Molecular Cancer Therapeutics* **2008,** *7* (3), 579-589.

86. Murata, M.; Narahara, S.; Umezaki, K.; Toita, R.; Tabata, S.; Piao, J. S.; Abe, K.; Kang, J.-H.; Ohuchida, K.; Cui, L., Liver cell specific targeting by the preS1 domain of hepatitis B virus surface antigen displayed on protein nanocages. *Int J Nanomedicine* **2012,** *7*, 4353-4362.

87. Schoonen, L.; van Hest, J. C. M., Functionalization of protein-based nanocages for drug delivery applications. *Nanoscale* **2014,** *6* (13), 7124-7141.

88. Ma, Y.; Nolte, R. J. M.; Cornelissen, J. J. L. M., Virus-based nanocarriers for drug delivery. *Advanced Drug Delivery Reviews* **2012,** *64* (9), 811-825.

89. Lin, T.; Chen, Z.; Usha, R.; Stauffacher, C. V.; Dai, J.-B.; Schmidt, T.; Johnson, J. E., The Refined Crystal Structure of Cowpea Mosaic Virus at 2.8 Å Resolution. *Virology* **1999,** *265* (1), 20-34.

90. Gillitzer, E.; Suci, P.; Young, M.; Douglas, T., Controlled Ligand Display on a Symmetrical Protein-

Cage Architecture Through Mixed Assembly. *Small* **2006,** *2* (8-9), 962-966.

91. Suci, P. A.; Varpness, Z.; Gillitzer, E.; Douglas, T.; Young, M., Targeting and Photodynamic Killing of a Microbial Pathogen Using Protein Cage Architectures Functionalized with a Photosensitizer. *Langmuir* **2007,** *23* (24), 12280-12286.

92. Brasch, M.; de la Escosura, A.; Ma, Y.; Uetrecht, C.; Heck, A. J. R.; Torres, T.; Cornelissen, J. J. L. M., Encapsulation of Phthalocyanine Supramolecular Stacks into Virus-like Particles. *Journal of the American Chemical Society* **2011,** *133* (18), 6878-6881.

93. Rhee, J.-K.; Hovlid, M.; Fiedler, J. D.; Brown, S. D.; Manzenrieder, F.; Kitagishi, H.; Nycholat, C.; Paulson, J. C.; Finn, M. G., Colorful Virus-Like Particles: Fluorescent Protein Packaging by the Qβ Capsid. *Biomacromolecules* **2011,** *12* (11), 3977-3981.

94. Hovlid, M. L.; Lau, J. L.; Breitenkamp, K.; Higginson, C. J.; Laufer, B.; Manchester, M.; Finn, M. G., Encapsidated Atom-Transfer Radical Polymerization in Qβ Virus-like Nanoparticles. *ACS Nano* **2014,** *8* (8), 8003-8014.

95. Pokorski, J. K.; Breitenkamp, K.; Finn, M. G., Functional Virus-Based Polymer-Protein Nanoparticles by Atom Transfer Radical Polymerization. *Journal of the American Chemical Society* **2011,** *133* (24), 9242-9245.

96. Patterson, D. P.; Schwarz, B.; El-Boubbou, K.; van der Oost, J.; Prevelige, P. E.; Douglas, T., Virus-like particle nanoreactors: programmed encapsulation of the thermostable CelB glycosidase inside the P22 capsid. *Soft Matter* **2012,** *8* (39), 10158-10166.

97. O'Neil, A.; Prevelige, P. E.; Basu, G.; Douglas, T., Coconfinement of Fluorescent Proteins: Spatially Enforced Communication of GFP and mCherry Encapsulated within the P22 Capsid. *Biomacromolecules* **2012,** *13* (12), 3902-3907.

98. Kang, S.; Prevelige Jr, P. E., Domain Study of Bacteriophage P22 Coat Protein and Characterization of the Capsid Lattice Transformation by Hydrogen/Deuterium Exchange. *Journal of Molecular Biology* **2005,** *347* (5), 935-948.

99. Patterson, D. P.; Schwarz, B.; Waters, R. S.; Gedeon, T.; Douglas, T., Encapsulation of an Enzyme Cascade within the Bacteriophage P22 Virus-Like Particle. *ACS Chemical Biology* **2014,** *9* (2), 359-365.

100. Kang, S.; Uchida, M.; O'Neil, A.; Li, R.; Prevelige, P. E.; Douglas, T., Implementation of P22 Viral Capsids as Nanoplatforms. *Biomacromolecules* **2010,** *11* (10), 2804-2809.

101. Jordan, P. C.; Patterson, D. P.; Saboda, K. N.; Edwards, E. J.; Miettinen, H. M.; Basu, G.; Thielges, M. C.; Douglas, T., Self-assembling biomolecular catalysts for hydrogen production. *Nat Chem* **2016,** *8* (2), 179-185.

102. Qazi, S.; Liepold, L. O.; Abedin, M. J.; Johnson, B.; Prevelige, P.; Frank, J. A.; Douglas, T., P22

viral capsids as nanocomposite high-relaxivity MRI contrast agents. *Molecular pharmaceutics* **2013,** *10* (1), 11-17.

103. Sutter, M.; Boehringer, D.; Gutmann, S.; Gunther, S.; Prangishvili, D.; Loessner, M. J.; Stetter, K. O.; Weber-Ban, E.; Ban, N., Structural basis of enzyme encapsulation into a bacterial nanocompartment. *Nat Struct Mol Biol* **2008,** *15* (9), 939-947.

104. Rahmanpour, R.; Bugg, T. D. H., Assembly in vitro of Rhodococcus jostii RHA1 encapsulin and peroxidase DypB to form a nanocompartment. *FEBS Journal* **2013,** *280* (9), 2097-2104.

105. Rurup, W. F.; Snijder, J.; Koay, M. S. T.; Heck, A. J. R.; Cornelissen, J. J. L. M., Self-Sorting of Foreign Proteins in a Bacterial Nanocompartment. *Journal of the American Chemical Society* **2014,** *136* (10), 3828-3832.

106. Tamura, A.; Fukutani, Y.; Takami, T.; Fujii, M.; Nakaguchi, Y.; Murakami, Y.; Noguchi, K.; Yohda, M.; Odaka, M., Packaging guest proteins into the encapsulin nanocompartment from Rhodococcus erythropolis N771. *Biotechnology and bioengineering* **2015,** *112* (1), 13-20.

107. Giessen, T. W.; Silver, P. A., Converting a Natural Protein Compartment into a Nanofactory for the Size-Constrained Synthesis of Antimicrobial Silver Nanoparticles. *ACS Synthetic Biology* **2016,** *5* (12), 1497-1504.

108. Löfblom, J.; Feldwisch, J.; Tolmachev, V.; Carlsson, J.; Ståhl, S.; Frejd, F. Y., Affibody molecules: Engineered proteins for therapeutic, diagnostic and biotechnological applications. *FEBS Letters* **2010,** *584* (12), 2670-2680.

109. Betzig, E.; Patterson, G. H.; Sougrat, R.; Lindwasser, O. W.; Olenych, S.; Bonifacino, J. S.; Davidson, M. W.; Lippincott-Schwartz, J.; Hess, H. F., Imaging Intracellular Fluorescent Proteins at Nanometer Resolution. *Science* **2006,** *313* (5793), 1642-1645.

110. Nagai, T.; Ibata, K.; Park, E. S.; Kubota, M.; Mikoshiba, K.; Miyawaki, A., A variant of yellow fluorescent protein with fast and efficient maturation for cell-biological applications. *Nat Biotech* **2002,** *20* (1), 87-90.

111. Zakeri, B.; Fierer, J. O.; Celik, E.; Chittock, E. C.; Schwarz-Linek, U.; Moy, V. T.; Howarth, M., Peptide tag forming a rapid covalent bond to a protein, through engineering a bacterial adhesin. *Proceedings of the National Academy of Sciences* **2012,** *109* (12), E690-E697.

112. Schoene, C.; Fierer, J. O.; Bennett, S. P.; Howarth, M., SpyTag/SpyCatcher cyclization confers resilience to boiling on a mesophilic enzyme. *Angewandte Chemie International Edition* **2014,** *53* (24), 6101-6104.

113. Li, L.; Fierer, J. O.; Rapoport, T. A.; Howarth, M., Structural Analysis and Optimization of the Covalent Association between SpyCatcher and a Peptide Tag. *Journal of Molecular Biology* **2014,** *426* (2), 309-317.

114. Veggiani, G.; Zakeri, B.; Howarth, M., Superglue from bacteria: unbreakable bridges for protein nanotechnology. *Trends in Biotechnology* **2014,** *32* (10), 506-512.

115. Peer, D.; Karp, J. M.; Hong, S.; Farokhzad, O. C.; Margalit, R.; Langer, R., Nanocarriers as an emerging platform for cancer therapy. *Nat Nano* **2007,** *2* (12), 751-760.

116. Uchida, M.; Terashima, M.; Cunningham, C. H.; Suzuki, Y.; Willits, D. A.; Willis, A. F.; Yang, P. C.; Tsao, P. S.; McConnell, M. V.; Young, M. J.; Douglas, T., A human ferritin iron oxide nano-composite magnetic resonance contrast agent. *Magnetic Resonance in Medicine* **2008,** *60* (5), 1073-1081.

117. Moon, H.; Kim, W. G.; Lim, S.; Kang, Y. J.; Shin, H.-H.; Ko, H.; Hong, S. Y.; Kang, S., Fabrication of uniform layer-by-layer assemblies with complementary protein cage nanobuilding blocks via simple His-tag/metal recognition. *Journal of Materials Chemistry B* **2013,** *1* (35), 4504-4510.

118. Willner, D.; Trail, P. A.; Hofstead, S. J.; King, H. D.; Lasch, S. J.; Braslawsky, G. R.; Greenfield, R. S.; Kaneko, T.; Firestone, R. A., (6-Maleimidocaproyl)hydrazone of doxorubicin--a new derivative for the preparation of immunoconjugates of doxorubicin. *Bioconjugate chemistry* **1993,** *4* (6), 521-527.

119. Enterina, J. R.; Wu, L.; Campbell, R. E., Emerging fluorescent protein technologies. *Current Opinion in Chemical Biology* **2015,** *27*, 10-17.

120. Wahlfors, J.; Loimas, S.; Pasanen, T.; Hakkarainen, T., Green fluorescent protein (GFP) fusion constructs in gene therapy research. *Histochemistry and Cell Biology* **2001,** *115* (1), 59-65.

121. Yu, Z.; Schmaltz, R. M.; Bozeman, T. C.; Paul, R.; Rishel, M. J.; Tsosie, K. S.; Hecht, S. M., Selective Tumor Cell Targeting by the Disaccharide Moiety of Bleomycin. *Journal of the American Chemical Society* **2013,** *135* (8), 2883-2886.

122. Lee, J.; Song, E. K.; Bae, Y.; Min, J.; Rhee, H.-W.; Park, T. J.; Kim, M.; Kang, S., An enhanced ascorbate peroxidase 2/antibody-binding domain fusion protein (APEX2–ABD) as a recombinant target-specific signal amplifier. *Chemical Communications* **2015,** *51* (54), 10945-10948.

123. Min, J.; Song, E. K.; Kim, H.; Kim, K. T.; Park, T. J.; Kang, S., A Recombinant Secondary Antibody Mimic as a Target-specific Signal Amplifier and an Antibody Immobilizer in Immunoassays. *Scientific reports* **2016,** *6*.

124. Rabhi-Essafi, I.; Sadok, A.; Khalaf, N.; Fathallah, D. M., A strategy for high-level expression of soluble and functional human interferon α as a GST-fusion protein in E. coli. *Protein Engineering Design and Selection* **2007,** *20* (5), 201-209.

125. Moulder, S. L.; Yakes, F. M.; Muthuswamy, S. K.; Bianco, R.; Simpson, J. F.; Arteaga, C. L., Epidermal growth factor receptor (HER1) tyrosine kinase inhibitor ZD1839 (Iressa) inhibits HER2/neu (erbB2)-overexpressing breast cancer cells in vitro and in vivo. *Cancer research* **2001,** *61* (24), 8887-8895.

126. Subik, K.; Lee, J.-F.; Baxter, L.; Strzepek, T.; Costello, D.; Crowley, P.; Xing, L.; Hung, M.-C.; Bonfiglio, T.; Hicks, D. G., The expression patterns of ER, PR, HER2, CK5/6, EGFR, Ki-67 and AR by immunohistochemical analysis in breast cancer cell lines. *Breast cancer: basic and clinical research* **2010,** *4*, 35.

127. Lyakhov, I.; Zielinski, R.; Kuban, M.; Kramer-Marek, G.; Fisher, R.; Chertov, O.; Bindu, L.; Capala, J., HER2- and EGFR-Specific Affiprobes: Novel Recombinant Optical Probes for Cell Imaging. *ChemBioChem* **2010,** *11* (3), 345-350.

128. Thorn, C. F.; Oshiro, C.; Marsh, S.; Hernandez-Boussard, T.; McLeod, H.; Klein, T. E.; Altman, R. B., Doxorubicin pathways: pharmacodynamics and adverse effects. *Pharmacogenetics and Genomics* **2011,** *21* (7), 440-446.

129. Müller, I.; Jenner, A.; Bruchelt, G.; Niethammer, D.; Halliwell, B., Effect of Concentration on the Cytotoxic Mechanism of Doxorubicin—Apoptosis and Oxidative DNA Damage. *Biochemical and Biophysical Research Communications* **1997,** *230* (2), 254-257.

130. Wu, L.-Q.; Payne, G. F., Biofabrication: using biological materials and biocatalysts to construct nanostructured assemblies. *Trends in Biotechnology* **2004,** *22* (11), 593-599.

131. Gudiksen, M. S.; Lauhon, L. J.; Wang, J.; Smith, D. C.; Lieber, C. M., Growth of nanowire superlattice structures for nanoscale photonics and electronics. *Nature* **2002,** *415* (6872), 617-620.

132. Lowe, C. R., Nanobiotechnology: the fabrication and applications of chemical and biological nanostructures. *Current Opinion in Structural Biology* **2000,** *10* (4), 428-434.

133. Yoo, P. J.; Nam, K. T.; Belcher, A. M.; Hammond, P. T., Solvent-Assisted Patterning of Polyelectrolyte Multilayers and Selective Deposition of Virus Assemblies. *Nano Letters* **2008,** *8* (4), 1081-1089.

134. Udit, A. K.; Brown, S.; Baksh, M. M.; Finn, M. G., Immobilization of bacteriophage Qβ on metal-derivatized surfaces via polyvalent display of hexahistidine tags. *Journal of Inorganic Biochemistry* **2008,** *102* (12), 2142-2146.

135. Franken, K. L. M. C.; Hiemstra, H. S.; van Meijgaarden, K. E.; Subronto, Y.; den Hartigh, J.; Ottenhoff, T. H. M.; Drijfhout, J. W., Purification of His-Tagged Proteins by Immobilized Chelate Affinity Chromatography: The Benefits from the Use of Organic Solvent. *Protein Expression and Purification* **2000,** *18* (1), 95-99.

136. Wörsdörfer, B.; Woycechowsky, K. J.; Hilvert, D., Directed Evolution of a Protein Container. *Science* **2011,** *331* (6017), 589-592.

137. Wörsdörfer, B.; Pianowski, Z.; Hilvert, D., Efficient in Vitro Encapsulation of Protein Cargo by an Engineered Protein Container. *Journal of the American Chemical Society* **2011,** *134* (2), 909-911.

138. Seebeck, F. P.; Woycechowsky, K. J.; Zhuang, W.; Rabe, J. P.; Hilvert, D., A Simple Tagging

System for Protein Encapsulation. *Journal of the American Chemical Society* **2006,** *128* (14), 4516-4517.

139. Schmid, E. L.; Keller, T. A.; Dienes, Z.; Vogel, H., Reversible Oriented Surface Immobilization of Functional Proteins on Oxide Surfaces. *Analytical Chemistry* **1997,** *69* (11), 1979-1985.

140. Kang, S.; Lander, G. C.; Johnson, J. E.; Prevelige, P. E., Development of Bacteriophage P22 as a Platform for Molecular Display: Genetic and Chemical Modifications of the Procapsid Exterior Surface. *ChemBioChem* **2008,** *9* (4), 514-518.

141. He, M.; Stoevesandt, O.; Palmer, E. A.; Khan, F.; Ericsson, O.; Taussig, M. J., Printing protein arrays from DNA arrays. *Nature methods* **2008,** *5* (2), 175-177.

142. Zhang, X.; Meining, W.; Fischer, M.; Bacher, A.; Ladenstein, R., X-ray structure analysis and crystallographic refinement of lumazine synthase from the hyperthermophile Aquifex aeolicus at 1.6 Å resolution: determinants of thermostability revealed from structural comparisons. *Journal of Molecular Biology* **2001,** *306* (5), 1099-1114.

143. Khan, F.; He, M.; Taussig, M. J., Double-Hexahistidine Tag with High-Affinity Binding for Protein Immobilization, Purification, and Detection on Ni−Nitrilotriacetic Acid Surfaces. *Analytical Chemistry* **2006,** *78* (9), 3072-3079.

144. Höök, F.; Rodahl, M.; Brzezinski, P.; Kasemo, B., Energy Dissipation Kinetics for Protein and Antibody−Antigen Adsorption under Shear Oscillation on a Quartz Crystal Microbalance. *Langmuir* **1998,** *14* (4), 729-734.

145. Hayashi, T.; Sano, K.-I.; Shiba, K.; Kumashiro, Y.; Iwahori, K.; Yamashita, I.; Hara, M., Mechanism Underlying Specificity of Proteins Targeting Inorganic Materials. *Nano Letters* **2006,** *6* (3), 515-519.

Acknowledgements

지난 5 년 동안 느리고 부족한 저를 믿어주시고 이끌어주신 교수님께 감사의 말씀을 드립니다. 실험실 생활을 하는 동안 힘든 일들도 있었지만 돌이켜보면 늘 저에게 도움이 되는 일이었던 것 같습니다.

바쁘신 일정에도 학위 논문 심사에 시간을 내어주신 박태주 교수님, 홍성유 교수님, 이현우 교수님 진심으로 감사드립니다. 대전에서도 기꺼이 참석해 주신 김문일 박사님 정말 감사드립니다. 교수님들의 조언이 저에게 많은 응원이 되었습니다.

어떤 일이든 제 입장에서 생각해주시는 부모님, 늦은 나이에 학업을 시작할 때도 응원부터 해주셔서 든든했습니다. 이제는 친구 같은 내 동생 효정아, 우리 앞으로 같은 길을 걸어가자. 너를 생각하면 힘이 난다! 작은 일에도 기쁘게 칭찬해 주시고 크게 사랑해주는 가족들이 있었기에 잘 견딜 수 있었습니다. 고맙습니다. 늘 사랑합니다.

대학원 생활을 하면서 멋진 동료들을 알게 되어 행복했습니다. 친구처럼 늘 따뜻하게 조언해주신 현희 언니, 언니 덕분에 실험실이 편안했던 것 같아요! 감사합니다. 어디를 가든 언니의 따뜻함을 늘 잊지 않겠습니다. 내 짝 은경이, 너 없었다면 내 대학원 생활이 힘들었을 거야. 항상 편하게 대해주고 챙겨줘서 많이 의지했던 것 같아! 고마워~ 힘내고 건강 잘 챙겨! 늘 응원할게! 이제 두 아이의 엄마가 된 영지야, 친구지만 너를 통해 많이 배운 것 같아! 아프지 말고 잘 지내! 생각이 잘 통하는 준선이... 마음에 있는 이야기를 털어놓을 수 있어서 힘든 내 실험실 생활이 오히려 즐겁게 지나갔던 것 같아. 항상 고마워. 하는 일 늘 잘되길 바라. 예의 바른 지수, 지금까지 안부 인사해주고 고마워! 너의 귀엽고, 긍정적인 생각 덕분에 실험실에서 재미있었어.

윤지야, 지금은 힘들겠지만 이 모든 일이 너에게 반드시 도움이 될 것이라는 생각을 잊지 말고, 최선을 다하길... 긍정적인 생각으로 연구해서 좋은 결과 있기를 바란다. 가끔 애교로 어이없는 웃음 유발한 한솔이, 내 눈치 보느라 그 동안 고생많았다. 랩 장 봉서, 후배들 잘 챙겨서 즐거운 실험실 생활하길! 혁준, 성국... 모두 목표한 대로 좋은 결과가 있기를 바랍니다. 서로의 입장을 생각하고 배려해 일한다면 더 많은 것을 얻게 될 것이라고 생각합니다.

다 언급하지는 못했지만 저를 도와주신 모든 분들께 이 기회를 통해 정말 감사의 인사를 전합니다.

부족하지만 논문을 완성할 수 있도록 힘써주신 교수님께 다시 한번 감사드립니다.

APPENDIX A

Analytical techniques

Electrospray ionization-time of flight mass spectrometry (ESI-TOF Mass spectrometry)

- Principle of electrospray ionization

Since the electrospray ionization method and mass spectrometry have been developed, it has been widely used for the analysis of biopolymers and synthetic polymers including proteins, DNAs. The solution containing the substance to be analyzed is flowed through a capillary with a high potential. When the solution exits through the capillary end, the solution creates a mist of ionic droplets with a high charge due to the high electric potential effect. More specifically, the solution-phase cations accumulate on the surface and are dragged toward the mass spectrometry to form a 'Taylor cone'. When the electrostatic force generated by the accumulated cations increased above the surface tension, ion droplets are ejected through the capillary end. This ion droplet travels along the electric field and potential and pressure gradient to the entrance of the mass spectrometer, where the solvent in the ionic droplet evaporates and secondary fissions (Coulomb explosion) results in smaller droplets that ultimately leave only monomolecular ions.[1-3]

In order to help evaporate the solvent in the ionic droplets, the nebulizer gas is flowed together. At this time, the ejection rate of the ion spray, the composition of the solvent, and the intensity of the electric field applied to the capillary are the main factors determining the nebulizer gas and rate. The ejection speed of the ion spray determines the required amount of material to be analyzed, and is divided into micro-spray or nano-spray depending on the ejection speed. When mass spectrometric analysis of minute amounts of biomolecules, the ejection rate is an important consideration, but it is not so important when analyzing large amount of synthetic polymers.[4]

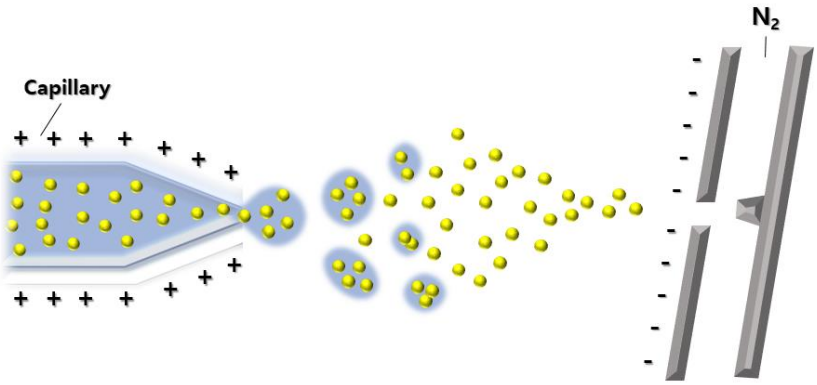

Figure A1. Scheme of ion droplet formation and principle of electrospray ionization. The solution containing the substance to be analyzed is flowed through a capillary with a high potential.

- Solution of electrospray

In general, the decision of solvent used in electrospray is determined by factors such as polarity, viscosity, surface tension, and electrical conductivity. Particularly, the selection of the solvent used for the polymer electrospray is largely dependent on two factors. Firstly, the solvent should be a solvent capable of dissolving the polymer well and the electric spray must be stable. When the solvent contains a protonic atom such as oxygen or nitrogen, or a double bond or a benzene ring, it may be relatively easily used as a solvent by adding a small amount of acid to a protic solvent such as water, methanol or AcCN.

- Mass analyzer: Time-of-flight (TOF)

Time-of-flight mass spectrometry is a method of mass spectrometry in which an ion's mass-to-charge ratio is determined via a time measurement. Ions are accelerated by an electric field of known strength. (ref) This acceleration results in an ion having the same kinetic energy as any other ion that has the same charge. The velocity of the ion depends on the mass-to-charge ratio (heavier ions of the same charge reach lower speeds, although ions with higher charge will also increase in velocity). The time that it subsequently takes for the ion to reach a detector at a known distance is measured. This time will depend on the velocity of the ion, and therefore is a measure of its mass-to-charge ratio. Form this ratio and known experimental parameters, one can identify the ion.

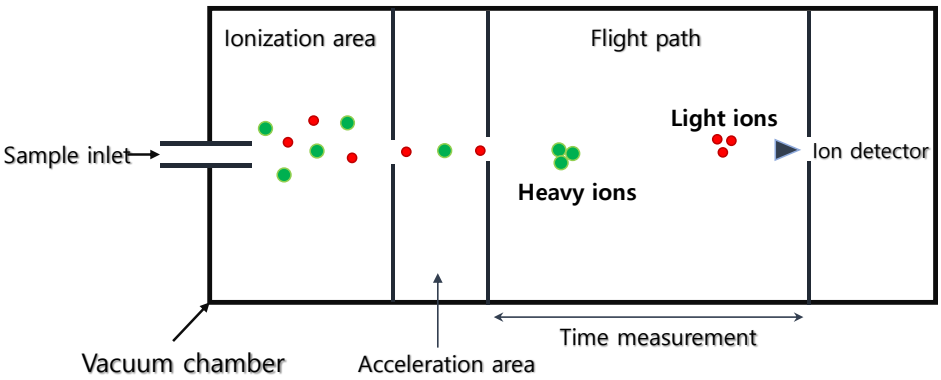

Figure A2. Scheme of time-of-flight mass analysis method. Time-of-flight mass spectrometry is a method of mass spectrometry in which an ion's mass-to-charge ratio is determined via a time measurement.

Quartz Crystal Microbalance (QCM)

A biosensor means a measuring device that binds biological components such as enzymes, microorganisms, antibodies, and receptors to an electrical or physicochemical device, detects the electrode active material or physical change caused by a reaction with a specific target analyte as an electrical signal. Transducer is to converts biological signals from biological reactions into electrical signals, they are classified electrochemical[5], optic[6], thermal, piezoelectric[7-8] according to the principle of transducers.[9] The most widely used electrochemical biosensor has a disadvantage in that the detection limit range is rather high, and the optical biosensor can overcome the disadvantages of the electrophoresis biosensor, however the equipment is expensive and difficult to miniaturize.

On the other hand, the piezoelectric effect type biosensor has a very low detection limit rage, and is composed of only a small reactor including a quartz oscillator and a simple amplification circuit, so that the device is cheap and can be miniaturized. In addition, since the high selectivity of the antibody is utilized, only the substance to be measured can be accurately measured and the interference caused by the interference substance can be minimized.

When mechanical pressure is applied to the surface of several crystals such as quartz, rochelle salt, tourmaline, a voltage is applied between the two surfaces of the crystal, and this magnitude is proportional to the applied pressure, which is called the piezoelectric effect. In addition, when oscillating the crystal by alternating the voltage, a vibrating motion generates a transverse wave, and the frequency of this wave is the unique resonance frequency of crystal. This principle is the basis concept of QCM system currently in use.

- *Electromechanical coupling*

The QCM consists of a thin piezoelectric plate with electrodes evaporated onto both sides. Due to the piezo-effect, an AC voltage across the electrodes induces a shear deformation and vice versa. The electromechanical coupling provides a simple way to detect an acoustic resonance by electrical means. Otherwise, it is of minor importance. However, electromechanical coupling can have a slight influence on the resonance frequency via piezoelectric stiffening. This effect can be used for sensing[10], but is usually avoided. It is essential to have the electric and dielectric boundary conditions well under control. Grounding the front electrode (the electrode in contact with the sample) is one option. A π-network sometimes is employed for the same reason[11]. A π-network is an arrangement of resistors, which almost short-circuit the two electrodes. This makes the device less susceptible to electrical perturbations.

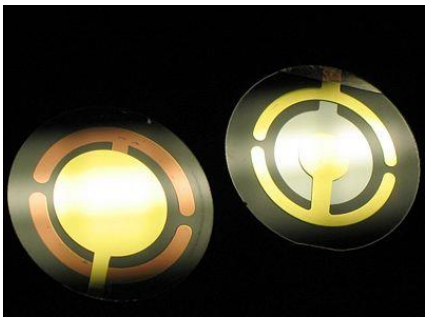

Figure A3. Photograph of typical quartz crystal resonators as used for QCM, metallized with gold electrodes (left: front electrode, right: back electrode) by vapor deposition.

The QCM system is limited to the gaseous state. In the liquid state, the resonance frequency of the quartz crystal depends on various factors such as the viscosity and density of the solution, as well as the mass change of the quartz crystal surface. In the liquid phase, the resistance of the surface of quartz crystal is increased, which is less sensitive than the resonance frequency of the gas phase, but it is advantageous in real time measurement in terms of biosensor.

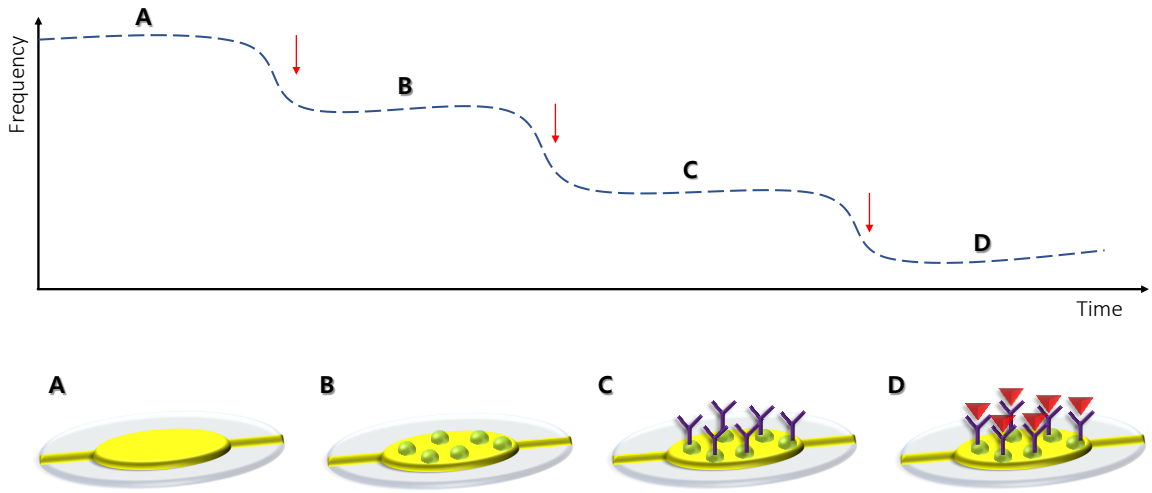

Figure A4. Working principle of Quartz crystal microbalance. (Red arrows indicate each sample injection.)

Surface Plasmon Resonance (SPR)

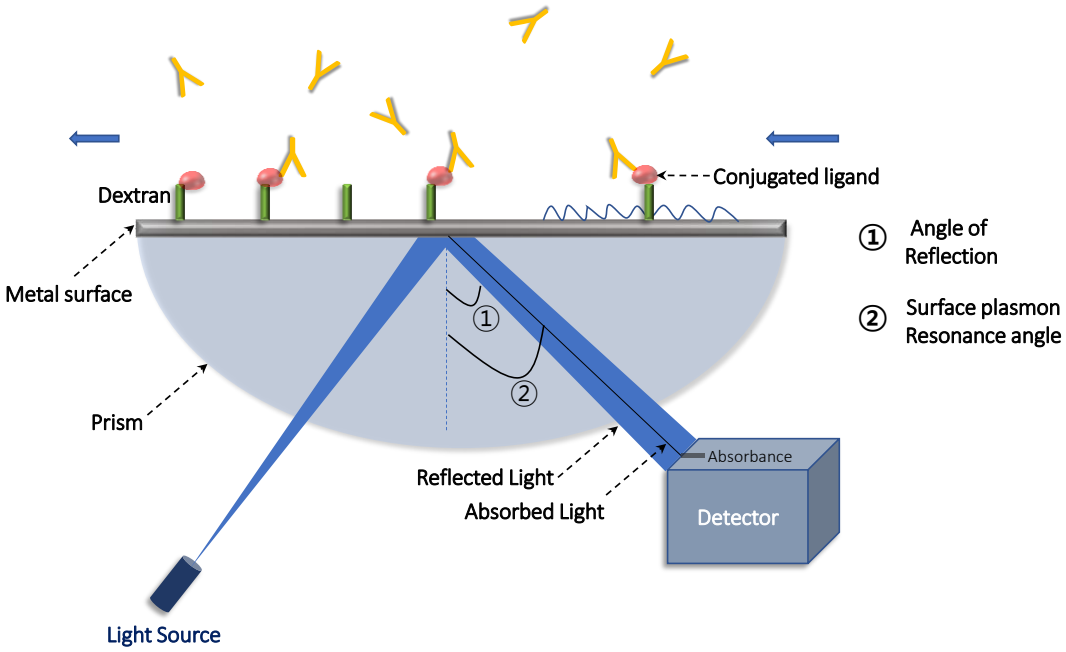

Figure A5. Surface plasmon resonance. The collective oscillation of electrons in a solid or liquid stimulated by incident light.

Surface plasmon resonance (SPR) is the resonant oscillation of conduction electrons at the interface between negative and positive permittivity material stimulated by incident light. SPR is the basis of many standard tools for measuring absorption of material onto planar metal (typically gold or silver) surfaces or onto the surface of metal nanoparticles. It is the fundamental principle behind many color-based biosensor applications and different lab-on-chip sensors.

The surface plasmon polariton is a non-radiative electromagnetic surface wave that propagates in a direction parallel to the negative permittivity/dielectric material interface. Since the wave is on the boundary of the conductor and the external medium (air, water or vacuum for example), these oscillations are very sensitive to any change of this boundary, such as the adsorption of molecules to the conducting surface.[12]

To describe the existence and properties of surface plasmon polaritons, one can choose from various models (quantum theory, Drude model, etc.). The simplest way to approach the problem is to treat each material as a homogeneous continuum, described by a frequency-dependent relative

permittivity between the external medium and the surface. This quantity, hereafter referred to as the materials' "dielectric function," is the complex permittivity. In order for the terms that describe the electronic surface plasmon to exist, the real part of the dielectric constant of the conductor must be negative and its magnitude must be greater than that of the dielectric. This condition is met in the infrared-visible wavelength region for air/metal and water/metal interfaces (where the real dielectric constant of a metal is negative and that of air or water is positive).

Sensor chip CM5 is a general-purpose chip for interaction analysis involving all types of biomolecules such as small organic molecules, proteins, lipids, carbohydrates, and nucleic acids. The sensor chip design to allow detailed quantitative studies of these reagents to yield data on e.g. interaction kinetics, affinity, concentration and binding ratios. The ligand is covalently bound to the sensor chip surface via carboxyl moieties on the dextran. Functional groups on the ligand that can be used for coupling include NH2, SH, CHO and COOH.[13] CM5 is regenerated by selective dissociation of the analyte from the covalently immobilized ligand. Conditions should be chosen to achieve complete dissociation of the analyte without affecting the binding characteristics of the ligand.

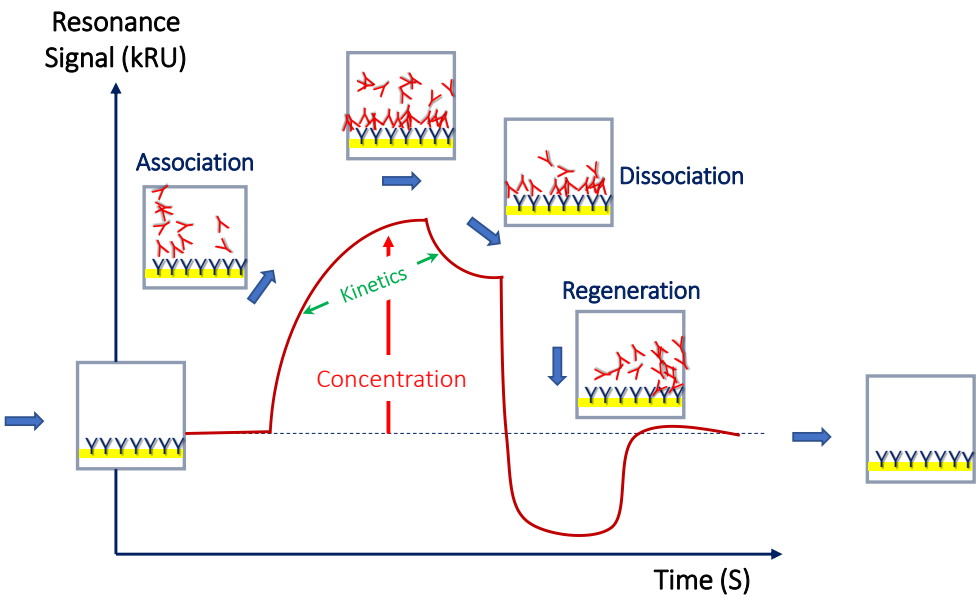

Figure A6. Working principle of surface plasmon resonance. Prepare ligand and analyte select in first step and insert a suitable sensor chip immobilize the ligand and next a control ligand to sensor surface inject analyte and a control analyte over sensor surfaces and record response. Finally, regenerate surfaces if necessary and analyze data.

APPENDIX B

Encapsulin fusion protein cages

Encapsulation of Nano-luciferase in N-termini of Encapsulin-linker-SpyTag

Compartmentalization of biochemical pathways and biological processes is an important feature of all cells. Complex metabolisms often rely on a space control that represents incompatible responses at any given time. Encapsulation of enzymes within protein compartments offers microbes a way to regulate the interconnected network of biochemical reactions comprising their metabolism.[14-15] In particular, encapsulation can increase the local concentration of metabolites and enzymes, prevent leakage of volatile or toxic intermediates, avoid undesired side reactions and create unique microenvironments necessary or the activity of specialized enzymes. Protein cage-based enzyme compartmentalization should be valuable for other cargoes loading and presented targeting moiety to bind specific cancer cell lines.

Encapsulin protein cage is well known to contains ferritin-like proteins or peroxidase, both enzymes involved in oxidative-stress response. These enzymes are targeted to the interior of encapsulin via unique C-terminal extensions. The ferritin-like protein (Flp) and dye decolorizing peroxidase (DyP) with GGDLGIRK peptide well interact with binding pocket on the interior of the spherical shell.[16] However, since this reaction is due to hydrophobicity, it is not easy to apply to other guest molecules encapsulation.

In this study, we tried to encapsulate nano-luciferase enzyme in *T. maritima* encapsulin using genetic modification. To compare the enzyme activity depends on location in encapsulin, nano-luciferase was inserted in N-termini and loop region at 42 which were already confirmed facing inward and in loop138 position which exposure to the exterior surface (Figure B1).[17] In here, we utilized encapsulin-linker-spytag (E-L-ST) as a template for enzyme encapsulation because spytag peptide can bind with spycatcher-molecules to display targeting moieties or other active molecules.[18-19]

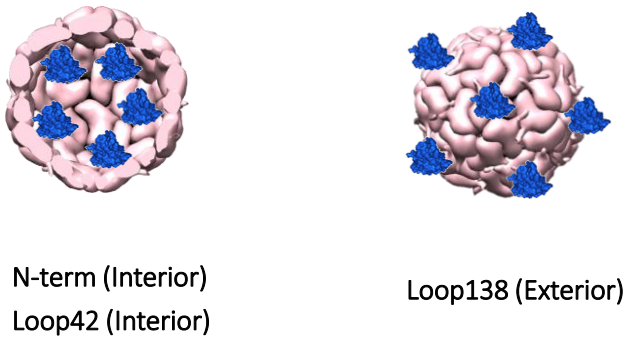

Figure B1. Scheme of nano-luciferase encapsulation in N-termini, Loop42 which exposure to interior surfaces and Loop138 which exposure to exterior surfaces.

Nano-luciferase (Nlluc) is a 19 kDa, ATP independent luciferase that utilizes a novel coelenterazine analog (furimazine) to produce high intensity, glow-type luminescence. Nluc has excellent physical properties with thermal stable, active over broad pH range. In addition, Nluc is very sensitive and can be used for enzyme activity assays. It is expected that cell imaging can be taken with only substrate without external stimulus such as laser.[20]

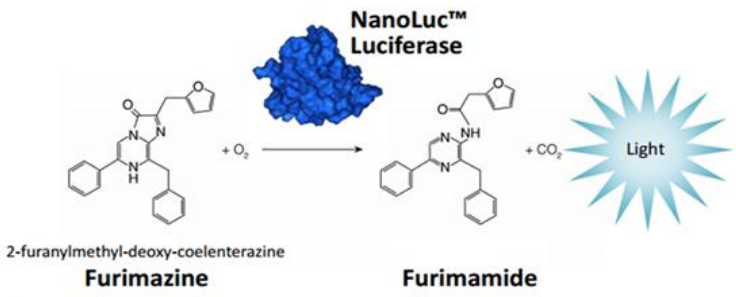

Figure B2. Scheme of nano-luciferase activity with blue light when treated substrate called furimazine.

Nano-luciferase in loop42 (E-L-ST-L42-Nluc), N-termini (E-L-ST-N-Nluc), and loop138 (E-L-ST-L138-Nluc) of Encapsulin-linker-spytag (E-L-ST) were over-expressed and purified using size exclusion chromatography. Although E-L-ST-L138-Nluc was over-expressed and little soluble, E-L-ST-L42-Nluc and E-L-ST-N-Nluc were soluble and heat stable. Soluble fraction of E-L-ST-N-Nluc presented blue light when treated substrate called furimazine.

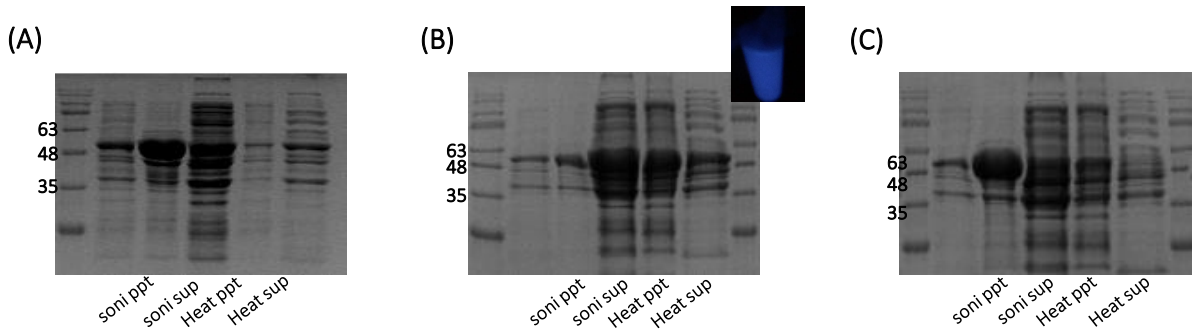

Figure B3. Expression, solubility and heat stability test of E-L-ST-L42-Nluc (A), E-L-ST-N-Nluc (B), and E-L-ST-L138-Nluc (C) using SDS-PAGE.

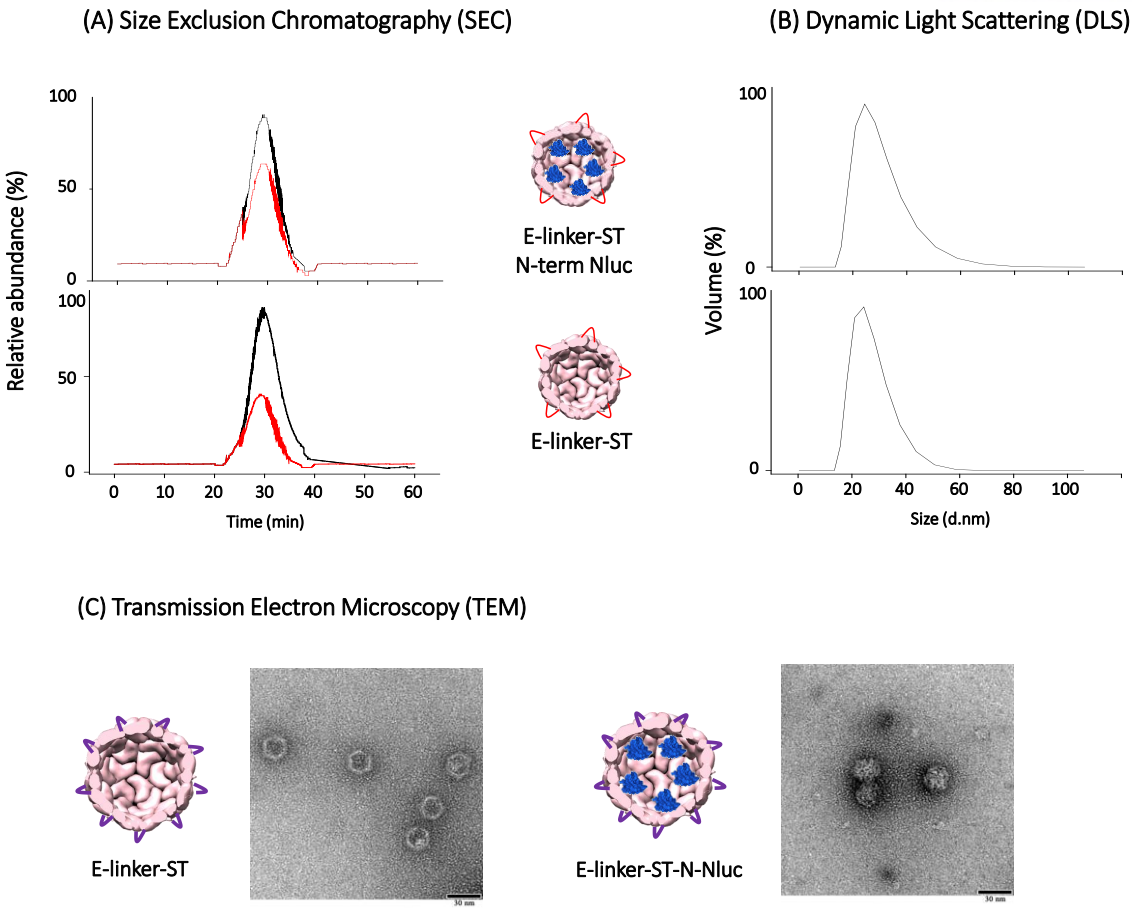

Figure B4. Characterization of E-L-ST-N-Nluc. (A) Size exclusion elution profiles of E-L-ST-N-Nluc (top), E-L-ST (bottom). (B) Dynamic light scattering measurements of E-L-ST-N-Nluc (top), E-L-ST (bottom). (C) Transmission electron microscopy images of E-L-ST-N-Nluc (Right), E-L-ST (left).

To verify Nluc encapsulation in E-L-ST, the biophysical properties of E-L-ST-N-Nluc were examined using size exclusion chromatography (SEC), dynamic light scattering (DLS) and transmission electron microscopy compared with E-L-ST. The SEC elution profile of E-L-ST-N-Nluc (Figure B4 (A) top) was same as that of E-L-ST (Figure B4 (A) bottom). The DLS measurement of E-L-ST-N-Nluc and that of E-L-ST were similar hydrodynamic diameter. The TEM image also indicated their intact cage architecture with uniform size. Although E-L-ST was showed empty inside of cage through negatively stained with uranyl acetate, E-L-ST-N-Nluc was presented fully encapsulate with Nluc.

These data demonstrated that Nluc enzymes were genetically well-encapsulated in encapsulin protein cages and enzyme packaging did not alter their intact cage architectures.

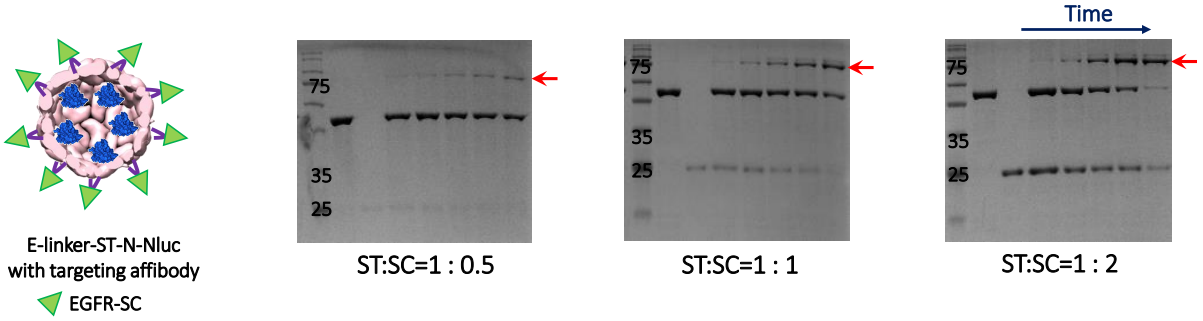

Figure B5. Scheme of binding E-L-ST-N-Nluc and EGFR-SC (left) and binding affinity test depending on time and ratio with SDS-PAGE. (lane 1: E-L-ST-N-Nluc, lane 2: EGFR-SC, lane 3: 10min, lane 4: 30min, lane 5: 1hr, lane 6: 6hr, lane 7: 12hr)

To investigate whether genetically engineered E-L-ST-N-Nluc and EGFR-SpyCatcher (EGFR-SC) can form isopeptide bonds to covalently conjugated to each other, they were mixed together, sampled at various times, and the reaction products were analyzed *via* SDS-PAGE (Figure B5). SDS-PAGE data showed that the covalent ligation between E-L-ST-N-Nluc and EGFR-SC was completed within 12hr.

To date, it has been confirmed through enzymatic activity that the nano-luciferase enzyme is genetically inserted into the encapsulin protein cages without changing the structural intactness. We have also demonstrated that molecules with various functions can be ligated using spytag exterior surface of the cages. Based on the results thus far, it is possible to test the activity of the enzyme to see if it can be used in the assay, and the number of enzymes can be controlled to see how the enzyme activity changes.

References

1. Thomson, B. A.; Iribarne, J. V., Field induced ion evaporation from liquid surfaces at atmospheric pressure. *The Journal of Chemical Physics* **1979,** *71* (11), 4451-4463.

2. Fenn, J. B., Ion formation from charged droplets: roles of geometry, energy, and time. *Journal of the American Society for Mass Spectrometry* **1993,** *4* (7), 524-535.

3. Gaskell, S. J., Electrospray: principles and practice. *Journal of mass spectrometry* **1997,** *32* (7), 677-688.

4. Latourte, L.; Blais, J.-C.; Tabet, J.-C.; Cole, R. B., Desorption Behavior and Distributions of Fluorinated Polymers in MALDI and Electrospray Ionization Mass Spectrometry. *Analytical Chemistry* **1997,** *69* (14), 2742-2750.

5. Russell, L. J.; Rawson, K. M., The commercialisation of sensor technology in clinical chemistry: an outline of the potential difficulties. *Biosensors* **1986,** *2* (5), 301-318.

6. Alarie, J. P.; Sepaniak, M. J.; Vo-Dinh, T., Evaluation of antibody immobilization technqiues for fiber optic-based fluoroimmunosensing. *Analytica Chimica Acta* **1990,** *229*, 169-176.

7. Prusak-Sochaczewski, E.; Luong, J.; Guilbault, G., Development of a piezoelectric immunosensor for the detection of Salmonella typhimurium. *Enzyme and microbial technology* **1990,** *12* (3), 173-177.

8. Roederer, J. E.; Bastiaans, G. J., Microgravimetric immunoassay with piezoelectric crystals. *Analytical Chemistry* **1983,** *55* (14), 2333-2336.

9. Babacan, S.; Pivarnik, P.; Letcher, S.; Rand, A. G., Evaluation of antibody immobilization methods for piezoelectric biosensor application. *Biosensors and Bioelectronics* **2000,** *15* (11), 615-621.

10. Zhang, C.; Vetelino, J. F., Chemical sensors based on electrically sensitive quartz resonators. *Sensors and Actuators B: Chemical* **2003,** *91* (1), 320-325.

11. Koyama, M.; Akaike, K.; Aizawa, H.; Kurosawa, S. In *Electronic circuit system of high sensitivity mass detection for QCM-biosensor*, Frequency Control Symposium and Exposition, 2004. Proceedings of the 2004 IEEE International, IEEE: 2004; pp 813-816.

12. Zeng, S.; Baillargeat, D.; Ho, H.-P.; Yong, K.-T., Nanomaterials enhanced surface plasmon resonance for biological and chemical sensing applications. *Chemical Society Reviews* **2014,** *43* (10), 3426-3452.

13. Muguruma, H.; Nagata, R.; Nakamura, R.; Sato, K.; Uchiyama, S.; Karube, I., Sensor Chip Using a Plasma-polymerized Film for Surface Plasmon Resonance Biosensors: Reliable Analysis of Binding Kinetics. *Analytical Sciences* **2000,** *16* (4), 347-348.

14. Giessen, T. W., Encapsulins: microbial nanocompartments with applications in biomedicine, nanobiotechnology and materials science. *Current Opinion in Chemical Biology* **2016,** *34*, 1-10.

15. Giessen, T. W.; Silver, P. A., A catalytic nanoreactor based on in vivo encapsulation of multiple enzymes in an engineered protein nanocompartment. *ChemBioChem* **2016,** *17* (20), 1931-1935.

16. Sutter, M.; Boehringer, D.; Gutmann, S.; Gunther, S.; Prangishvili, D.; Loessner, M. J.; Stetter, K. O.; Weber-Ban, E.; Ban, N., Structural basis of enzyme encapsulation into a bacterial nanocompartment. *Nat Struct Mol Biol* **2008,** *15* (9), 939-947.

17. Moon, H.; Lee, J.; Min, J.; Kang, S., Developing Genetically Engineered Encapsulin Protein Cage Nanoparticles as a Targeted Delivery Nanoplatform. *Biomacromolecules* **2014,** *15* (10), 3794-3801.

18. Schoene, C.; Fierer, J. O.; Bennett, S. P.; Howarth, M., SpyTag/SpyCatcher cyclization confers resilience to boiling on a mesophilic enzyme. *Angewandte Chemie International Edition* **2014,** *53* (24), 6101-6104.

19. Moon, H.; Bae, Y.; Kim, H.; Kang, S., Plug-and-playable fluorescent cell imaging modular toolkits using the bacterial superglue, SpyTag/SpyCatcher. *Chemical Communications* **2016,** *52* (97), 14051-14054.

20. Sun, Q.; Chen, Q.; Blackstock, D.; Chen, W., Post-Translational Modification of Bionanoparticles as a Modular Platform for Biosensor Assembly. *ACS Nano* **2015,** *9* (8), 8554-8561.